UC Berkeley
UC Berkeley Electronic Theses and Dissertations

Title

Homogeneous Non-Equilibrium Molecular Dynamics Methods for Calculating the Heat Transport Coefficient of Solids and Mixtures

Permalink

https://escholarship.org/uc/item/9h02x1md

Author

Mandadapu, Kranthi Kiran

Publication Date

2011

Peer reviewed|Thesis/dissertation

eScholarship.org Powered by the California Digital Library
University of California

Homogeneous Non-Equilibrium Molecular Dynamics Methods for Calculating the Heat Transport Coefficient of Solids and Mixtures

by

Kranthi Kiran Mandadapu

A dissertation submitted in partial satisfaction
of the requirements for the degree of

Doctor of Philosophy

in

Engineering - Mechanical Engineering

in the

Graduate Division

of the

University of California, Berkeley

Committee in charge:

Professor Panayiotis Papadopoulos, Chair
Professor David J. Steigmann
Professor Alexandre J. Chorin

Spring 2011

Homogeneous Non-Equilibrium Molecular Dynamics Methods for Calculating the Heat Transport Coefficient of Solids and Mixtures

Copyright © 2011

by

Kranthi Kiran Mandadapu

Abstract

Homogeneous Non-Equilibrium Molecular Dynamics Methods for Calculating the Heat Transport Coefficient of Solids and Mixtures

by

Kranthi Kiran Mandadapu

Doctor of Philosophy in Mechanical Engineering

University of California, Berkeley

Professor Panayiotis Papadopoulos, Chair

This thesis presents a class of homogeneous non-equilibrium molecular dynamics (HNEMD) methods for obtaining the heat transport coefficient that relates the heat flux and temperature gradient in the linear irreversible regime. These methods are based on the linear response theory of statistical mechanics. The proposed HNEMD methods are parallelizable, and yield better statistical averages at lower overall computational cost than the existing direct and Green-Kubo methods.

The HNEMD method, as it was initially proposed, is applicable only to single-species systems with two-body interactions. In this thesis, the HNEMD method is extended to single species systems with many-body interactions, and is applied to silicon systems where three-body interactions are taken into account.

The HNEMD method developed for single-species systems is inadequate for obtaining the heat transport coefficient of multi-species systems. A further development of the HNEMD method, the Mixture-HNEMD (M-HNEMD) method, is presented for multi-species systems with many-body interactions. This M-HNEMD method satisfies all the requirements of linear response theory and is compatible with periodic boundary conditions. Applications of the M-HNEMD method to liquid argon-krypton systems with two-body interactions and to perfectly crystalline gallium-nitride systems with three-body interactions are presented, and the results are consistent with the results from the Green-Kubo method. This is the first HNEMD method which can be used for calculating the heat-transport coefficient of multi-species systems.

The expressions for stress tensor and heat-flux vector needed for the development of HNEMD method for single-species systems and of the M-HNEMD method for multi-species systems with many-body interactions require an extension of the statistical mechanical theory of transport processes proposed by Irving and Kirkwood. This extension forms an integral part of the thesis.

Acknowledgements

My doctoral work at Berkeley would not be possible and enjoyable without the support of my advisor Professor Panos Papadopoulos. He was always supportive of my research and was always willing to have long discussions on many of my ideas. His understanding, clarity and presentation of Finite Element Methods motivated me to become his student. I would like to thank him for always trying to impart the qualities of rigorousness and clarity in solving research problems. I would also like to thank him for the long paper writing sessions which focused on presenting the solutions of research problems with clarity.

It would not be possible to publish this thesis without the collaborative work and valuable help of Dr. Reese Jones from Sandia National Laboratories. He was always there whenever I was stuck on a problem. I would like to thank him for helping me develop the software codes. Also, I would like to thank my future advisors, Dr. Jeremy Templeton and Dr. Jonathan Zimmerman, from Sandia National Laboratories for funding my last semester of stay at Berkeley.

I would like to thank my dissertation committee members Professor Alexandre Chorin and Professor David Steigmann for their guidance. They were my constant source of inspiration. I would like to thank Professor Steigmann for his inspirational teaching on various topics such as stability, electrodynamics of continuous media, elasticity and shell theory.

My entrance to Berkeley would not be possible without the help of Professor Sanjay Govindjee. I would like to thank him for providing me funding so that I could come to Berkeley. I have enjoyed working with him and I would like to thank him for being available for long discussions on a wide variety of topics. I have really enjoyed being his assistant for the course Statistical Mechanics of Elasticity.

I would like to thank all the members of Computational Solid Mechanics Laboratory for their support through out my stay in Berkeley. I would especially like to thank Arkaprabha Sengupta for the never ending discussions that I had with him, and Neil Hodge for helping me set up my computer and getting used to Linux.

My stay at Berkeley would not be so memorable without my roommate, Adarsh Krishnamurthy, and my friends Ugljesa and Vesna. I am very grateful to have had such a cheerful roommate. A special thanks to Ugljesa and Vesna for the support they have given me through out my Ph. D. Also, I would like to thank my friends Athulan and Sriram for the endless discussion sessions both in general and academic matters. It would have been very boring to stay at Berkeley without my friends Aditya, Debanjan, Brinda, Anuj, Sharanya, Yasaswini, Dilip, Mary, Subbu, Praveena, Archana, Dimitris, Katerina, Hugo and Jayakanth. I would specially remember Debanjan for the discussions I had with him.

I would like to thank my friends Vamsi, Shanti, Varun, Rajesh, Aparna and Phani in San Jose for entertaining my endless visits whenever I wanted to leave Berkeley. A special thanks to my friend Vamsi for the support that he has given me throughout my Ph. D. I would also like to thank my undergraduate friends Bharath, Rekha, Amit, Sougandh, Sumanth, Sharanya and Raghavender

for their support.

My doctoral work would not be possible without the constant support of my parents and my sister. I am grateful to my parents who always tried to teach me the importance of hard work. Finally, I would like to thank my wife, Deepthi, for her love, patience and support when I was finishing the doctoral work. She was always there for discussing all the problems I had during my Ph. D.

Dedicated to my family and friends.

Contents

Chapter 1

Introduction

Heat conduction is a process involving transfer of energy between regions due to a temperature gradient. In the linear irreversible thermodynamic regime, *i.e.*, when systems are close to thermodynamic equilibrium, the heat flux $\mathbf{J}_Q$ is often modeled as directly proportional to the temperature gradient $\boldsymbol{\nabla} T$, where T is the temperature. This is very well known as the Fourier's law $\mathbf{J}_Q = -\boldsymbol{\kappa} \boldsymbol{\nabla} T$. The constant of proportionality $\boldsymbol{\kappa}$ relating the heat flux to the temperature gradient is called the heat transport coefficient.

Heat transport coefficient estimates are very important in many applications, such as thermoelectric devices which convert heat to electricity [3, 44], semiconductor devices [20], *etc*. In thermoelectrics, the efficiency of the device depends on the thermal conductivity through a dimensionless factor ZT, also called as the *figure of merit*, by

$$ZT \;=\; \frac{\sigma S^2 T}{\kappa}\,, \tag{1.1}$$

where $Z = \dfrac{\sigma S^2}{\kappa}$, S is the Seebeck coefficient and σ is the electrical conductivity. If ZT is high, the efficiency of such devices is high. One way of increasing ZT is to create a material which keep σS^2 constant and to reduce the thermal conductivity κ, showing the importance of the heat transport coefficient [44, 36].

The heat transport coefficient is usually obtained by experiment. However, in some cases, it can be very expensive to perform such experiments. Consider the example of Indium-Gallium-Arsenide ($\mathrm{In}_x - \mathrm{Ga}_{1-x} - \mathrm{As}$) alloy semiconductors as thermoelectric devices. The thermal conductivity of these semiconductors varies with the alloy composition x and exhibits a minimum for $x = 0.53$ [52]. It was later found by experiments that adding Erbium-Arsenide (ErAs) nanoparticles to ($\mathrm{In}_{0.53} - \mathrm{Ga}_{0.47} - \mathrm{As}$) reduced the thermal conductivity by 50% and the numerator in (1.1) did not change, thereby doubling the ZT [36]. In order to find a better thermoelectric material, *i.e.*, higher ZT, than $\mathrm{ErAs} : \mathrm{In}_{0.53} - \mathrm{Ga}_{0.47} - \mathrm{As}$, one needs to alloy further using group III and group V compounds from the periodic table. However, there exist many possible choices

of elements in groups III and V, therefore the task of doing experiments may become very expensive. Molecular dynamics (MD) simulations provide a valuable tool in the above problem by reducing the pool of choices for which experiments can be performed, thereby reducing the total cost of experiments. Another important case involves problems related to mechanics, where the thermal conductivity tensor $\boldsymbol{\kappa}$ is often strongly dependent on the deformation gradient $\mathbf{F}$ and the temperature T. The task of designing experiments that measure $\boldsymbol{\kappa}(\mathbf{F}, T)$ is generally complex and expensive owing to the size of the parametric space of $\mathbf{F}$ and T. Moreover, it is often difficult to identify from the experimental results the contribution of, say, a distribution of defects or impurities. Molecular dynamics (MD) simulations provide an efficient supplement to such experiments.

Heat transport coefficient can be computed using MD simulations given sufficient information regarding the inherent molecular structure and an interatomic potential that accurately describes the interactions among the particles in the system [31, 42, 11, 69, 21, 25, 48, 51, 70, 67, 33, 73, 46, 45, 47]. The two most commonly used methods for estimating the heat transport coefficient are (i) the direct method [69, 67, 73] and (ii) the GreenKubo (GK) method [38, 40, 28, 70, 67, 33]. In the direct method, a fixed heat flux $\mathbf{J}_Q$ is driven through the system and the corresponding temperature gradient is estimated [67, 73]. The heat transport coefficient is then obtained by using Fourier's law ($\mathbf{J}_Q = -\boldsymbol{\kappa}\boldsymbol{\nabla}T$). This is a non-equilibrium molecular dynamics (NEMD) method as the system is driven to a non-equilibrium thermodynamic state due to the temperature gradient and is called as the direct method, as it is analogous to the experimental measurement. Another variant of the direct method exists, where a fixed temperature gradient is maintained by using two reservoirs with different temperatures at the two ends of the system and the corresponding heat flux is estimated [31, 69]. The heat transport coefficient is then obtained using Fourier' law. This method is fraught with finite-size effects and unrealistically large temperature gradients making it difficult to obtain an estimate of the heat transport coefficient at the desired temperature. On the other hand, the Green-Kubo (GK) method is an equilibrium molecular dynamics method, where fluctuations of the heat flux from equilibrium MD simulations are employed to calculate the heat transport coefficient via the Green-Kubo formulae [70, 67, 33]. These formulae are obtained by employing Onsager' regression hypothesis [57, 58], and are given by integrals of autocorrelation functions of the heat fluxes [40, 28]. In this method, the heat flux autocorrelation function is obtained from the heat flux fluctuations and is then integrated. Typically, the GK method requires very long simulation times to yield values of heat transport coefficients that are converged to within statistical uncertainties, largely due to the inaccuracy of the calculation of the autocorrelation function. An alternative to these methods, the so-called homogeneous nonequilibrium molecular dynamics (HNEMD) method [21, 24, 46, 45, 47], with which this thesis is chiefly concerned, has advantages over both the GK method and the direct method. Relative to the former it is free of difficulties involving the calculation and integration of the heat flux autocorrelation tensor, while relative to the latter it does not have strong size effects and unrealistically large temperature gradients. In addition, the HNEMD method typically yields better statistical averages than both the direct and the GK method at a lower overall computational cost.

The HNEMD method, initially proposed by Evans [21], defines a mechanical analog to the

thermal transport process and uses the linear response theory to calculate the transport coefficients. This method is synthetic, in the sense that a fictitious external force field is used to mimic the effect of a thermal gradient, thereby reducing the thermal transport problem to a mechanical problem. This external force field appears in the equations of motion. If this force field is sufficiently small, the long-time ensemble average of the heat flux vector corresponding to the resultant nonequilibrium system is proportional to the field with the constant of proportionality being the Green-Kubo formula for the heat transport coefficient. Therefore, the heat transport coefficient at a desired temperature can be computed from the response of the heat flux vector to the fictitious force field, thereby avoiding the tedious calculation and integration of the heat flux autocorrelation function.

The HNEMD method was initially formulated by Evans for "single-species" systems modeled by interaction potentials consisting of two-body (or pair) potentials. Therefore, in its original incarnation, it was not applicable to materials that contain different species and are modeled by higher order potentials. Also, if this initially developed HNEMD method is applied to multi-species systems, *e.g.*, a semi-conductor gallium-nitride (GaN) system, the long-time average of the heat flux vector still remains proportional to the external field. However, the constant of proportionality is not just equal to heat transport coefficient, but involves additional correlation integrals. These correlation integrals need to be evaluated from an equilibrium simulation in addition to running the HNEMD algorithm. To this end, a new class of HNEMD method is developed in this thesis to address the shortcomings of the original HNEMD method.

The contributions from this thesis can be grouped into three parts: (i) extension of the HNEMD method to single species systems modeled by three-body and many-body potentials, (ii) a new HNEMD method for multi-species systems, called here as *Mixture*-HNEMD (M-HNEMD) method, modeled by interaction potentials containing terms of any order, and (iii) extension of Irving and Kirkwood's statistical mechanical theory of transport processes to systems modeled by many body potentials, so as to be able to derive the expressions for stress tensor and heat flux vector which can be used in the HNEMD and M-HNEMD methods.

The thesis is organized as follows: In Chapter 2, a review of the basic continuum thermomechanics is given within the context of heat conduction in solids and liquid mixtures. Here, the balance laws of mass, momentum, energy and entropy are introduced. Explicit formulae for the internal entropy production rate in terms of the flux vectors, such as heat flux and diffusive flux, and thermodynamic forces, such as temperature gradient and chemical potential gradient that drive the irreversible processes, are obtained. Assuming that the system is not far from equilibrium, linear phenomenological laws are introduced between the fluxes and thermodynamic forces and heat transport coefficient is identified as a constant of proportionality between the heat flux and the temperature gradient. In Chapter 3, a review of statistical mechanics is given. Here, Green-Kubo formulae required for the evaluation of heat transport coefficient are also introduced. Later, the statistical mechanical theory of transport processes given by Irving and Kirkwood is extended to systems modeled by many-body interaction potentials. In Chapter 4, a review of the existing molecular dynamics methods, such as the direct method and Green-Kubo methods for evaluating the heat transport coefficients is given and their advantages and disadvantages are highlighted.

Also, the HNEMD method, which forms the main contribution of this thesis, is introduced. Chapter 5 introduces the linear response theory necessary for the application of the HNEMD method to compute the heat transport coefficient. Here, a review of the equations of motion required to maintain a constant temperature in the form of a Nosé-Hoover thermostat is presented, and it is proved that these equations of motion reproduce the canonical phase-space distribution. Subsequently, these equations of motion are perturbed by an external field in a particular way and the long-time average of any phase variable is shown to be proportional to the external field with the constant of proportionality being an integral of an autocorrelation function. Three basic conditions required for the application of this theory to evaluate the heat transport coefficient are obtained by equating the above integral of the autocorrelation function to the Green-Kubo formula for the heat transport coefficient. In Chapter 6, the equations of motion necessary for the application of HNEMD method to single-species systems are introduced for the case of two-body potentials and applied to an argon (Ar) system at the triple point. These are then extended to three-body and many-body potentials and applied to a silicon (Si) system. In Chapter 7, it is shown that the HNEMD method in its original form is inadequate to estimate the heat transport coefficient for a multi-species system. Next, the M-HNEMD equations of motion are developed and applied to a pure argon system, an argon-krypton (Ar-Kr) binary mixture, and a perfect GaN crystal. Chapter 8 summarizes the findings of the thesis and describes potential directions of future work.

Chapter 2

Continuum Thermomechanics

In this chapter, the macroscopic balance laws of mass, momentum and energy are introduced. The Second Law of Thermodynamics is introduced as a form of entropy balance with positive internal entropy production rate. For the case of solids and liquid mixtures, explicit formulae for the internal entropy production rate in terms of the flux vectors and the thermodynamic forces driving the irreversible processes are obtained. Further, in the linear irreversible thermodynamical regime, linear phenomenological relations are proposed between fluxes and thermodynamic forces, thereby identifying thermal conductivity as a constant of proportionality between the heat flux and the temperature gradient vectors.

2.1 Kinematics and Balance Laws

Consider a body $\mathcal{B}$, defined as a collection of material points, whose reference configuration is denoted by $\mathcal{R}_0$ at time t_0 and whose current configuration is $\mathcal{R}$ at time t. Let $\mathbf{X}$ be the position vector of any material point in the reference configuration and let corresponding position vector $\mathbf{x}$ in the current configuration be defined by a mapping $\chi \ : \ \mathcal{R}_0 \times t \rightarrow \mathcal{R}$ such that $\mathbf{x} = \chi(\mathbf{X}, t)$. Deformation in the body is characterized by the deformation gradient $\mathbf{F}$ defined as $\mathbf{F}(\mathbf{X}, t) = \dfrac{\partial \mathbf{x}}{\partial \mathbf{X}}$.

The local forms of macroscopic balances of mass, momentum and energy with respect to the current configuration are expressed as

$$\dot{\rho}(\mathbf{x}, t) + \rho(\mathbf{x}, t) \frac{\partial}{\partial \mathbf{x}} \cdot \mathbf{v}(\mathbf{x}, t) \ = \ 0 \ , \tag{2.1}$$

$$\rho(\mathbf{x}, t) \dot{\mathbf{v}}(\mathbf{x}, t) \ = \ \frac{\partial}{\partial \mathbf{x}} \cdot \mathbf{T}(\mathbf{x}, t) + \rho(\mathbf{x}, t) \mathbf{b}(\mathbf{x}, t) \ , \tag{2.2}$$

and

$$\rho(\mathbf{x},t)\dot{e}(\mathbf{x},t) \;=\; \rho(\mathbf{x},t)\mathbf{b}(\mathbf{x},t)\cdot\mathbf{v}(\mathbf{x},t) + \rho(\mathbf{x},t)r(\mathbf{x},t) + \frac{\partial}{\partial\mathbf{x}}\cdot(\mathbf{T}(\mathbf{x},t)\mathbf{v}(\mathbf{x},t)) - \frac{\partial}{\partial\mathbf{x}}\cdot\mathbf{J}_Q(\mathbf{x},t)\;, \tag{2.3}$$

where $\rho(\mathbf{x},t) > 0$ is the mass density, $\mathbf{v}(\mathbf{x},t) = \dfrac{\mathrm{d}\mathbf{x}}{\mathrm{d}t}$ is the velocity, $\mathbf{T}(\mathbf{x},t)$ is the Cauchy stress tensor, $\mathbf{b}(\mathbf{x},t)$ is the body force per unit mass, $\mathbf{J}_Q(\mathbf{x},t)$ is the heat flux vector, $r(\mathbf{x},t)$ is the heat source per unit mass at the macroscopic point $\mathbf{x}$ at time t, and $e(\mathbf{x},t)$ is the total energy per unit mass defined as

$$e \;=\; \frac{1}{2}\mathbf{v}\cdot\mathbf{v} + \epsilon \tag{2.4}$$

with ϵ being the internal energy per unit mass. Here, "$\dfrac{\partial}{\partial\mathbf{x}}\cdot$" denotes the divergence operator and $\dot{\overline{(\cdot)}} = \dfrac{d}{dt}(\cdot)$ denotes the material time-derivative of $(\cdot)$.

The local form of the Second Law of Thermodynamics is expressed as

$$\rho(\mathbf{x},t)\dot{\eta}(\mathbf{x},t) \;=\; -\frac{\partial}{\partial\mathbf{x}}\cdot\mathbf{J}_\eta(\mathbf{x},t) + \rho(\mathbf{x},t)s_e(\mathbf{x},t) + \rho(\mathbf{x},t)s_i(\mathbf{x},t)\;, \tag{2.5}$$

where $\eta(\mathbf{x},t)$ is the entropy per unit mass, $\mathbf{J}_\eta(\mathbf{x},t)$ is the entropy flow per unit area, $s_e(\mathbf{x},t)$ is the external entropy production rate per unit mass (*e.g.*, radiation) and $s_i(\mathbf{x},t)$ is the internal entropy production rate per unit mass which is positive for irreversible processes and zero for reversible processes, *i.e.*,

$$s_i(\mathbf{x},t) \geq 0\;, \tag{2.6}$$

see [61, Chapter 3] and [18, 26, 27]. Using (2.4), the balance of energy (2.3) can be rewritten as

$$\rho\dot{\epsilon} \;=\; -\frac{\partial}{\partial\mathbf{x}}\cdot\mathbf{J}_Q + \rho r + \mathbf{T}:\mathbf{L} \tag{2.7}$$

using (2.2), where $\mathbf{L} = \dfrac{\partial\mathbf{v}}{\partial\mathbf{x}}$ is the velocity gradient, and ":" denotes the double dot product of any two tensors.

2.2 Heat Conduction in an Elastic Solid

In an elastic solid, the internal energy ϵ and entropy η are assumed to depend on the deformation gradient $\mathbf{F}$ and temperature T, *i.e.*,

$$\epsilon \;=\; \hat{\epsilon}(\mathbf{F},T)\;, \tag{2.8}$$

$$\eta \;=\; \hat{\eta}(\mathbf{F},T)\;. \tag{2.9}$$

Now, defining the Helmholtz free energy per unit mass $\psi = \hat{\psi}(\mathbf{F}, T)$ as

$$\psi \;=\; \epsilon - T\eta \,, \tag{2.10}$$

the rate of change of entropy is given by

$$\begin{aligned} \rho\dot{\eta} \;&=\; \frac{\rho\dot{\epsilon} - \rho\dot{T}\eta - \rho\dot{\psi}}{T} \\ &=\; -\frac{\partial}{\partial \mathbf{x}} \cdot \left(\frac{\mathbf{J}_Q}{T}\right) + \rho\frac{r}{T} - \left(\rho\eta + \rho\frac{\partial\psi}{\partial T}\right)\frac{\dot{T}}{T} + \left(\mathbf{T} - \rho\frac{\partial\psi}{\partial\mathbf{F}}\mathbf{F}^T\right) : \frac{\mathbf{L}}{T} - \mathbf{J}_Q \cdot \frac{\boldsymbol{\nabla} T}{T^2} \,, \end{aligned} \tag{2.11}$$

where the second equality is obtained by using (2.7). Comparing (2.11) to the balance of entropy given by (2.5), it can be seen that the entropy flow $\mathbf{J}_\eta$, externally supplied entropy rate s_e and the internal entropy production rate s_i are given by

$$\mathbf{J}_\eta \;=\; \frac{\mathbf{J}_Q}{T} \,, \tag{2.12}$$

$$\rho s_e \;=\; \rho\frac{r}{T} \,, \tag{2.13}$$

$$\rho s_i = -\left(\rho\eta + \rho\frac{\partial\psi}{\partial T}\right)\frac{\dot{T}}{T} + \left(\mathbf{T} - \rho\frac{\partial\psi}{\partial\mathbf{F}}\mathbf{F}^T\right) : \frac{\mathbf{L}}{T} + \mathbf{J}_Q \cdot \mathbf{X}_Q \;\geq\; 0 \,, \tag{2.14}$$

respectively, where $\mathbf{X}_Q = -\dfrac{\boldsymbol{\nabla} T}{T^2}$. Since inequality (2.14) holds for all $\mathbf{F}$ and T, and also T may vary independently of $\mathbf{F}$ for homothermal processes, ($\boldsymbol{\nabla} T = \mathbf{0}$) one can obtain

$$\mathbf{T} \;=\; \rho\frac{\partial\psi}{\partial\mathbf{F}}\mathbf{F}^T \,, \tag{2.15}$$

$$\eta \;=\; -\frac{\partial\psi}{\partial T} \,, \tag{2.16}$$

therefore one is left with the inequality

$$\mathbf{J}_Q \cdot \mathbf{X}_Q \;\geq\; 0 \,. \tag{2.17}$$

Here, $\mathbf{X}_Q$ is called the thermodynamic force driving the irreversible process of heat conduction. In the linear irreversible thermodynamic regime, the heat flux vector $\mathbf{J}_Q$ may be assumed to be linearly dependent on the thermodynamic force $\mathbf{X}_Q$, *i.e.*,

$$\mathbf{J}_Q \;= \mathbf{L}_{QQ}\mathbf{X}_Q \,, \tag{2.18}$$

where $\mathbf{L}_{QQ}$ is the constant of proportionality tensor. Admitting Fourier' law in the form $\mathbf{J}_Q = -\boldsymbol{\kappa}\boldsymbol{\nabla}T$, and recalling the definition of $\mathbf{X}_Q$, the thermal conductivity tensor can be obtained as

$$\boldsymbol{\kappa} = \frac{\mathbf{L}_{QQ}}{T^2} \ . \tag{2.19}$$

2.3 Heat Conduction in Liquid Mixtures

It is well known that mixtures consisting of different species are capable of heat conduction, diffusion and cross phenomena such as the thermo diffusion (commonly called Sorét effect) and the Dufour effect [18, Section 49]. Sorét effect is a phenomenon where a concentration gradient is set up due to a temperature gradient [35]. Dufour effect is a phenomenon where a temperature gradient arises when two substances diffuse each other [66]. In a mixture consisting of n different species, one may write balance laws of mass, momentum and energy for each species [55]. However, for the present purpose, only balances of mass for the species are written separately and combined balance laws of momentum and energy are used to define the internal entropy production rate [18, 19].

At the macroscopic point $\mathbf{x}$, the system of liquid mixtures has a density $\rho(\mathbf{x}, t)$ such that

$$\rho(\mathbf{x}, t) \ = \ \sum_{k=1}^{n} \rho_k(\mathbf{x}, t) \ , \tag{2.20}$$

where $\rho_k(\mathbf{x}, t)$ is the density of species k [18, Chapter 43]. The local form of the balance of mass for the species k, when there are no chemical reactions, is expressed as

$$\frac{\partial \rho_k}{\partial t} \ = \ -\frac{\partial}{\partial \mathbf{x}} \cdot (\rho_k \mathbf{v}_k) \ , \tag{2.21}$$

where $\mathbf{v}_k$ is the velocity of the species k. Summing (2.21) over all the species, one may obtain

$$\frac{\partial}{\partial t}\left(\sum_{k=1}^{n} \rho_k\right) \ = \ -\frac{\partial}{\partial \mathbf{x}} \cdot \left(\sum_{k=1}^{n} \rho_k \mathbf{v}_k\right) \ . \tag{2.22}$$

Now, defining the barycentric velocity $\mathbf{v}$ at the macroscopic point $\mathbf{x}$ as

$$\mathbf{v} \ = \ \frac{\displaystyle\sum_{k=1}^{n} \rho_k \mathbf{v}_k}{\rho} \ , \tag{2.23}$$

and using (2.20), (2.22) can be written as

$$\frac{\partial \rho}{\partial t} \;=\; -\frac{\partial}{\partial \mathbf{x}} \cdot (\rho \mathbf{v}) \;. \tag{2.24}$$

Also, the material time derivative of the density of species k can be written as

$$\dot{\rho_k} = = \; -\rho_k \frac{\partial}{\partial \mathbf{x}} \cdot \mathbf{v} - \frac{\partial}{\partial \mathbf{x}} \cdot \mathbf{J}_k \tag{2.25}$$

using (2.21) and (2.22), where $\mathbf{J}_k \;=\; \rho_k(\mathbf{v}_k - \mathbf{v})$ is the diffusive flux. It can be seen from the definition of diffusive flux and barycentric velocity (2.23) that

$$\sum_{k=1}^{n} \mathbf{J}_k \;=\; \sum_{k=1}^{n} \rho_k(\mathbf{v}_k - \mathbf{v}) = \mathbf{0} \;. \tag{2.26}$$

Again, summing up (2.25) over all the species and using (2.20), one may obtain

$$\dot{\rho} \;=\; -\rho \frac{\partial}{\partial \mathbf{x}} \cdot \mathbf{v} \;, \tag{2.27}$$

which is the balance of mass at the macroscopic point $\mathbf{x}$ when all of the species are taken together. Now, defining the concentration of each species c_k as

$$c_k \;=\; \frac{\rho_k}{\rho} \;, \tag{2.28}$$

the rate of concentration of species may be obtained as

$$\rho \dot{c_k} \;=\; -\frac{\partial}{\partial \mathbf{x}} \cdot \mathbf{J}_k \;. \tag{2.29}$$

The local form of the combined balance of momentum is expressed as

$$\rho \dot{\mathbf{v}} \;=\; \frac{\partial}{\partial \mathbf{x}} \cdot \mathbf{T} + \sum_{k=1}^{n} \rho_k \mathbf{b}_k \;, \tag{2.30}$$

where $\mathbf{b}_k$ is the body force per unit mass on the species k. Similarly, the local form of the balance of energy is expressed as

$$\rho \dot{e} \;=\; \sum_{k=1}^{n} \rho_k \mathbf{b}_k \cdot \mathbf{v}_k + \rho r + \frac{\partial}{\partial \mathbf{x}} \cdot (\mathbf{T}\mathbf{v}) - \frac{\partial}{\partial \mathbf{x}} \cdot \mathbf{J}_Q \;. \tag{2.31}$$

Again, defining the total energy $e = \frac{1}{2}\mathbf{v}\cdot\mathbf{v} + \epsilon$ for the liquid mixture, (2.31) may be written as

$$\rho\dot{\epsilon} = -\rho r + \mathbf{T} : \mathbf{L} + \sum_{k=1}^{n} \mathbf{b}_k \cdot \mathbf{J}_k - \frac{\partial}{\partial \mathbf{x}} \cdot \mathbf{J}_Q \, . \tag{2.32}$$

At this stage, the derivations are specialized to the case of a liquid mixture system, which is assumed to be constitutively dependent on specific volume $\nu = \frac{1}{\rho}$, temperature T and concentrations c_k, *i.e.*,

$$\epsilon \;=\; \hat{\epsilon}(\nu, T, c_1, c_2, \ldots, c_n) \, , \tag{2.33}$$

$$\eta \;=\; \hat{\eta}(\nu, T, c_1, c_2, \ldots, c_n) \, . \tag{2.34}$$

Again, similar to the case of solids, introducing the Helmholtz energy to be $\psi = \hat{\psi}(\nu, T, c_1, c_2, \ldots, c_n)$ $= \epsilon - T\eta$, the rate of entropy is obtained as

$$\begin{aligned} \rho\dot{\eta} \;&=\; \frac{\rho\dot{\epsilon} - \rho\dot{T}\eta - \rho\dot{\psi}}{T} \\ &=\; -\frac{\partial}{\partial \mathbf{x}} \cdot \left(\frac{\mathbf{J}_Q}{T}\right) + \rho\frac{r}{T} - \left(\rho\eta + \rho\frac{\partial\psi}{\partial T}\right)\frac{\dot{T}}{T} + \left(\mathbf{T} - \frac{\partial\psi}{\partial\nu}\mathbf{I}\right) : \frac{\mathbf{L}}{T} - \mathbf{J}_Q \cdot \frac{\boldsymbol{\nabla} T}{T^2} \\ &\qquad - \rho\sum_{k=1}^{n} \frac{\partial\psi}{\partial c_k}\frac{\dot{c}_k}{T} + \sum_{k=1}^{n} \mathbf{b}_k \cdot \mathbf{J}_k \, . \end{aligned} \tag{2.35}$$

Using (2.29) and letting $\mu_k = \dfrac{\partial\psi}{\partial c_k}$ be the chemical potential of species k, (2.35) can be reduced to

$$\begin{aligned} \rho\dot{\eta} \;=\; -\frac{\partial}{\partial \mathbf{x}} \cdot \left(\frac{\mathbf{J}_Q - \sum_{k=1}^{n} \mu_k \mathbf{J}_k}{T}\right) + \rho\frac{r}{T} - \left(\rho\eta + \rho\frac{\partial\psi}{\partial T}\right)\frac{\dot{T}}{T} + \left(\mathbf{T} - \frac{\partial\psi}{\partial\nu}\mathbf{I}\right) : \frac{\mathbf{L}}{T} \\ - \mathbf{J}_Q \cdot \frac{\boldsymbol{\nabla} T}{T^2} + \sum_{k=1}^{n} \left[\mathbf{b}_k - \boldsymbol{\nabla}\left(\frac{\mu_k}{T}\right)\right] \mathbf{J}_k \, . \end{aligned} \tag{2.36}$$

where $\mathbf{I}$ is the identity tensor. Comparing (2.36) to (2.5), the entropy flow $\mathbf{J}_\eta$, the external entropy supply rate s_e, and the internal entropy production rate are obtained as

$$\mathbf{J}_\eta \;=\; \frac{\mathbf{J}_Q - \sum_{k=1}^{n} \mu_k \mathbf{J}_k}{T} \, , \tag{2.37}$$

$$\rho s_e \;= \frac{r}{T} \, , \tag{2.38}$$

$$\rho s_i \;=\; -\left(\rho\eta + \rho\frac{\partial\psi}{\partial T}\right)\frac{\dot{T}}{T} + \left(\mathbf{T} - \frac{\partial\psi}{\partial\nu}\mathbf{I}\right) : \frac{\mathbf{L}}{T} + \mathbf{J}_Q \cdot \mathbf{X}_Q + \sum_{k=1}^{n} \mathbf{J}_k \cdot \mathbf{X}_k \;\geq\; 0\,, \tag{2.39}$$

respectively, where $\mathbf{X}_Q$ and $\mathbf{X}_k = \mathbf{b}_k - \boldsymbol{\nabla}\left(\frac{\mu_k}{T}\right)$ are the thermodynamic forces driving the irreversible processes of heat transfer and diffusion, respectively. Again, as (2.39) is valid for all ν and T assuming no viscous effects, one can obtain the following results

$$\eta \;=\; -\rho\frac{\partial\psi}{\partial T}\,, \tag{2.40}$$

$$\mathbf{T} \;=\; \frac{\partial\psi}{\partial\nu}\mathbf{I}\,, \tag{2.41}$$

$$\rho s_i \;=\; \mathbf{J}_Q \cdot \mathbf{X}_Q + \sum_{k=1}^{n} \mathbf{J}_k \cdot \mathbf{X}_k \;\geq\; 0\,. \tag{2.42}$$

Taking into account (2.26), the total rate of entropy production (2.42) can be equivalently expressed as

$$\rho s_i \;=\; \mathbf{J}_Q \cdot \mathbf{X}_Q + \sum_{k=1}^{n-1} \mathbf{J}_k \cdot (\mathbf{X}_k - \mathbf{X}_n) \;\geq\; 0\,. \tag{2.43}$$

Reducing (2.43) to the special case of binary mixture ($n = 2$) results in

$$\rho s_i \;=\; \mathbf{J}_Q \cdot \mathbf{X}_Q + \mathbf{J}_1 \cdot (\mathbf{X}_1 - \mathbf{X}_n) \;\geq\; 0\,. \tag{2.44}$$

Assuming the irreversible processes are close to thermodynamic equilibrium, the linear phenomenological relations

$$\mathbf{J}_1 \;=\; \mathbf{L}_{11}(\mathbf{X}_1 - \mathbf{X}_2) + \mathbf{L}_{1Q}\mathbf{X}_Q \tag{2.45}$$

$$\mathbf{J}_Q \;=\; \mathbf{L}_{Q1}(\mathbf{X}_1 - \mathbf{X}_2) + \mathbf{L}_{QQ}\mathbf{X}_Q \tag{2.46}$$

are proposed, where $\mathbf{L}_{11}$, $\mathbf{L}_{1Q}$, $\mathbf{L}_{Q1}$ and $\mathbf{L}_{QQ}$ are phenomenological coefficient matrices. Using (2.45), (2.46) and (2.44) it can be seen that

$$\begin{bmatrix} \mathbf{X}_Q & \mathbf{X}_1 - \mathbf{X}_2 \end{bmatrix} \begin{bmatrix} \mathbf{L}_{QQ} & \mathbf{L}_{Q1} \\ \mathbf{L}_{1Q} & \mathbf{L}_{11} \end{bmatrix} \begin{bmatrix} \mathbf{X}_Q \\ \mathbf{X}_1 - \mathbf{X}_2 \end{bmatrix} \;\geq\; 0 \tag{2.47}$$

for any $\mathbf{X}_Q$ and $\mathbf{X}_1 - \mathbf{X}_2$. It can be seen from (2.47) that the tensor $\begin{bmatrix} \mathbf{L}_{QQ} & \mathbf{L}_{Q1} \\ \mathbf{L}_{1Q} & \mathbf{L}_{11} \end{bmatrix}$ is positive definite. Hence $\mathbf{L}_{QQ}$ and $\mathbf{L}_{11}$ are also positive definite and are therefore invertible.

It is important to emphasize that in the case of binary liquid mixtures the evaluation of $\mathbf{L}_{QQ}$ is

not sufficient for estimating the thermal conductivity $\boldsymbol{\kappa}$. Indeed, experiments measuring thermal conductivity of binary liquid mixtures are typically conducted using the stationary state ($\mathbf{J}_1 = \mathbf{0}$). In this case, (2.45) implies $\mathbf{X}_1 - \mathbf{X}_2 = -\mathbf{L}_{11}^{-1}\mathbf{L}_{1Q}\mathbf{X}_Q$, which reduces (2.46) to

$$\mathbf{J}_Q \;=\; (\mathbf{L}_{QQ} - \mathbf{L}_{Q1}\mathbf{L}_{11}^{-1}\mathbf{L}_{1Q})\mathbf{X}_Q \; . \tag{2.48}$$

Therefore, for binary liquid mixtures, admitting Fourier's law in the form $\mathbf{J}_Q = -\boldsymbol{\kappa}\boldsymbol{\nabla}T$ and recalling the definition of $\mathbf{X}_Q$, the thermal conductivity tensor may be obtained as

$$\boldsymbol{\kappa} \;=\; \frac{1}{T^2}(\mathbf{L}_{QQ} - \mathbf{L}_{Q1}\mathbf{L}_{11}^{-1}\mathbf{L}_{1Q}) \; . \tag{2.49}$$

In contrast to liquid mixtures, in a crystalline solid, if no significant mass diffusion exits, one may neglect diffusion and the cross phenomena associated with it. In this case, $\mathbf{X}_Q$ is the only thermodynamic force, and therefore the heat flux vector in the linear irreversible regime follows the phenomenological law $\mathbf{J}_Q = \mathbf{L}_{QQ}\mathbf{X}_Q$, thus yielding the thermal conductivity as $\kappa = \dfrac{\mathbf{L}_{QQ}}{T^2}$, as shown in Section 2.2.

The main objective of this work is to estimate the heat transport coefficient $\dfrac{\mathbf{L}_{QQ}}{T^2}$ using molecular dynamics simulations in an accurate and time efficient manner. Hence, a connection needs to be established between macroscopic quantities such as energy, heat flux, diffusive flux etc., with the molecular variables such as positions and momenta of atoms or molecules that form the system. This will be accomplished in Chapter 3.

Chapter 3

Statistical Mechanics

It is well-known that every macroscopic system is made up of atoms or molecules whose dynamics is governed by certain laws (*e.g.*, Newton's Laws) with specified interparticle interactions. It is very difficult to determine the state of the macroscopic system by determining the position and momenta of each and every atom referred to together as *molecular variables* . Hence, the behavior of the system is governed by a set of few macroscopic observables (*e.g.*, energy, temperature, etc.) which can reproduce a phenomenon. Consistent with these governing macroscopic observables, there exist many *microstates*, *i.e.*, sets of positions and momenta of all atoms, which together form an *ensemble*. Any macroscopic observable measured under the governing set is defined as an average over all members of the ensemble, and any deviation from the average value is called a *fluctuation*. Statistical mechanics deals with the relationship between the microscopic dynamics and the set of macroscopic observables that govern the macroscopic behavior of the system [10, 8, 41].

A fundamental result in statistical mechanics is the expression for specific heat C_v, an equilibrium property, in terms of fluctuations of energy in the "canonical" ensemble where the governing set of macroscopic variables are the number of particles N, volume V and temperature T [8]. In a similar manner, it is possible to obtain expressions for the nonequilibrium properties $\mathbf{L}_{11}$, $\mathbf{L}_{1Q}$, $\mathbf{L}_{Q1}$, and $\mathbf{L}_{QQ}$ in terms of the fluctuations of the diffusive and heat flux vectors in an equilibrium system [57, 58, 40]. In this chapter, explicit expressions for the heat transport coefficients are given as integrals of correlations of diffusive and heat flux vectors in an equilibrium system. Also, a detailed derivation of the expression for the instantaneous heat flux vector is given in terms of positions and momenta of atoms of a system modeled by M-body potentials, which can then be used to obtain the required transport coefficient $\mathbf{L}_{QQ}$.

3.1 Green-Kubo Formulae

Consider an isolated system which can exchange neither energy nor matter with the surroundings. The governing set of macroscopic variables in this case are the number of particles N, volume V

and energy E. Assume that the system reached equilibrium, where the macroscopic variables when averaged do not change with time. Imagine that the total system is divided into subsystems where local temperature and concentrations may be defined. It is known from equilibrium statistical mechanics that on an average (over all the members in the ensemble corresponding to the isolated system), the temperature and concentrations of the constituents are uniform throughout the system and hence no average thermodynamic forces such as $\mathbf{X}_k$ and $\mathbf{X}_Q$ in the case of mixtures. However, there may be spontaneous local fluctuations (in any member of the ensemble) resulting in non-zero thermodynamic forces $\mathbf{X}_k$ and $\mathbf{X}_Q$, which, though small, drive the irreversible process of diffusion and heat transfer in the system. Hence, it may be possible to model the fluctuations using the phenomenological laws (2.45)-(2.46).

To model the fluctuations, it was hypothesized by Onsager that the "decay of a system from a given nonequilibrium state produced by a spontaneous fluctuation obeys, *on the average*, the (empirical) law for the decay from the same state back to equilibrium, when it has been produced by a constraint which is then suddenly removed" [57, 58, 59]. Let $a_1, a_2, \ldots, a_n$ be a set of macroscopic observables which are of interest for the isolated system in equilibrium. These can either be defined for the whole system (such as pressure in the total system), or for subsystems (such as energy of a subsystem) making up the total system. These macroscopic variables are stochastic variables since they are not constant across the members of the ensemble. Let $\bar{a}_1, \bar{a}_2, \ldots, \bar{a}_n$ be the average values (over the members of the ensemble corresponding to N,V,E) of $a_1, a_2, \ldots, a_n$ respectively. Let the fluctuations in the variable a_i be α_i, where

$$\alpha_i \;=\; a_i - \bar{a}_i \;, \qquad \text{for } i \in 1, \ldots, n \;. \tag{3.1}$$

When the macroscopic variables of interest are equal to their averages, the entropy of the system $S(\alpha_1, \alpha_2, \ldots, \alpha_n)$ is at its maximum [64]. Therefore,

$$\left.\frac{\partial S}{\partial \alpha_i}\right|_{\alpha_1=0,\ldots,\alpha_n=0} \;=\; 0 \;. \tag{3.2}$$

When the fluctuations are small, the entropy can be expanded by Taylor series as

$$S(\alpha_1, \ldots, \alpha_n) - S(0, \ldots, 0) \;=\; \Delta S \;=\; -\frac{1}{2}\sum_{i,j} g_{ij}\alpha_i\alpha_j + h.o.t \;, \tag{3.3}$$

where g_{ij} are the elements of the matrix $\mathbf{g}$ such that

$$g_{ij} \;=\; -\frac{\partial^2 S}{\partial \alpha_i \partial \alpha_j} \;. \tag{3.4}$$

The probability of a fluctuation in which α_i lies between α_i and $\alpha_i + \mathrm{d}\alpha_i$ is given by

$$P\mathrm{d}\alpha_1, \ldots, \mathrm{d}\alpha_n \;=\; \frac{1}{C}\exp\left(\frac{\Delta S}{k_B}\right)\mathrm{d}\alpha_1, \ldots, \mathrm{d}\alpha_n \;, \tag{3.5}$$

where C is the normalization constant such that the integration of the probability density function yields unity [39]. Using (3.5), one can obtain the relation

$$\langle \alpha_i \alpha_j \rangle \;=\; k_B g_{ij}^{-1} \;, \tag{3.6}$$

where k_B is the Boltzmann constant, g_{ij}^{-1} are the elements of the inverse of $\mathbf{g}$ and $\langle \cdot \rangle$ denotes the average over the ensemble corresponding to the isolated system in equilibrium.

At this stage, it is assumed that the decay of macroscopic variables, when they are perturbed from their average values due to the external constraints (for example, heating), can be modeled by linear transport laws of the form

$$\frac{\mathrm{d}}{\mathrm{d}t}(a_i(t) - \bar{a}_i(t)) \;=\; \sum_j M_{ij}(a_j - \bar{a}_j) \;, \tag{3.7}$$

where M_{ij} are constants. For example, one such linear transport law is the Fourier' law for heat conduction. Now, when a fluctuation occurs, it has to decay to maintain equilibrium. It was hypothesized by Onsager, as stated earlier, that this decay of fluctuations can also be modeled by the same transport laws which are used to model the perturbations of the system due to external constraints. Let $\alpha_1(t), \ldots, \alpha_n(t)$ be the fluctuations in $a_1, \ldots, a_n$ respectively at time t. It is known that certain section of the ensemble corresponding to the isolated system are consistent with this fluctuation. Following the molecular dynamics (or trajectory) of each and every member of this subsection of the ensemble, one can note the fluctuation at time $t + \tau$. Let the fluctuation in a_i at time $t + \tau$ given that the system had a set of fluctuations of $\alpha_1(t), \ldots, \alpha_n(t)$ at time t be denoted by $\alpha_i(t+\tau)\big|_{\alpha_1(t),\ldots,\alpha(t)}$. Following each and every member of this subsection of the ensemble, one can calculate the average (over this subsection of the ensemble) of $\alpha_i(t+\tau)\big|_{\alpha_1(t),\ldots,\alpha(t)}$ denoted by $\overline{\alpha_i(t+\tau)\big|_{\alpha_1(t),\ldots,\alpha(t)}}$. Using Onsager' hypothesis for this average over the subsection of the ensemble, the equation for the decay of the fluctuation occurring at time t is written in a time-difference sense as

$$\overline{\alpha_i(t+\tau)\big|_{\alpha_1(t),\ldots,\alpha_n(t)}} - \alpha_i(t) \;=\; \tau \sum_{j=1}^{n} M_{ij}\alpha_j(t) \;. \tag{3.8}$$

To be able to write linear laws (3.7) in the time-difference schemes, the time interval of observation

τ should be such that

$$\tau \ll \frac{1}{M_{ij}} , \qquad \text{for all } i, j . \tag{3.9}$$

Multiplying both sides of (3.8) by $\alpha_k(t)$, taking averages over the whole ensemble and following the derivations in [40, 75], it can be shown that

$$k_B \sum_j M_{ij} g_{jk}^{-1} \;=\; \int_0^\tau \left(1 - \frac{s}{\tau}\right) \langle \dot{\alpha}_i(0) \dot{\alpha}_k(s) \rangle \, \mathrm{d}s , \tag{3.10}$$

where $\dot{\alpha}_k(s)$ is the time derivative with respect to the molecular time scale τ_m, which is smaller than the observation time τ. The term $\langle \dot{\alpha}_i(0) \dot{\alpha}_k(s) \rangle$ is called the time-correlation function, which is obtained by taking the time dependent quantity $\dot{\alpha}_i(t)$ at time $t = 0$ and multiplying it by the other time dependent quantity $\dot{\alpha}_k(t)$ at time $t = s$, and then averaging the product over the entire ensemble. Usually, these correlation functions decay in time and have a decay time τ_c, after which they vanish. Assuming that the decay time τ_c of the correlation function $\langle \dot{\alpha}_i(0) \dot{\alpha}_k(s) \rangle$ is smaller than the time interval τ, (3.10) can be reduced to

$$k_B \sum_j M_{ij} g_{jk}^{-1} \;=\; \int_0^\infty \langle \dot{\alpha}_i(0) \dot{\alpha}_k(s) \rangle \, \mathrm{d}s , \tag{3.11}$$

yielding the left hand side to be an integral over infinite time interval. Now, introducing the thermodynamic force $X_i(\alpha) = \dfrac{\partial S}{\partial \alpha_i}$, (3.8) can be written as

$$\frac{\overline{\alpha_i(t+\tau)|_{\alpha_1(t),\ldots,\alpha_n(t)}} - \alpha_1(t)}{\tau} \;=\; \sum_{j=1}^{n} L_{ij} X_j(t) , \tag{3.12}$$

where $L_{ij} = \sum_k M_{ik} g_{kj}^{-1}$. Interpreting the time derivative on left hand side of (3.12) as flux J_i, (3.12) is of the form

$$J_i \;=\; \sum_j L_{ij} X_j , \tag{3.13}$$

which is equivalent to the form of the transport laws (2.45) and (2.46) connecting the forces and fluxes in the linear irreversible regime, with L_{ij} being the transport coefficient. Thus, using (3.8) and (3.11), the transport coefficient L_{ij} relating the thermodynamic current J_i and the thermodynamic force X_j can be obtained in terms of the correlation function as

$$L_{ij} \;=\; \frac{1}{k_B} \int_0^\infty \langle \dot{\alpha}_i(0) \dot{\alpha}_j(s) \rangle \, \mathrm{d}s , \tag{3.14}$$

famously known as the Green-Kubo relations. Here, it is very important to note that, in obtaining the (3.14), it is crucial to find the time interval τ such that

$$\tau_m \ll \tau_c \ll \tau \ll \frac{1}{M_{ij}} \, . \tag{3.15}$$

However, all the Green-Kubo relations derived above are for the case of discrete macroscopic variables. In order to obtain the transport coefficient $\mathbf{L}_{11}$, $\mathbf{L}_{1Q}$ and $\mathbf{L}_{QQ}$, it is important to derive the theory for continuous systems, *i.e.*, systems where the macroscopic quantities are defined at every macroscopic point $\mathbf{x}$ as described in Chapter 2. Using Onsager' hypothesis and following the derivations in [40], it can be shown that the phenomenological coefficient matrices for a binary liquid mixture can be obtained in terms of the correlation functions as

$$\mathbf{L}_{11} = \frac{V}{k_B} \int_0^\infty \left\langle \tilde{\mathbf{J}}_1(t) \otimes \tilde{\mathbf{J}}_1(0) \right\rangle \mathrm{d}t \, , \tag{3.16}$$

$$\mathbf{L}_{1Q} = \frac{V}{k_B} \int_0^\infty \left\langle \tilde{\mathbf{J}}_1(t) \otimes \tilde{\mathbf{J}}_Q(0) \right\rangle \mathrm{d}t \, , \tag{3.17}$$

$$\mathbf{L}_{QQ} = \frac{V}{k_B} \int_0^\infty \left\langle \tilde{\mathbf{J}}_Q(t) \otimes \tilde{\mathbf{J}}_Q(0) \right\rangle \mathrm{d}t \, , \tag{3.18}$$

where $\tilde{\mathbf{J}}_1(t)$ and $\tilde{\mathbf{J}}_Q(t)$ are the instantaneous diffusive and heat flux vectors respectively in any member of the ensemble. For solids, as there is no diffusion, there exists only one transport coefficient $\mathbf{L}_{QQ}$ given by (3.18). As the objective of this thesis is to estimate $\dfrac{\mathbf{L}_{QQ}}{T^2}$ using (3.18), one needs expressions for the instantaneous heat flux vector $\tilde{\mathbf{J}}_Q(t)$ [32, 24].

3.2 Stress and Heat Flux from Molecular Dynamics Simulations

In this section, the local forms of balance of mass, linear momentum and energy are obtained from the principles of classical statistical mechanics, where the particles obey Newton's laws of motion, in the absence of heat sources, body forces or external interaction potentials. The stress tensor and heat flux vector in terms of molecular variables are obtained from the derivations of balance of linear momentum and the balance of energy respectively following the Irving and Kirkwood procedure [32, 24].

Consider a system consisting of N atoms whose positions are denoted by $\mathbf{r}_1, \mathbf{r}_2, \ldots, \mathbf{r}_N$ and momenta by $\mathbf{p}_1, \mathbf{p}_2, \ldots, \mathbf{p}_N$. The 6N-dimensional space of positions and momenta denoted by $\mathbf{\Gamma} = \{(\mathbf{r}_i, \mathbf{p}_i) \, , \; i = 1, 2, \ldots, N\}$ is called the phase space. The instantaneous state of the system may be represented by a point in the *phase space*. As mentioned earlier, there are many pos-

sible microstates (choices of positions and momenta of atoms) consistent with few macroscopic variables that govern the behavior of the system. Hence, there exists a phase-space distribution function $f(\mathbf{\Gamma}, t)$ that denotes the probability of the system occupying a microstate $\mathbf{\Gamma}$ at time t, such that the distribution function is normalized to unity, *i.e.*,

$$\int f(\mathbf{\Gamma}, t)\, \mathrm{d}\mathbf{\Gamma} \;=\; 1\,. \tag{3.19}$$

Consider any subset Ω of the phase space. Then, $\int_\Omega f(\mathbf{\Gamma}, t)\, \mathrm{d}\mathbf{\Gamma}$ gives the fraction of members of the ensemble that are within Ω. If one follows this set in time then the fraction of members within this set should remain constant in time, as members are neither created nor destroyed. Therefore

$$\frac{\mathrm{d}}{\mathrm{d}t} \int_\Omega f(\mathbf{\Gamma}, t) \;=\; 0\,. \tag{3.20}$$

Assuming that $f(\mathbf{\Gamma}, t)$ is continuous in $\mathbf{\Gamma}$ and time t, using Reynolds transport theorem, (3.20) can be reduced to

$$\int_\Omega \left[\frac{\partial f(\mathbf{\Gamma}, t)}{\partial t} + f(\mathbf{\Gamma}, t) \frac{\partial}{\partial \mathbf{\Gamma}} \cdot \dot{\mathbf{\Gamma}} + \dot{\mathbf{\Gamma}} \cdot \frac{\partial}{\partial \mathbf{\Gamma}} f(\mathbf{\Gamma}, t) \right] \mathrm{d}\mathbf{\Gamma} \;=\; 0\,, \tag{3.21}$$

where $\dfrac{\partial}{\partial \mathbf{\Gamma}} \cdot \dot{\mathbf{\Gamma}} = \displaystyle\sum_i \left(\frac{\partial}{\partial \mathbf{p}_i} \cdot \dot{\mathbf{p}}_i + \frac{\partial}{\partial \mathbf{r}_i} \cdot \dot{\mathbf{r}}_i \right)$. Since Ω is any arbitrary subset of the phase space, localizing (3.21) to a point yields the Liouville equation for evaluating the phase space distribution function as

$$\frac{\partial f(\mathbf{\Gamma}, t)}{\partial t} \;=\; -\left[\frac{\partial}{\partial \mathbf{\Gamma}} \cdot \dot{\mathbf{\Gamma}} + \dot{\mathbf{\Gamma}} \cdot \frac{\partial}{\partial \mathbf{\Gamma}} \right] f(\mathbf{\Gamma}, t) \;=\; -iL f(\mathbf{\Gamma}, t)\,, \tag{3.22}$$

where iL is called as f-*Liouvillean* operator. The solution of (3.22) is formally represented as

$$f(\mathbf{\Gamma}, t) \;=\; \exp(-iLt) f(\mathbf{\Gamma}, 0)\,, \tag{3.23}$$

where $f(\mathbf{\Gamma}, 0)$ is the initial phase space distribution consistent with the initial preparation of the system [24]. It should be noted that if $\dfrac{\partial}{\partial \mathbf{\Gamma}} \cdot \dot{\mathbf{\Gamma}} = 0$, the phase space is incompressible. This is equivalent to the concept of material incompressibility in continuum mechanics.

Consider a general phase variable $G(\mathbf{\Gamma}) = \tilde{G}(t)$. The time derivative of G is given by

$$\dot{G}(\mathbf{\Gamma}) \;=\; \left[\dot{\mathbf{\Gamma}} \cdot \frac{\partial}{\partial \mathbf{\Gamma}} \right] G(\mathbf{\Gamma}) \;=\; \mathrm{iL} G(\mathbf{\Gamma})\,, \tag{3.24}$$

where iL is called as p-*Liouvillean* operator. The solution of (3.24) is formally represented as

$$\tilde{G}(t) \;=\; \exp(\mathrm{iL}t)\tilde{G}(0)\;. \tag{3.25}$$

The ensemble average of G at time t, $\langle G(t)\rangle$, can be evaluated in two ways. First, one can choose choose an initial configuration $\mathbf{\Gamma}$ from the initial probability distribution and then evaluate the phase variable G at time t by following the trajectory starting from $\mathbf{\Gamma}$. Finally, one can obtain the average by multiplying this value with a weighing factor determined by the initial probability distribution $f(\mathbf{\Gamma}, 0)$, *i.e.*,

$$\langle G(t)\rangle \;=\; \int G(t) f(\mathbf{\Gamma}, 0)\,\mathrm{d}\mathbf{\Gamma}\;. \tag{3.26}$$

This is the Heisenberg picture and is equivalent to the Lagrangian formulation in continuum mechanics, where one follows the material point. Second, one can choose any particular point $\mathbf{\Gamma}$ in the phase space and evaluate the change in the probability function $f(\mathbf{\Gamma}, t)$ at that point as a function of time. Then, one can calculate the average by evaluating the phase variable at that point $G(\mathbf{\Gamma})$ and multiplying it with the probability function at time t, *i.e.*,

$$\langle \tilde{G}(t)\rangle \;=\; \int G(\mathbf{\Gamma}) f(\mathbf{\Gamma}, t)\,\mathrm{d}\mathbf{\Gamma}\;. \tag{3.27}$$

This is called the Schrödinger picture and is equivalent to the Eulerian formulation in continuum mechanics, where one stays at a fixed point and monitors the particles coming in to the differential volume around the fixed point. It can be proved that the averages calculated by Heisenberg and Schrödinger representations are equivalent, see [24, Section 3.3]. A schematic of the Heisenberg and Schrödinger representations is shown in Figure 3.1.

Using the properties of Liouvillean operators, the following identities can be established:

$$\int f(\mathbf{\Gamma}, t)\mathrm{iL}G(\mathbf{\Gamma})\,\mathrm{d}\mathbf{\Gamma} \;=\; -\int G(\mathbf{\Gamma}) iL f(\mathbf{\Gamma}, t)\,\mathrm{d}\mathbf{\Gamma}\;, \tag{3.28}$$

$$\int G(\mathbf{\Gamma})\Big[\exp\big(-iL_0 t\big) g(\mathbf{\Gamma}, 0)\Big]\,\mathrm{d}\mathbf{\Gamma} \;=\; \int g(\mathbf{\Gamma}, 0)\Big[\exp\big(\mathrm{iL}_0 t\big) G(\mathbf{\Gamma})\Big]\,\mathrm{d}\mathbf{\Gamma}\;, \tag{3.29}$$

where the first identity is obtained using integration by parts and the second identity is the equivalence of Heisenberg and Schrödinger representations, see [24, Chapter 3].

At this stage, the particles in the system are assumed to obey Newton' laws of motion, *i.e.*, the rates of position and momentum of atom i are given by

$$\begin{aligned} \dot{\mathbf{r}}_i \;&=\; \frac{\mathbf{p}_i}{m_i}\;, \\ \dot{\mathbf{p}}_i \;&=\; \mathbf{F}_i\;, \end{aligned} \tag{3.30}$$

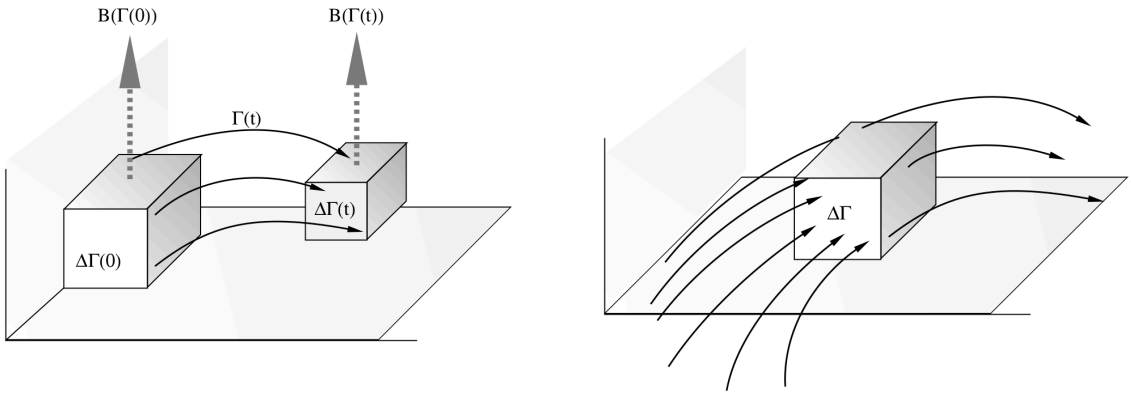

(a) *The Heisenberg picture.* **(b)** *The Schrödinger picture.*

Figure 3.1: *The Heisenberg-Schrödinger picture, from [24].*

respectively, where $\mathbf{F}_i$ is the interaction force on atom i given by

$$\mathbf{F}_i \;=\; -\frac{\partial \Phi}{\partial \mathbf{r}_i}\,, \tag{3.31}$$

with $\Phi(\mathbf{r}_1, \mathbf{r}_2, \ldots, \mathbf{r}_N)$ being the total interaction potential of the system. The latter is of the general form

$$\begin{aligned}\Phi(\mathbf{r}_1, \mathbf{r}_2, \ldots, \mathbf{r}_N) \;=\; \frac{1}{2!}\sum_{i_1,i_2} u_2(\mathbf{r}_{i_1}, \mathbf{r}_{i_2}) + \frac{1}{3!}\sum_{i_1,i_2,i_3} u_3(\mathbf{r}_{i_1}, \mathbf{r}_{i_2}, \mathbf{r}_{i_3}) + \ldots + \\ \frac{1}{M!}\sum_{i_1,i_2,\cdots i_M} u_M(\mathbf{r}_{i_1}, \mathbf{r}_{i_2}, \ldots, \mathbf{r}_{i_M})\,,\end{aligned} \tag{3.32}$$

where $M \leq N$ and $u_M(\mathbf{r}_{i_1}, \mathbf{r}_{i_2}, \ldots, \mathbf{r}_{i_M})$ describes M-body interactions [49]. The total interatomic force $\mathbf{F}_i$ on atom i is given by

$$\mathbf{F}_i = -\frac{\partial \Phi}{\partial \mathbf{r}_i} = \frac{1}{1!}\sum_{i_2} \mathbf{F}_{ii_2} + \frac{1}{2!}\sum_{i_2,i_3} \mathbf{F}_{ii_2i_3} + \ldots + \frac{1}{(M-1)!}\sum_{i_2,\ldots,i_M} \mathbf{F}_{ii_2\ldots i_M}\,, \tag{3.33}$$

where $\mathbf{F}_{ii_2\ldots i_M} = -\dfrac{\partial}{\partial \mathbf{r}_i} u_M(\mathbf{r}_i, \mathbf{r}_{i_2}, \ldots, \mathbf{r}_{i_M})$ is the M-body force contribution on atom i.

To obtain the local forms of balances of mass, linear momentum and balance of energy from the principles of classical statistical mechanics, a connection needs to be established between the macroscopic and molecular variables. Firstly, the probability per unit volume of finding an atom i

at the macroscopic point $\mathbf{x}$ is $\int \delta(\mathbf{x}-\mathbf{r}_i) f(\mathbf{\Gamma},t)\,\mathrm{d}\mathbf{\Gamma}$, and the contribution of mass of atom i to the density at $\mathbf{x}$ is then given by $\int m_i \delta(x-\mathbf{r}_i) f(\mathbf{\Gamma},t)\,\mathrm{d}\mathbf{\Gamma}$ at time t. Therefore, the total mass density at $\mathbf{x}$ due to the contribution from all molecules is given at time t by

$$\rho(\mathbf{x},t) \;=\; \int \sum_i m_i \delta(\mathbf{x}-\mathbf{r}_i) f(\mathbf{\Gamma},t)\,\mathrm{d}\mathbf{\Gamma}\;. \tag{3.34}$$

Similarly, the linear momentum at $\mathbf{x}$ is given at time t as

$$\rho(\mathbf{x},t)\mathbf{v}(\mathbf{x},t) \;=\; \int \sum_i \mathbf{p}_i \delta(\mathbf{x}-\mathbf{r}_i) f(\mathbf{\Gamma},t)\,\mathrm{d}\mathbf{\Gamma}\;. \tag{3.35}$$

In order to define the energy density from the molecular quantities, one needs to define the energy E_i of each atom i. This is taken to be of the form

$$E_i = \underbrace{\frac{\mathbf{p}_i\cdot\mathbf{p}_i}{2m_i}}_{kinetic} + \underbrace{\frac{1}{2!}\sum_{i_2} u_2(\mathbf{r}_i,\mathbf{r}_{i_2}) + \frac{1}{3!}\sum_{i_2,i_3} u_3(\mathbf{r}_i,\mathbf{r}_{i_2},\mathbf{r}_{i_3}) + \ldots + \frac{1}{M!}\sum_{i_2,\ldots,i_M} u_M(\mathbf{r}_i,\mathbf{r}_{i_2},\ldots,\mathbf{r}_{i_M})}_{potential}\;. \tag{3.36}$$

based on the assumption that the energy from any K-body term $u_K(\mathbf{r}_{i_1},\mathbf{r}_{i_2},\ldots,\mathbf{r}_{i_K})$ is divided equally among the atoms $i_1,i_2,\ldots,i_K$. For this choice of energy of each atom i, the energy density at $\mathbf{x}$ is given at time t as

$$\rho(\mathbf{x},t)\mathbf{e}(\mathbf{x},t) \;=\; \int \sum_i \Big[\frac{\mathbf{p}_i\cdot\mathbf{p}_i}{2m_i} + E_i\Big]\delta(\mathbf{x}-\mathbf{r}_i) f(\mathbf{\Gamma},t)\,\mathrm{d}\mathbf{\Gamma}\;, \tag{3.37}$$

assuming no external interaction potentials.

3.2.1 Balance of Mass

Taking the partial time derivative of (3.34),

$$\begin{aligned}
\frac{\partial \rho}{\partial t} &= \int \sum_i m_i \delta(\mathbf{x} - \mathbf{r}_i) \frac{\partial f(\mathbf{\Gamma}, t)}{\partial t} \, \mathrm{d}\mathbf{\Gamma} \\
&= -\int \sum_i m_i \delta(\mathbf{x} - \mathbf{r}_i) \; iL f(\mathbf{\Gamma}, t) \, \mathrm{d}\mathbf{\Gamma} \\
&= \int f(\mathbf{\Gamma}, t) \; \mathrm{iL}\Big(\sum_i m_i \delta(\mathbf{x} - \mathbf{r}_i) \Big) \, \mathrm{d}\mathbf{\Gamma} \\
&= \int f(\mathbf{\Gamma}, t) \sum_i m_i \frac{\partial \delta(\mathbf{x} - \mathbf{r}_i)}{\partial \mathbf{r}_i} \cdot \dot{\mathbf{r}}_i
\end{aligned} \tag{3.38}$$

where the second, third and fourth equalities follow from (3.22), (3.28) and (3.24), respectively. Using (3.30), (3.35) and the property of the delta function

$$\frac{\partial}{\partial \mathbf{r}_i} \delta(\mathbf{x} - \mathbf{r}_i) = -\frac{\partial}{\partial \mathbf{x}} \delta(\mathbf{x} - \mathbf{r}_i) \tag{3.39}$$

obtained by chain rule, equation (3.38) can be reduced to

$$\begin{aligned}
\frac{\partial \rho}{\partial t} &= -\int f(\mathbf{\Gamma}, t) \sum_i \frac{\partial \delta(\mathbf{x} - \mathbf{r}_i)}{\partial \mathbf{x}} \cdot \frac{\mathbf{p}_i}{m_i} \\
&= -\frac{\partial}{\partial \mathbf{x}} \cdot \int \sum_i \mathbf{p}_i \delta(\mathbf{x} - \mathbf{r}_i) f(\mathbf{\Gamma}, t) \, \mathrm{d}\mathbf{\Gamma} \\
&= -\frac{\partial}{\partial \mathbf{x}} \cdot (\rho \mathbf{v}) \, ,
\end{aligned} \tag{3.40}$$

which is the local form of balance of mass given by (2.1). Hence, the microscopic definition of mass density given by (3.34) exactly satisfies the balance of mass given by (2.1).

3.2.2 Balance of Momentum

Following the same procedure as for the balance of mass, the partial time derivative on the left and right hand sides of (3.35) yields

$$\begin{aligned}\frac{\partial}{\partial t}(\rho\mathbf{v}) &= \int \sum_i \mathbf{p}_i \delta(\mathbf{x}-\mathbf{r}_i)\frac{\partial f(\mathbf{\Gamma},t)}{\partial t}\,\mathrm{d}\mathbf{\Gamma} \\ &= -\int \sum_i \mathbf{p}_i \delta(\mathbf{x}-\mathbf{r}_i)\; iLf(\mathbf{\Gamma},t)\,\mathrm{d}\mathbf{\Gamma} \\ &= \int f(\mathbf{\Gamma},t)\;\mathrm{iL}\Big(\sum_i \mathbf{p}_i\delta(\mathbf{x}-\mathbf{r}_i)\Big)\,\mathrm{d}\mathbf{\Gamma} \\ &= \int f(\mathbf{\Gamma},t)\sum_i\Big[\dot{\mathbf{p}}_i\delta(\mathbf{x}-\mathbf{r}_i)+\mathbf{p}_i\Big(\frac{\partial\delta(\mathbf{x}-\mathbf{r}_i)}{\partial\mathbf{r}_i}\cdot\dot{\mathbf{r}}_i\Big)\Big]\,\mathrm{d}\mathbf{\Gamma}\,,\end{aligned} \tag{3.41}$$

where the second, third and fourth equalities follow from (3.22), (3.28) and (3.24), respectively. Now, using (3.30) and (3.39), equation (3.41) can be reduced to

$$\frac{\partial}{\partial t}(\rho\mathbf{v}) = \int f(\mathbf{\Gamma},t)\sum_i \mathbf{F}_i\delta(\mathbf{x}-\mathbf{r}_i)\,\mathrm{d}\mathbf{\Gamma} - \frac{\partial}{\partial\mathbf{x}}\cdot\int f(\mathbf{\Gamma},t)\sum_i\frac{\mathbf{p}_i\otimes\mathbf{p}_i}{m_i}\delta(\mathbf{x}-\mathbf{r}_i)\,\mathrm{d}\mathbf{\Gamma}\,, \tag{3.42}$$

where the second term on the right hand side can be rewritten as

$$\begin{aligned}\frac{\partial}{\partial\mathbf{x}}\cdot\int f(\mathbf{\Gamma},t)\sum_i\frac{\mathbf{p}_i\otimes\mathbf{p}_i}{m_i}\delta(\mathbf{x}-\mathbf{r}_i)\,\mathrm{d}\mathbf{\Gamma} &= \frac{\partial}{\partial\mathbf{x}}\cdot\int f(\mathbf{\Gamma},t) \\ &\sum_i m_i\Big(\frac{\mathbf{p}_i}{m_i}-\mathbf{v}\Big)\otimes\Big(\frac{\mathbf{p}_i}{m_i}-\mathbf{v}\Big)\delta(\mathbf{x}-\mathbf{r}_i)\,\mathrm{d}\mathbf{\Gamma} + \frac{\partial}{\partial\mathbf{x}}\cdot(\rho\mathbf{v}\otimes\mathbf{v})\,,\end{aligned} \tag{3.43}$$

upon using (3.34) and (3.35). Hence, equation (3.42) can be reduced to

$$\begin{aligned}\frac{\partial}{\partial t}(\rho\mathbf{v})+\frac{\partial}{\partial\mathbf{x}}\cdot(\rho\mathbf{v}\otimes\mathbf{v}) &= \int f(\mathbf{\Gamma},t)\sum_i\mathbf{F}_i\delta(\mathbf{x}-\mathbf{r}_i)\,\mathrm{d}\mathbf{\Gamma} \\ &- \frac{\partial}{\partial\mathbf{x}}\cdot\int f(\mathbf{\Gamma},t)\sum_i m_i\Big(\frac{\mathbf{p}_i}{m_i}-\mathbf{v}\Big)\otimes\Big(\frac{\mathbf{p}_i}{m_i}-\mathbf{v}\Big)\delta(\mathbf{x}-\mathbf{r}_i)\,\mathrm{d}\mathbf{\Gamma}\,.\end{aligned} \tag{3.44}$$

The first term on the right hand side of (3.44) can be written in terms of the interaction potential Φ as

$$\sum_i \mathbf{F}_i \delta(\mathbf{x}-\mathbf{r}_i) \;=\; \sum_i \delta(\mathbf{x}-\mathbf{r}_i)\Big[\frac{1}{1!}\sum_{i_2}\mathbf{F}_{ii_2} + \frac{1}{2!}\sum_{i_2,i_3}\mathbf{F}_{ii_2i_3} + \ldots + \frac{1}{(M-1)!}\sum_{i_2,\ldots,i_M}\mathbf{F}_{ii_2\ldots i_M}\Big]\,, \tag{3.45}$$

using the definition of the interatomic force $\mathbf{F}_i$ in (3.33). Assuming central forces, for any K-body term in the M-body potential (3.32)

$$\frac{\partial}{\partial \mathbf{r}_i}u_K(\mathbf{r}_i,\mathbf{r}_{i_2},\ldots,\mathbf{r}_{i_K}) + \frac{\partial}{\partial \mathbf{r}_{i_2}}u_K(\mathbf{r}_i,\mathbf{r}_{i_2},\ldots,\mathbf{r}_{i_K}) + \ldots + \frac{\partial}{\partial \mathbf{r}_K}u_K(\mathbf{r}_i,\mathbf{r}_{i_2},\ldots,\mathbf{r}_{i_K}) \;=\; \mathbf{0}\,. \tag{3.46}$$

Now, any K-body force term on the right hand side of (3.45) can be written as

$$\frac{1}{(K-1)!}\sum_{i,i_2,\ldots,i_K}\delta(\mathbf{x}-\mathbf{r}_i)\mathbf{F}_{ii_2\ldots i_K} \;=\; -\frac{1}{K!}\Big[(K-1)\sum_{i,i_2,\ldots,i_K}\delta(\mathbf{x}-\mathbf{r}_i)\frac{\partial}{\partial \mathbf{r}_i}u_K(\mathbf{r}_i,\mathbf{r}_{i_2},\ldots,\mathbf{r}_{i_K}) + \sum_{i,i_2,\ldots,i_K}\delta(\mathbf{x}-\mathbf{r}_i)\frac{\partial}{\partial \mathbf{r}_i}u_K(\mathbf{r}_i,\mathbf{r}_{i_2},\ldots,\mathbf{r}_{i_K})\,. \tag{3.47}$$

Substituting (3.46) in the last term of the right hand side of (3.47) and rearranging terms, equation (3.47) can be reduced to

$$\frac{1}{(K-1)!}\sum_{i,i_2,\ldots,i_K}\delta(\mathbf{x}-\mathbf{r}_i)\mathbf{F}_{ii_2\ldots i_K} \;=\; \frac{1}{K!}\sum_{i,i_2,\ldots,i_K}\Big[(K-1)\delta(\mathbf{x}-\mathbf{r}_i) - \delta(\mathbf{x}-\mathbf{r}_{i_2}) - \ldots - \delta(\mathbf{x}-\mathbf{r}_{i_K})\Big]\mathbf{F}_{ii_2\ldots i_K}\,. \tag{3.48}$$

Using the identity

$$\delta(\mathbf{x}-\mathbf{r}_i) - \delta(\mathbf{x}-\mathbf{r}_{i_2}) \;=\; -\frac{\partial}{\partial \mathbf{x}}\cdot(\mathbf{r}_{ii_2}b_{ii_2})\,, \tag{3.49}$$

where $\mathbf{r}_{ii_2} = \mathbf{r}_i - \mathbf{r}_{i_2}$ and the bond function $b_{ii_2} = b(\mathbf{x};\mathbf{r}_i,\mathbf{r}_{i_2}) = \int_0^1 \delta(\mathbf{x}-\mathbf{r}_i+\lambda\mathbf{r}_{ii_2})\,\mathrm{d}\lambda$, (3.48) can be reduced to

$$\frac{1}{(K-1)!}\sum_{i,i_2,\ldots,i_K}\delta(\mathbf{x}-\mathbf{r}_i)\mathbf{F}_{ii_2\ldots i_K} \;=\; -\frac{\partial}{\partial \mathbf{x}}\cdot\Big[\sum_{i,i_2,\ldots,i_K}\mathbf{F}_{ii_2\ldots i_K}\otimes\big(\mathbf{r}_{ii_2}b_{ii_2}+\ldots+\mathbf{r}_{ii_K}b_{ii_K}\big)\Big]\,. \tag{3.50}$$

The bond function $b(\mathbf{x};\mathbf{r}_i,\mathbf{r}_j)$ can be interpreted as follows: if, in Figure 3.2, $\mathbf{x}$ is on the line segment connecting $\mathbf{r}_i$ and $\mathbf{r}_j$ then $b(\mathbf{x};\mathbf{r}_i,\mathbf{r}_j) = 1$, otherwise, $b(\mathbf{x};\mathbf{r}_i,\mathbf{r}_j) = 0$. Using (3.50),

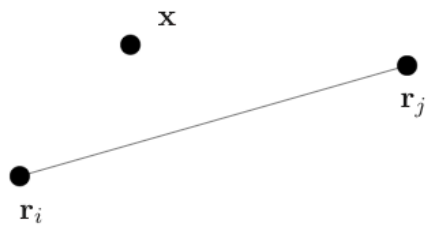

Figure 3.2: *A schematic showing the positions of atoms, $\mathbf{r}_i$ and $\mathbf{r}_j$, and the continuum point $\mathbf{x}$ to depict the bond function.*

equation (3.45) may be rewritten as

$$\sum_i \mathbf{F}_i\delta(\mathbf{x}-\mathbf{r}_i) \;=\; -\frac{\partial}{\partial\mathbf{x}}\cdot\Big[\frac{1}{2!}\sum_{i,i_2}\mathbf{F}_{ii_2}\otimes\mathbf{r}_{ii_2}b_{ii_2}+\frac{1}{3!}\sum_{i,i_2,i_3}\mathbf{F}_{ii_2i_3}\otimes(\mathbf{r}_{ii_2}b_{ii_2}+\mathbf{r}_{ii_3}b_{ii_3})+\ldots+ \frac{1}{M!}\sum_{i,i_2,\ldots,i_M}\mathbf{F}_{ii_2\ldots i_M}\otimes(\mathbf{r}_{ii_2}b_{ii_2}+\ldots+\mathbf{r}_{ii_M}b_{ii_M})\Big]\,. \tag{3.51}$$

Finally substituting (3.51) in (3.44), it can be shown that

$$\rho\dot{\mathbf{v}} \;=\; \frac{\partial}{\partial\mathbf{x}}\cdot\int(\mathbf{T}_K+\mathbf{T}_V)f(\mathbf{\Gamma},t)\,\mathrm{d}\mathbf{\Gamma}\,, \tag{3.52}$$

where

$$\mathbf{T}_K \;=\; -\sum_i m_i\Big(\frac{\mathbf{p}_i}{m_i}-\mathbf{v}\Big)\otimes\Big(\frac{\mathbf{p}_i}{m_i}-\mathbf{v}\Big)\delta(\mathbf{x}-\mathbf{r}_i)\,, \tag{3.53}$$

and

$$\mathbf{T}_V \;=\; -\Big[\frac{1}{2!}\sum_{i,i_2}\mathbf{F}_{ii_2}\otimes\mathbf{r}_{ii_2}b_{ii_2}+\frac{1}{3!}\sum_{i,i_2,i_3}\mathbf{F}_{ii_2i_3}\otimes(\mathbf{r}_{ii_2}b_{ii_2}+\mathbf{r}_{ii_3}b_{ii_3})+\ldots+ \frac{1}{M!}\sum_{i,i_2,\ldots,i_M}\mathbf{F}_{ii_2\ldots i_M}\otimes(\mathbf{r}_{ii_2}b_{ii_2}+\ldots+\mathbf{r}_{ii_M}b_{ii_M})\Big]\,. \tag{3.54}$$

It can be seen that (3.52), obtained from point function mass and momentum densities (3.34) and (3.35), becomes identical in form to the local form of balance of mass (2.2) when body forces are absent. However, to obtain the macroscopic balance of momentum, one needs to take appropriate space averages. Comparing terms in (3.52) and (2.2), the point wise stress tensor may be defined as

$$\mathbf{T}^p = \int (\mathbf{T}_K + \mathbf{T}_V) f(\mathbf{\Gamma}, t)\, \mathrm{d}\mathbf{\Gamma} \,. \tag{3.55}$$

Here, it can be seen that $\mathbf{T}_K$ consists of contributions only from velocities and is called as the *kinetic stress tensor*. Moreover, it is always symmetric. On the other hand, $\mathbf{T}_V$ is due to the forces between atoms and is called as the *virial stress tensor*. This is always symmetric if the interatomic potential describing the interactions between the atoms follows the central force model *i.e.*, equation (3.46), which is almost always the case [1]. It is important to note that in the case of gases, where the interaction forces are very weak, the contribution of the kinetic stress tensor to the total stress tensor is more than the virial stress tensor. However, when interaction forces become important as in the case of liquids and solids, the contribution from virial stress tensor is significantly higher than the kinetic part.

3.2.3 Balance of Energy

In this subsection, point-wise definition of the heat flux vector is obtained. Taking the partial time derivative on both sides of (3.37)

$$\begin{aligned}
\frac{\partial}{\partial t}(\rho e) &= \int \sum_i E_i \delta(\mathbf{x} - \mathbf{r}_i) \frac{\partial f(\mathbf{\Gamma}, t)}{\partial t}\, \mathrm{d}\mathbf{\Gamma} \\
&= -\int \sum_i E_i \delta(\mathbf{x} - \mathbf{r}_i)\; i\boldsymbol{L} f(\mathbf{\Gamma}, t)\, \mathrm{d}\mathbf{\Gamma} \\
&= \int f(\mathbf{\Gamma}, t)\, \mathrm{iL}\Big(\sum_i E_i \delta(\mathbf{x} - \mathbf{r}_i) \Big)\, \mathrm{d}\mathbf{\Gamma} \\
&= \int f(\mathbf{\Gamma}, t) \sum_i \dot{E}_i \delta(\mathbf{x} - \mathbf{r}_i)\, \mathrm{d}\mathbf{\Gamma} + \int f(\mathbf{\Gamma}, t) \sum_i E_i \Big(\frac{\partial \delta(\mathbf{x} - \mathbf{r}_i)}{\partial \mathbf{r}_i} \cdot \dot{\mathbf{r}}_i \Big) \Big]\, \mathrm{d}\mathbf{\Gamma} \\
&= \int f(\mathbf{\Gamma}, t) \sum_i \dot{E}_i \delta(\mathbf{x} - \mathbf{r}_i)\, \mathrm{d}\mathbf{\Gamma} - \frac{\partial}{\partial \mathbf{x}} \cdot \Big(\int f(\mathbf{\Gamma}, t) \sum_i E_i \dot{\mathbf{r}}_i \delta(\mathbf{x} - \mathbf{r}_i)\, \mathrm{d}\mathbf{\Gamma} \Big) \,,
\end{aligned} \tag{3.56}$$

where the second, third and fourth equalities follow from (3.22), (3.28) and (3.24), respectively. The first term on the right hand side of (3.56) can be written as

$$\begin{aligned}\sum_i \dot{E}_i \delta(\mathbf{x}-\mathbf{r}_i) \;&=\; \sum_i \Big[\frac{\mathbf{p}_i}{m_i}\cdot\dot{\mathbf{p}}_i + \frac{1}{2!}\sum_{i_2}\dot{u}_2(\mathbf{r}_i,\mathbf{r}_{i_2}) + \frac{1}{3!}\sum_{i_2,i_3}\dot{u}_3(\mathbf{r}_i,\mathbf{r}_{i_2},\mathbf{r}_{i_3}) + \ldots \\ &\qquad\qquad + \frac{1}{M!}\sum_{i_2,\ldots,i_M}\dot{u}_M(\mathbf{r}_i,\mathbf{r}_{i_2},\ldots,\mathbf{r}_{i_M})\Big]\delta(\mathbf{x}-\mathbf{r}_i) \\ &=\; \frac{1}{2!}\sum_{i,i_2}\Big(2\frac{\mathbf{p}_i}{m_i}\cdot\mathbf{F}_{ii_2} + \dot{u}_2(\mathbf{r}_i,\mathbf{r}_{i_2})\Big)\delta(\mathbf{x}-\mathbf{r}_i) + \ldots + \\ &\quad \frac{1}{M!}\sum_{i,i_2,\ldots,i_M}\Big(M\frac{\mathbf{p}_i}{m_i}\cdot\mathbf{F}_{ii_2\ldots i_M} + \dot{u}_M(\mathbf{r}_i,\mathbf{r}_{i_2},\ldots,\mathbf{r}_{i_M})\Big)\delta(\mathbf{x}-\mathbf{r}_i)\;,\end{aligned} \tag{3.57}$$

using the definition of E_i (3.36) and equations of motion (3.30). Now, any K-body term in (3.57) can be further simplified as

$$\begin{aligned}&\frac{1}{K!}\sum_{i,i_2,\ldots,i_K}\Big(K\frac{\mathbf{p}_i}{m_i}\cdot\mathbf{F}_{ii_2\ldots i_K} + \dot{u}_K(\mathbf{r}_i,\mathbf{r}_{i_2},\ldots,\mathbf{r}_{i_K})\Big)\delta(\mathbf{x}-\mathbf{r}_i) \\ &\quad= \frac{1}{K!}\sum_{i,i_2,\ldots,i_K}\Big(K\frac{\mathbf{p}_i}{m_i}\cdot\mathbf{F}_{ii_2\ldots i_K}\delta(\mathbf{x}-\mathbf{r}_i)\Big) + \frac{1}{K!}\sum_{i,i_2,\ldots,i_K}\Big(\frac{\partial u_K}{\partial\mathbf{r}_i}\cdot\frac{\mathbf{p}_i}{m_i} + \frac{\partial u_K}{\partial\mathbf{r}_{i_2}}\cdot\frac{\mathbf{p}_{i_2}}{m_{i_2}} + \\ &\qquad\qquad \ldots + \frac{\partial u_K}{\partial\mathbf{r}_K}\cdot\frac{\mathbf{p}_K}{m_K}\Big)\delta(\mathbf{x}-\mathbf{r}_i) \\ &\quad= \frac{1}{K!}\sum_{i,i_2,\ldots,i_K}\Big[\frac{\mathbf{p}_i}{m_i}\cdot\mathbf{F}_{ii_2\ldots i_K}\big(\delta(\mathbf{x}-\mathbf{r}_i)-\delta(\mathbf{x}-\mathbf{r}_{i_2})\big) + \\ &\qquad\qquad \ldots + \frac{\mathbf{p}_i}{m_i}\cdot\mathbf{F}_{ii_2\ldots i_K}\big(\delta(\mathbf{x}-\mathbf{r}_i)-\delta(\mathbf{x}-\mathbf{r}_{i_K})\big)\Big] \\ &\quad= -\frac{\partial}{\partial\mathbf{x}}\cdot\left(\frac{1}{K!}\sum_{i,i_2,\ldots,i_K}\Big[(\mathbf{r}_{ii_2}b_{ii_2}+\ldots+\mathbf{r}_{ii_K}b_{ii_K})\otimes\mathbf{F}_{i,i_2,\ldots,i_K}\Big]\frac{\mathbf{p}_i}{m_i}\right),\end{aligned} \tag{3.58}$$

where the third equality is obtained using (3.49) and the definition of $\mathbf{F}_{ii_2\ldots i_K}$. Using (3.58) and (3.54), the first term on the right hand side of (3.57) can be obtained as

$$\begin{aligned}\sum_i \dot{E}_i\delta(\mathbf{x}-\mathbf{r}_i) \;&=\; -\frac{\partial}{\partial\mathbf{x}}\cdot\Bigg(\sum_i\Big[\frac{1}{2!}\sum_{i_2}\mathbf{r}_{ii_2}b_{ii_2}\otimes\mathbf{F}_{ii_2}+\frac{1}{3!}\sum_{i_2}(\mathbf{r}_{ii_2}b_{ii_2}+\mathbf{r}_{ii_3}b_{ii_3})\otimes\mathbf{F}_{ii_2i_3}+\\ &\qquad\qquad \ldots+\frac{1}{M!}\sum_{i_2,\ldots,i_K}(\mathbf{r}_{ii_2}b_{ii_2}+\ldots+\mathbf{r}_{ii_K}b_{ii_M})\otimes\mathbf{F}_{ii_2\ldots i_M}\Big]\frac{\mathbf{p}_i}{m_i}\Bigg)\\ &=\; -\frac{\partial}{\partial\mathbf{x}}\cdot\Bigg(\sum_i\Big[\frac{1}{2!}\sum_{i_2}\mathbf{r}_{ii_2}b_{ii_2}\otimes\mathbf{F}_{ii_2}+\frac{1}{3!}\sum_{i_2}(\mathbf{r}_{ii_2}b_{ii_2}+\mathbf{r}_{ii_3}b_{ii_3})\otimes\mathbf{F}_{ii_2i_3}+\ldots\\ &\quad+\frac{1}{M!}\sum_{i_2,\ldots,i_K}(\mathbf{r}_{ii_2}b_{ii_2}+\ldots+\mathbf{r}_{ii_K}b_{ii_M})\otimes\mathbf{F}_{ii_2\ldots i_M}\Big]\Big(\frac{\mathbf{p}_i}{m_i}-\mathbf{v}\Big)\Bigg)+\frac{\partial}{\partial\mathbf{x}}\cdot\big(\mathbf{T}_V^T\mathbf{v}\big)\,.\end{aligned} \tag{3.59}$$

Now, the second term on the right hand side of (3.56) can be written as

$$\begin{aligned}\int f(\Gamma,t)\sum_i E_i\dot{\mathbf{r}}_i\delta(\mathbf{x}-\mathbf{r}_i)\,\mathrm{d}\mathbf{\Gamma} \;&=\; \int f(\Gamma,t)\sum_i E_i\Big(\frac{\mathbf{p}_i}{m_i}-\mathbf{v}\Big)\delta(\mathbf{x}-\mathbf{r}_i)\,\mathrm{d}\mathbf{\Gamma}+\rho e\mathbf{v}\\ &=\; \int f(\Gamma,t)\sum_i\Big[\big(\frac{\mathbf{p}_i}{m_i}-\mathbf{v}\big)\cdot\big(\frac{\mathbf{p}_i}{m_i}-\mathbf{v}\big)+\sum_{i_2}u_2+\sum_{i_2,i_3}u_3\\ &\quad+\ldots+\sum_{i_2,i_3,\ldots,i_M}u_M\Big]\Big(\frac{\mathbf{p}_i}{m_i}-\mathbf{v}\Big)\delta(\mathbf{x}-\mathbf{r}_i)\,\mathrm{d}\mathbf{\Gamma}+\rho e\mathbf{v}-\mathbf{T}_K^T\mathbf{v}\\ &=\; \int f(\Gamma,t)\sum_i\hat{E}_i\Big(\frac{\mathbf{p}_i}{m_i}-\mathbf{v}\Big)\delta(\mathbf{x}-\mathbf{r}_i)\,\mathrm{d}\mathbf{\Gamma}+\rho e\mathbf{v}-\mathbf{T}_K^T\mathbf{v}\end{aligned} \tag{3.60}$$

using (3.34) and (3.35), where $\mathbf{T}_K$ is given by (3.53) and

$$\hat{E}_i=\big(\frac{\mathbf{p}_i}{m_i}-\mathbf{v}\big)\cdot\big(\frac{\mathbf{p}_i}{m_i}-\mathbf{v}\big)+\sum_{i_2}u_2+\sum_{i_2,i_3}u_3+\ldots+\sum_{i_2,i_3,\ldots,i_M}u_M\,. \tag{3.61}$$

Substituting (3.59) and (3.60) in (3.56), using (3.37) and the pointwise stress tensor definition, equation (3.56) can be reduced to

$$\begin{aligned}\rho\dot{e} &= \frac{\partial}{\partial \mathbf{x}}\cdot\left(\mathbf{T}^{pT}\mathbf{v}\right) - \frac{\partial}{\partial \mathbf{x}}\cdot\left(\int\sum_i\left[\hat{E}_i\mathbf{I}\delta(\mathbf{x}-\mathbf{r}_i) + \frac{1}{2!}\sum_{i_2}\mathbf{r}_{ii_2}b_{ii_2}\otimes\mathbf{F}_{ii_2}+\ldots\right.\right.\\ &\left.\left.+\frac{1}{M!}\sum_{i_2,\ldots,i_K}(\mathbf{r}_{ii_2}b_{ii_2}+\ldots+\mathbf{r}_{ii_K}b_{ii_M})\otimes\mathbf{F}_{ii_2\ldots i_M}\right]\left(\frac{\mathbf{p}_i}{m_i}-\mathbf{v}\right)f(\mathbf{\Gamma},t)\,\mathrm{d}\mathbf{\Gamma}\right)\\ &= \frac{\partial}{\partial \mathbf{x}}\cdot\left(\mathbf{T}^{pT}\mathbf{v}\right) - \frac{\partial}{\partial \mathbf{x}}\cdot\mathbf{J}^p_Q\,,\end{aligned} \tag{3.62}$$

where

$$\begin{aligned}\mathbf{J}^p_Q &= \int\sum_i\left[\hat{E}_i\mathbf{I}\delta(\mathbf{x}-\mathbf{r}_i) + \frac{1}{2!}\sum_{i_2}\mathbf{r}_{ii_2}b_{ii_2}\otimes\mathbf{F}_{ii_2}+\ldots\right.\\ &\left.+\frac{1}{M!}\sum_{i_2,\ldots,i_K}(\mathbf{r}_{ii_2}b_{ii_2}+\ldots+\mathbf{r}_{ii_K}b_{ii_M})\otimes\mathbf{F}_{ii_2\ldots i_M}\right]\left(\frac{\mathbf{p}_i}{m_i}-\mathbf{v}\right)f(\mathbf{\Gamma},t)\,\mathrm{d}\mathbf{\Gamma}\,.\end{aligned} \tag{3.63}$$

It can be seen that (3.62) is identical in form to the balance of energy (2.3) in the absence of body forces and external heat source. Again comparing terms in (3.62) and (2.3), the point-wise heat flux vector is given by (3.63).

As mentioned earlier, in order to obtain the macroscopic balance of energy from (3.62) one has to perform appropriate space averaging over a microscopically large though macroscopically small domain, determined by the resolving power of one's measuring instruments, [32]. Therefore, averaging over a spatial domain of volume V and specializing to any one system in the ensemble, the macroscopic instantaneous stress tensor and heat flux vectors can be obtained in terms of the molecular variables from (3.55) and (3.63) as

$$\begin{aligned}\tilde{\mathbf{T}}(t) &= \frac{1}{V}\int_V\mathbf{T}^p\,\mathrm{d}\mathbf{x}\\ &= -\frac{1}{V}\sum_i m_i\left(\frac{\mathbf{p}_i}{m_i}-\mathbf{v}\right)\otimes\left(\frac{\mathbf{p}_i}{m_i}-\mathbf{v}\right) - \frac{1}{V}\Big[\frac{1}{2!}\sum_{i,i_2}\mathbf{F}_{ii_2}\otimes\mathbf{r}_{ii_2}+\\ &\frac{1}{3!}\sum_{i,i_2,i_3}\mathbf{F}_{ii_2i_3}\otimes(\mathbf{r}_{ii_2}+\mathbf{r}_{ii_3})+\ldots+\frac{1}{M!}\sum_{i,i_2,\ldots,i_M}\mathbf{F}_{ii_2\ldots i_M}\otimes(\mathbf{r}_{ii_2}+\ldots+\mathbf{r}_{ii_M})\Big]\end{aligned} \tag{3.64}$$

and

$$\begin{aligned}\tilde{\mathbf{J}}_Q(t) &= \frac{1}{V}\int_V \mathbf{J}_Q^p \,\mathrm{d}\mathbf{x} \\ &= \frac{1}{V}\sum_i \left[\hat{E}_i\mathbf{I} + \frac{1}{2!}\sum_{i_2}\mathbf{r}_{ii_2}\otimes\mathbf{F}_{ii_2} + \dots \right. \\ &\qquad \left. + \frac{1}{M!}\sum_{i_2,\dots,i_K}(\mathbf{r}_{ii_2}+\dots+\mathbf{r}_{ii_K})\otimes\mathbf{F}_{ii_2\dots i_M}\right]\left(\frac{\mathbf{p}_i}{m_i}-\mathbf{v}\right),\end{aligned} \tag{3.65}$$

respectively. The instantaneous heat flux vector thus obtained can be used with the Green-Kubo relations (3.16) to obtain the heat transport coeffiecient $\mathbf{L}_{QQ}$.

Chapter 4

Molecular Dynamics Methods

In this chapter, a review of the existing molecular dynamics methods for evaluating the heat transport coefficients, such as the direct method and the Green-Kubo method, is given and their advantages and limitations are highlighted. Also, an introduction to the HNEMD method is given which will be dealt in an elaborate manner in the subsequent chapters.

4.1 Direct Method

The direct method is a non-equilibrium molecular dynamics method and is analogous to the experimental measurement [67]. In this method, a known value of heat flux $\mathbf{J}_Q$ is constantly driven through the system, which is then left to evolve by Newton's equations of motion (3.30) resulting in a constant temperature gradient $\boldsymbol{\nabla} T$ when the system reaches steady-state. The value of thermal conductivity $\boldsymbol{\kappa}$ at a temperature T is then obtained by using Fourier's law $\mathbf{J}_Q = -\boldsymbol{\kappa}\boldsymbol{\nabla} T$. A detailed explanation and the application of the method is given in [67, 73].

The heat flux in the system is driven by the addition and removal of energy from the system at two different locations. The energy is added or removed by appropriate scaling of the velocities of atoms in the system. Figure 4.1 shows a schematic representation of the molecular dynamics system used to compute the thermal conductivity. As shown in Figure 4.1, energy $\Delta\epsilon$ is added by rescaling the velocities of atoms at every time step in the slab of thickness w centered at $z = -\dfrac{L_z}{4}$ and removed from the slab of same thickness w centered at $z = \dfrac{L_z}{4}$. Applying the balance law of energy to the slab at $z = -\dfrac{L_z}{4}$ when the system reaches a steady state, it can be seen that

$$\frac{1}{wA}\frac{\Delta\epsilon}{\Delta t} \;=\; \frac{J_{Qz} - (-J_{Qz})}{w}\,, \tag{4.1}$$

where, J_{Qz} is the heat flux in the z direction, A is the cross-sectional area of the MD system and

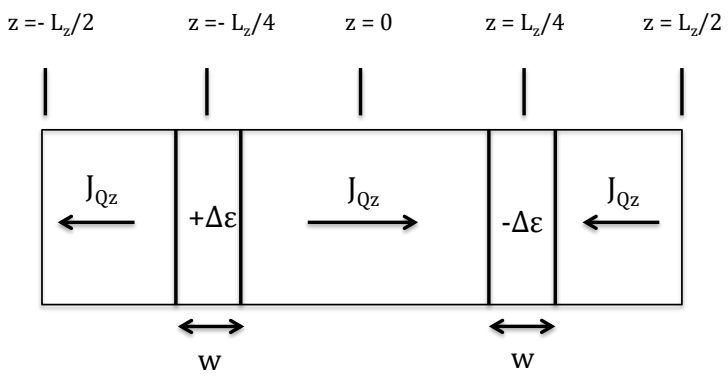

Figure 4.1: *Schematic representation of the molecular dynamics system in the direct method, where L_z is the total length of the system in the z-direction, from [67].*

Δt denotes the time step in solving the equations of motion (3.30). In this way, a heat flux of

$$J_{Qz} \;=\; \frac{\Delta\epsilon}{2A\Delta t} \tag{4.2}$$

is driven through the system. Here, the system is allowed to reach a steady state by solving (3.30) and imposing periodic boundary conditions (PBCs) in all three directions. PBCs are usually chosen to mimic the presence of an infinite bulk surrounding the N-particle model system in order to obtain the bulk estimates. In the case of PBCs, all atoms that exit the system from one side enter it again from the opposite side with the same momentum and forces, see, *e.g.*., [2, Section 1.5.2]. To determine the temperature as a function of z, the system is divided into small blocks along the z-axis. The temperature at z is then defined in terms of the kinetic energies of the atoms in the block centered at z using the equipartition theorem [64, Section 6.5] as

$$T(z) \;=\; \left\langle \sum_{i \,\in\, block} \frac{m_i \mathbf{v}_i \cdot \mathbf{v}_i}{3N_z k_B} \right\rangle \;=\; \langle T_b(z) \rangle \;, \tag{4.3}$$

where the summation is on the atoms in the block, $\langle \cdot \rangle$ denotes the ensemble average corresponding to the steady state phase space distribution, k_B is the Boltzmann's constant and N_z is the number of atoms in the block. Furthermore, assuming the system to be ergodic, the ensemble average in (4.3) is evaluated as a time average of the kinetic energy once the steady state is reached, *i.e.*,

$$\langle T_b(z) \rangle \;=\; \lim_{Y \to \infty} \frac{1}{Y} \int_{t_0}^{t_0+Y} \tilde{T}_{bz}(t)\, \mathrm{d}t, \tag{4.4}$$

where $T_b(z) = \tilde{T}_{bz}(t)$. Using (4.4), a typical temperature profile for the case of silicon modeled by

the Stillinger-Weber potential at 500K is shown in Figure 4.2 [67]. A linear fit can be applied to the

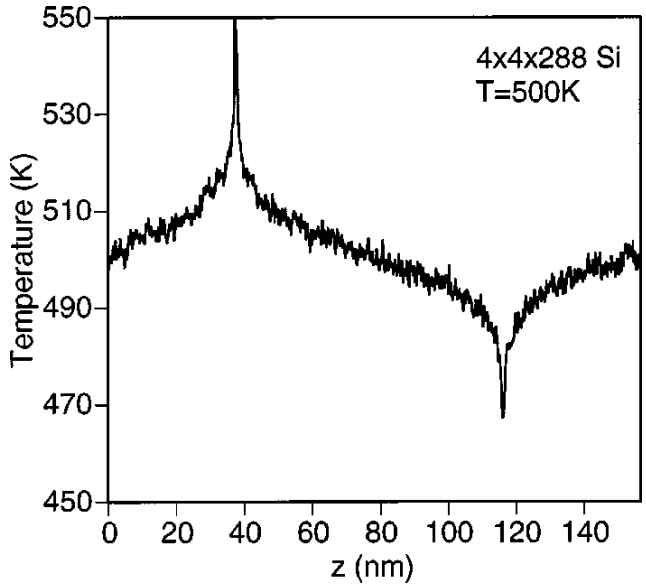

Figure 4.2: *Temperature profile along the length of a unit cell silicon system consisting of* $4 \times 4 \times 288$ *unit cells at an average temperature of* $T = 500K$*, from [67].*

temperature profile as shown in Figure 4.3 to estimate the temperature gradient. The temperature gradient thus obtained and the heat flux given by (4.2) can be used along with Fourier's law to obtain an estimate of the thermal conductivity. However, it is important to understand the behavior of the simulated system for various values of $\Delta\epsilon$, as one needs to identify a range of $\Delta\epsilon$ where the heat flux and the temperature gradient are directly proportional to each other, or equivalently, the thermal conductivity obtained should be independent of $\Delta\epsilon$. Figure 4.4 shows the effect of the magnitude $\Delta\epsilon$ of the energy difference on the thermal conductivity. Furthermore, using this method, it can be seen that the thermal conductivity attained is dependent on the length of the simulated system, as shown in Figure 4.5. To obtain meaningful values that may be compared with experiments, it is necessary to perform several simulations of increasing lengths and then extrapolate to the infinite-size limit. The thermal conductivity at infinite length κ_∞ may then be obtained from linear extrapolation using

$$\frac{1}{\kappa(L_z)} = \frac{1}{\kappa_\infty} + \frac{\alpha}{L_z}\,, \tag{4.5}$$

where $\kappa(L_z)$ is the thermal conductivity obtained corresponding to a length L_z and α is a length-independent coefficient.

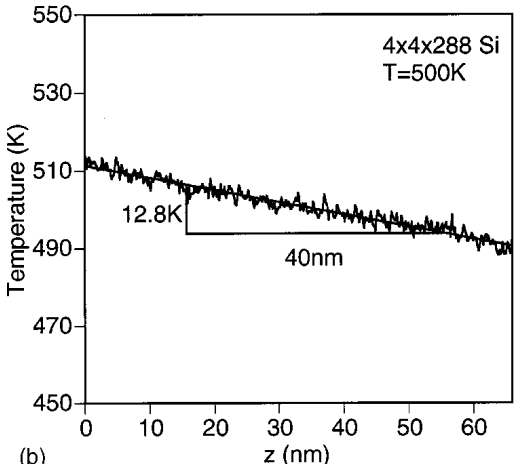

Figure 4.3: *Linear fit to a temperature profile along the length of a silicon molecular dynamics system consisting of* $4 \times 4 \times 288$ *unit cells at an average temperature of* $T = 500K$*, from [67].*

The preceding direct method has many disadvantages. First, it is only capable of obtaining the thermal conductivity component along the direction of the induced flux. Second, the temperature gradients in this method are found to be on the order of $10^9 \frac{K}{m}$, as seen in Figure 4.3, and therefore the validity of Fourier's law becomes questionable. Since the gradients are large, it is very difficult to identify the temperature at which the thermal conductivity is obtained. Third, the length of the system in the direction along which the thermal conductivity is estimated needs to be much larger than the mean-free path of the phonons in order to avoid scattering of phonons with the heat source ($+\Delta\epsilon$) and sink ($-\Delta\epsilon$) [67]. In the case of silicon at $500K$, where the phonon mean-free path is around $100\,nm$, the number of atoms in the system need to be on the order of 3×10^5 to avoid the size effects, hence making the simulation computationally costly in spite of imposing periodic boundary conditions. Fourth, the computational cost also increases since the direct method depends on identifying a range where the thermal conductivity is independent of $\Delta\epsilon$, as shown in Figure 4.4.

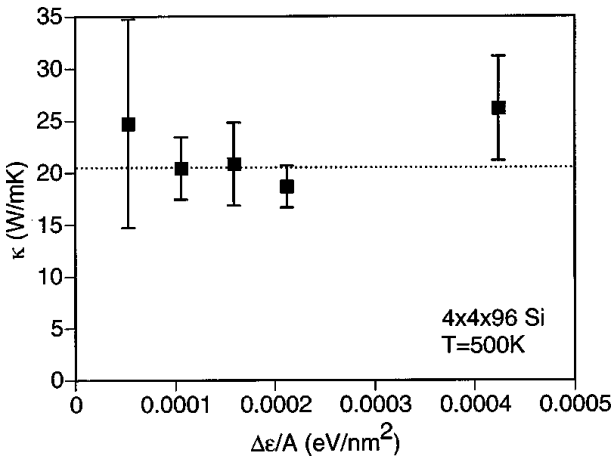

Figure 4.4: *Thermal conductivity dependence on the rescaling energy $\Delta\epsilon$ of a silicon system consisting of $4 \times 4 \times 96$ unit cells at an average temperature of $T = 500K$, from [67]. It can be seen that the heat-flux is directly proportionately to the temperature gradient following Fourier's law.*

4.2 Green-Kubo Method

The method of Green-Kubo is the second most commonly used method to obtain the heat transport coefficient $\frac{\mathbf{L}_{QQ}}{T^2}$ [70, 67]. In this method, a molecular dynamics system is allowed to reach equilibrium at a certain temperature T and volume V by imposing periodic boundary conditions in all three directions. Once the system reaches equilibrium, the average heat flux in the system is zero. However, there exist fluctuations of the heat flux vector whose instantaneous values $\tilde{\mathbf{J}}_Q(t)$ are continuously noted. Using these instantaneous heat flux values, the heat flux autocorrelation function is obtained as a function of time by

$$\mathcal{C}_{\mathbf{J}_Q}(\tau) \;=\; \langle \tilde{\mathbf{J}}_Q(\tau) \otimes \tilde{\mathbf{J}}_Q(0) \rangle \;=\; \lim_{Y \to \infty} \frac{1}{Y} \int_{t_0}^{t_0+Y} \tilde{\mathbf{J}}_Q(\tau + s) \otimes \tilde{\mathbf{J}}_Q(s)\, \mathrm{d}s \;, \tag{4.6}$$

where the second equality is obtained by appealing to the ergodic hypothesis. The autocorrelation function is used in the Green-Kubo formula (3.18) to obtain the heat transport coefficient tensor $\frac{\mathbf{L}_{QQ}}{T^2}$. As mentioned earlier, in the case of solids, this heat transport coefficient reduces to the thermal conductivity $\boldsymbol{\kappa}$. Figure 4.6 shows the normalized heat flux autocorrelation function of silicon

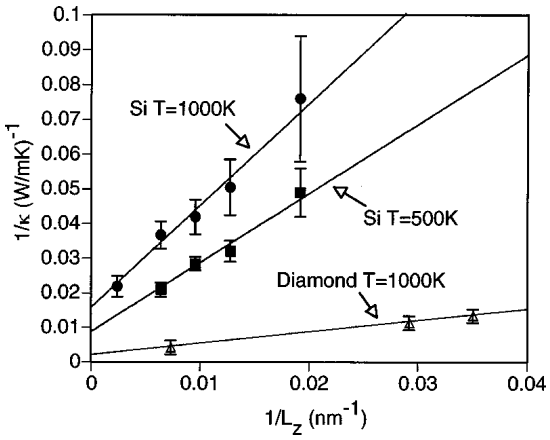

Figure 4.5: *Thermal conductivity dependence on the length L_z of the system in the z-direction for silicon and diamond, from [67].*

at $1000K$, modeled by Stillinger-Weber interatomic potential. It can be seen that the autocorrelation function decays abruptly for shorter times followed by a long tail. It is this long tail of the autocorrelation function that contributes significantly to the thermal conductivity tensor, especially in the case of solids. Figure 4.7 shows the integration of autocorrelation function yielding the thermal conductivity as a function of time.

There are two main advantages in using the Green-Kubo method. First, thermal conductivity converges quickly with the system size which is on the order of 2000 atoms for the case of silicon at $1000K$, as shown in Table 4.1. Second, running a single simulation yields all the components of thermal conductivity tensor $\boldsymbol{\kappa}$ unlike the direct method. However, the most important shortcoming of the Green-Kubo method is the convergence of autocorrelation function with the simulation time for a particular system size. As mentioned earlier, in the Green-Kubo approach, the heat transport coefficient is obtained by integration of the corresponding auto-correlation function (4.6). Hence, the result directly depends on the accuracy of the auto-correlation function. For a finite simulation time τ_M, using ergodic hypothesis (4.6), the estimate $\bar{\mathcal{C}}_{\mathbf{J}_Q}(\tau)$ of the autocorrelation function $\mathcal{C}_{\mathbf{J}_Q}(\tau)$ is given by

$$\bar{\mathcal{C}}_{\mathbf{J}_Q}(\tau) \;=\; \frac{1}{\tau_M}\int_0^{\tau_M} \tilde{\mathbf{J}}_Q(s) \otimes \tilde{\mathbf{J}}_Q(s+\tau)\,\mathrm{d}s \tag{4.7}$$

Assuming that the process $\tilde{\mathbf{J}}_Q(t)$ follows Gaussian statistics, the variance in the estimate of $\mathcal{C}_{\mathbf{J}_Q}$ can be calculated theoretically for the following two cases: (i) $\tau \to 0$, *i.e.*, at short correlation

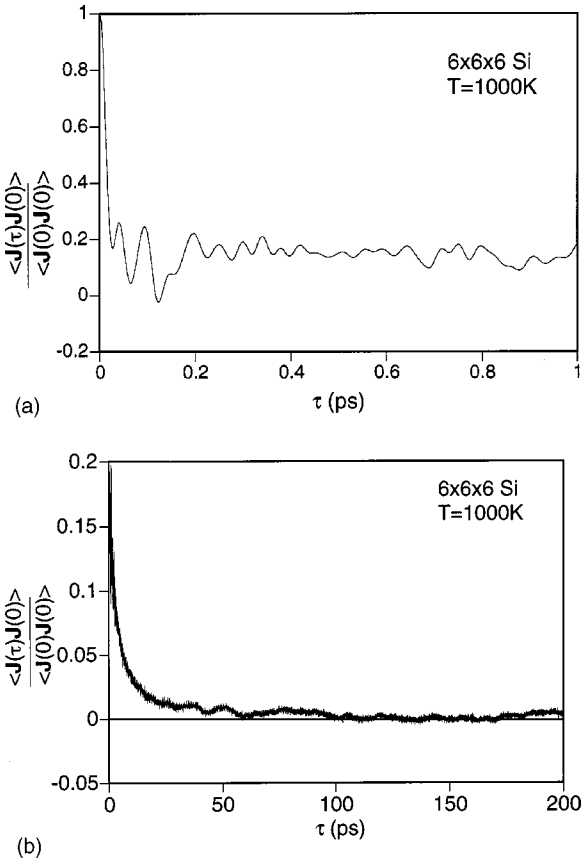

Figure 4.6: *Normalized heat flux autocorrelation for silicon at $T = 1000K$, from [67]. (a) Normalized correlation function at short correlation times (b) Normalized correlation function at all times.*

times, and (ii) $\tau \to \infty$, *i.e.*, at long correlation times [2]. For $\tau \to 0$,

$$\frac{\langle \bar{\mathcal{C}}_{\mathbf{J}_Q}(\tau)^2 \rangle - \langle \bar{\mathcal{C}}_{\mathbf{J}_Q}(\tau) \rangle^2}{\langle \mathcal{C}_{\mathbf{J}_Q}(0) \rangle^2} = 4\frac{\tau_c}{\tau_M} \tag{4.8}$$

where τ_c is given by

$$\tau_c = \frac{\int_0^\infty \langle \mathcal{C}_{\mathbf{J}_Q}(s) \rangle^2 \, \mathrm{d}s}{\langle \mathcal{C}_{\mathbf{J}_Q}(0) \rangle^2} \tag{4.9}$$

which again depends on the decay of the auto-correlation function. For $\tau \to \infty$, the variance in

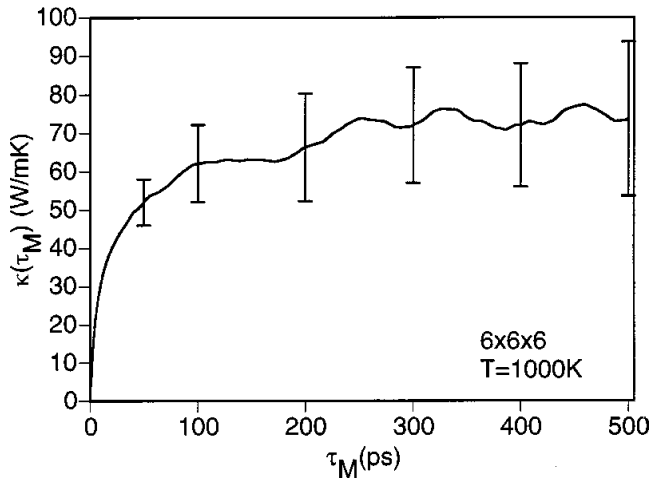

Figure 4.7: *Thermal conductivity estimation as a function of time by the integration of heat flux autocorrelation function of silicon at $T = 1000K$, from [67].*

the estimate of $\mathcal{C}_{\mathbf{J}_Q}(\tau)$ is shown to be

$$\frac{\langle \bar{\mathcal{C}}_{\mathbf{J}_Q}(\tau)^2 \rangle - \langle \bar{\mathcal{C}}_{\mathbf{J}_Q}(\tau) \rangle^2}{\langle \mathcal{C}_{\mathbf{J}_Q}(0) \rangle^2} = 2\frac{\tau_c}{\tau_M} \,, \tag{4.10}$$

see [2]. Here, it is important to mention that (4.8) and (4.10) are obtained by assuming that the total simulation time τ_M is much longer than the characterisitic decay time of the fluctuations of $\mathbf{J}_Q$ and also that equal number of samples are used to obtain the estimates of $\mathcal{C}_{\mathbf{J}_Q}(\tau)$ at both shorter and longer correlation times. From (4.8) and (4.10), it can be seen that the variance in $\bar{\mathcal{C}}_{\mathbf{J}_Q}(\tau)$ relative to the zero time correlation changes very small when one goes from shorter times to longer times. The values of $\bar{\mathcal{C}}_{\mathbf{J}_Q}(\tau)$ may not be reliable when they are of the order of their variances. For example, in the case of Silicon at 1000K where the decay of the normalized heat flux autocorrelation function is shown in Figure 4.6, the value of τ_c is approximately $0.4ps$. If one assumes the total simulation time to be 30 million time steps of $0.5fs$ each, then the relative standard deviation of $\bar{\mathcal{C}}_{\mathbf{J}}(\tau)$ for short times is approximately 0.03 using (4.8) and for long times is 0.015 using (4.10). Hence, all the values of $\bar{\mathcal{C}}_{\mathbf{J}_Q}(\tau)$ for correlation times greater than $25ps$ may not be reliable and when integrated these correspond to $15 - 20\%$ of the total thermal conductivity. One way to reduce these errors is to continue the simulation for a long time thereby making the Green-Kubo method computationally costly.

Size (unit cells)	Number of atoms	κ (W/mK)
$4 \times 4 \times 4$	512	22
$5 \times 5 \times 5$	1000	82
$6 \times 6 \times 6$	1728	66
$8 \times 8 \times 8$	4096	62

Table 4.1: *Comparison of thermal conductivity (κ) of silicon at $T = 1000K$ obtained by the GK method for different system sizes, from [67]. It can be seen that the thermal conductivity converges for a system size of $6 \times 6 \times 6$ unit cells.*

4.3 HNEMD Method

In addition to the two methods described above, there exists another method known as the HNEMD method initially proposed by Evans which forms the main contribution of this thesis [24, 21, 46, 45, 47]. The HNEMD method of Evans defines a mechanical analogue to the thermal transport process and uses the linear response theory to calculate the transport coefficients. This method is synthetic, in the sense that a fictitious force field is used to mimic the effect of a thermal gradient, thereby reducing the thermal transport problem to a mechanical problem. Using the linear response theory [24, 45], the long-time ensemble average of the heat flux vector for the resulting non-equilibrium system can be shown to be proportional to the external force field (when the latter is sufficiently small), with the constant of proportionality being the Green-Kubo formula for the heat transport coefficient tensor. In this way, one can obtain the heat transport coefficient tensor without explicitly calculating the autocorrelation functions. Hence, one can circumvent the problems related to the calculation and integration of autocorrelation functions.

In the following sections, the linear response theory required for the HNEMD method is developed and then applied to single or multicomponent systems modeled by pair potentials. Subsequently, the method is extended to three-body potentials and many-body potentials [21, 46, 45, 47].

Chapter 5

Linear Response Theory

In many problems, one needs to calculate the heat transport coefficient tensor at a particular temperature. This corresponds to the situation where the governing set of macroscopic variables are the number of particles N, volume V and temperature T. The ensemble and the probability distribution corresponding to this governing set are called the *canonical ensemble* and the *canonical phase space distribution*. The dynamics of particles evolving using Newtons laws given by (3.30) correspond to a constant energy and hence cannot reproduce the canonical phase space distribution function. Therefore, one needs to model the dynamics of particles such that the canonical distribution at a particular temperature is reproduced. In this chapter, the equations of motion required to maintain constant temperature are presented [56, 30]. These are called the Nosé-Hoover (NH) thermostatted equations of motion. These are then used to derive the extended canonical phase-space distribution function. Next, the Nose-Hoover thermostatted equations of motion perturbed by an external field are considered to derive the linear response theory necessary for the application of the HNEMD method [45, 24].

5.1 Nosé-Hoover Thermostat

In problems related to canonical ensemble (N, V, T), it is important that the equations of motion used to model the system preserve the canonical phase space distribution

$$f(\mathbf{\Gamma}) \;=\; \frac{e^{-\beta H_0(\mathbf{\Gamma})}}{Z(\beta)}\,, \tag{5.1}$$

where H_0 is the total energy, $Z(\beta) = \int e^{-\beta H_0(\mathbf{\Gamma})}\, \mathrm{d}\mathbf{\Gamma}$ is the partition function, $\beta = \dfrac{1}{k_B T}$ [64]. Here, the total energy of the N-body system is given by

$$H_0 \;=\; \sum_{i=1}^{N} \frac{\mathbf{p}_i \cdot \mathbf{p}_i}{2m_i} + \Phi(\mathbf{r}_1, \mathbf{r}_2, \ldots, \mathbf{r}_N)\;, \tag{5.2}$$

where $\Phi(\mathbf{r}_1, \mathbf{r}_2, \ldots, \mathbf{r}_N)$ is the inter-atomic potential given by (3.32).

Thermostatted equations of motion corresponding to this canonical ensemble were given initially by Nosé [56] and later amended by Hoover [30] in to the form

$$\begin{aligned} \dot{\mathbf{r}}_i \;&=\; \frac{\mathbf{p}_i}{m}\;, \\ \dot{\mathbf{p}}_i \;&=\; \mathbf{F}_i - \zeta \mathbf{p}_i\;, \\ \dot{\zeta} \;&=\; \frac{1}{Q}\left(\sum_{i=1}^{N} \frac{\mathbf{p}_i \cdot \mathbf{p}_i}{m_i} - 3Nk_BT \right). \end{aligned} \tag{5.3}$$

Here, ζ is the thermodynamic friction coefficient and Q is an arbitrary parameter chosen to yield the canonical phase space distribution. The equations follow the integral feedback mechanism to generate the canonical distribution and are referred to as Nosé-Hoover equations of motion. Taking into account (3.22), the distribution function $f(\mathbf{\Gamma}, \zeta, t)$ corresponding to (5.3) is given by the Liouville equation

$$\frac{\partial f(\mathbf{\Gamma}, t)}{\partial t} \;=\; -\left[\frac{\partial}{\partial \mathbf{\Gamma}} \cdot \dot{\mathbf{\Gamma}} + \dot{\mathbf{\Gamma}} \cdot \frac{\partial}{\partial \mathbf{\Gamma}} + \dot{\zeta} \frac{\partial}{\partial \zeta} + \frac{\partial}{\partial \zeta} \dot{\zeta} \right] f(\mathbf{\Gamma}, t)\;, \tag{5.4}$$

which can be rewritten as

$$\frac{df(\mathbf{\Gamma}, t)}{dt} \;=\; -\left[\frac{\partial}{\partial \mathbf{\Gamma}} \cdot \dot{\mathbf{\Gamma}} + \frac{\partial}{\partial \zeta} \dot{\zeta} \right] f(\mathbf{\Gamma}, t)\;. \tag{5.5}$$

Now, using the NH equations of motion (5.3), the term on the right hand side of (5.5) can be evaluated as

$$\begin{aligned} \frac{\partial}{\partial \mathbf{\Gamma}} \cdot \dot{\mathbf{\Gamma}} + \frac{\partial}{\partial \zeta} \dot{\zeta} \;&=\; \sum_{i=1}^{N} \frac{\partial}{\partial \mathbf{r}_i} \cdot \dot{\mathbf{r}}_i + \sum_{i=1}^{N} \frac{\partial}{\partial \mathbf{p}_i} \cdot \dot{\mathbf{p}}_i + \frac{\partial}{\partial \zeta} \dot{\zeta} \\ &=\; 3N\zeta\;, \end{aligned} \tag{5.6}$$

thereby reducing (5.5) to

$$\frac{df(\mathbf{\Gamma}, t)}{dt} \;=\; 3N\zeta\;. \tag{5.7}$$

Taking the time derivative of $H_0 + \frac{1}{2}Q\zeta^2$, it follows that

$$\begin{aligned} \frac{d}{dt}\big(H_0 + \frac{1}{2}Q\zeta^2\big) &= \sum_i \left(\frac{\mathbf{p}_i \cdot \dot{\mathbf{p}}_i}{m_i} + \frac{\partial \Phi}{\partial \mathbf{r}_i} \cdot \dot{\mathbf{r}}_i \right) + Q\zeta\dot{\zeta} \\ &= -3N\zeta k_B T \,, \end{aligned} \tag{5.8}$$

where use is made of the equations of motion (5.3) and the definition of (3.33) interatomic force $\mathbf{F}_i$ on atom i. Therefore, using (5.8) and (5.7), a differential equation can be obtained for the phase space distribution in the form

$$\frac{1}{f}\frac{df(\mathbf{\Gamma}, t)}{dt} = -\beta \frac{d}{dt}\big(H_0 + \frac{1}{2}Q\zeta^2\big) \,, \tag{5.9}$$

whose solution yields $f(\mathbf{\Gamma}, \zeta, t)$ to be the extended canonical distribution given by

$$f(\mathbf{\Gamma}, \zeta, t) = f_c(\mathbf{\Gamma}, \zeta) = \frac{e^{-\beta\left(H_0(\mathbf{\Gamma}) + \frac{1}{2}Q\zeta^2\right)}}{\int e^{-\beta\left(H_0(\mathbf{\Gamma}) + \frac{1}{2}Q\zeta^2\right)} \, \mathrm{d}\mathbf{\Gamma} \, \mathrm{d}\zeta} \,. \tag{5.10}$$

Hence, the NH equations of motion (5.3) produces the desired canonical distribution accurately.

5.2 Isothermal Linear Response Theory for HNEMD Method

The general form of the equations of motion in the linear response theory is obtained by a perturbative external field $\mathbf{F}_e$ in the presence of a Nosé-Hoover (NH) thermostat thus leading to

$$\begin{aligned} \dot{\mathbf{r}}_i &= \frac{\mathbf{p}_i}{m_i} + \mathbf{C}_i(\mathbf{\Gamma})\mathbf{F}_e \,, \\ \dot{\mathbf{p}}_i &= \mathbf{F}_i + \mathbf{D}_i(\mathbf{\Gamma})\mathbf{F}_e - \zeta \mathbf{p}_i \,, \\ \dot{\zeta} &= \frac{1}{Q}\left(\sum_{i=1}^{N} \frac{\mathbf{p}_i \cdot \mathbf{p}_i}{m_i} - 3Nk_B T \right) , \end{aligned} \tag{5.11}$$

where $\mathbf{C}_i(\mathbf{\Gamma})$ and $\mathbf{D}_i(\mathbf{\Gamma})$ are the second-order tensor phase variables which describe the coupling of the system to the applied external field $\mathbf{F}_e$ [23]. It can be seen that when $\mathbf{F}_e = \mathbf{0}$, the phase-space distribution $f(\mathbf{\Gamma}, \zeta, t)$ becomes the (extended) canonical distribution f_c given by (5.10). Assuming that the external field $\mathbf{F}_e$ is applied at time $t = 0$, the perturbed distribution $f(\mathbf{\Gamma}, \zeta, t)$ corresponding

to field dependent equations of motion (5.11) is obtained by solving the Liouville equation

$$\begin{aligned} \frac{\partial f(\mathbf{\Gamma},\zeta,t)}{\partial t} &= \left[\frac{\partial}{\partial \mathbf{\Gamma}}\cdot\dot{\mathbf{\Gamma}} + \dot{\mathbf{\Gamma}}\cdot\frac{\partial}{\partial \mathbf{\Gamma}} + \dot{\zeta}\frac{\partial}{\partial\zeta} + \frac{\partial}{\partial\zeta}\dot{\zeta}\right] f(\mathbf{\Gamma},\zeta,t) \\ &= -iLf(\mathbf{\Gamma},\zeta,t)\ , \end{aligned} \tag{5.12}$$

with initial condition $f(\mathbf{\Gamma},\zeta,0) = f_c(\mathbf{\Gamma},\zeta)$. Here, iL represents the f-Liouvillean operator corresponding to (5.11). Assuming the external field $\mathbf{F}_e$ to be small enough and independent of time, the Liouvillean iL^c and the perturbed distribution function $f(\mathbf{\Gamma},\zeta,t)$ may be approximated by

$$\begin{aligned} iL &= iL_0 + i\Delta L(t)\ , \\ f(\mathbf{\Gamma},\zeta,t) &= f_c(\mathbf{\Gamma},\zeta) + \Delta f(\mathbf{\Gamma},\zeta,t)\ , \end{aligned} \tag{5.13}$$

where $i\Delta L(t)$ and $\Delta f(\mathbf{\Gamma},\zeta,t)$ are linear perturbations to the field-free Liouvillean iL_0 and the extended canonical distribution $f_c(\mathbf{\Gamma},\zeta)$, respectively, due to the presence of the external field $\mathbf{F}_e$. Here, iL_0 corresponds to the field-free equations of motion, *i.e.*, equation (5.11) with $\mathbf{F}_e = \mathbf{0}$, while f_c satisfies $\dfrac{\partial}{\partial t}f = -iL_0 f$. Using the approximation (5.13), the Liouville equation (5.12) can be linearized as

$$\frac{\partial}{\partial t}\Delta f(\mathbf{\Gamma},\zeta,t) + iL_0\Delta f(\mathbf{\Gamma},\zeta,t) = -i\Delta L(t) f_c(\mathbf{\Gamma},\zeta)\ , \tag{5.14}$$

while satisfying an initial condition $\Delta f(\mathbf{\Gamma},\zeta,0) = 0$. The solution $\Delta f(\mathbf{\Gamma},\zeta,t)$ of the linearized Liouville equation (5.14) can be obtained formally as

$$\Delta f(\mathbf{\Gamma},\zeta,t) = -\int_0^t \exp\big(-iL_0(t-s)\big) i\Delta L(s) f_c(\mathbf{\Gamma},\zeta)\,\mathrm{d}s\ ,\ , \tag{5.15}$$

where $i\Delta L(s)f_c(\mathbf{\Gamma},\zeta) = iL(s)f_c(\mathbf{\Gamma},\zeta) - iL_0 f_c(\mathbf{\Gamma},\zeta)$. The validity of the solution can be verified by the following two steps: (i) substituting $t = 0$ and observing that $\Delta f(\mathbf{\Gamma},\zeta,0) = 0$ thereby satisfying the initial condition and (ii) substituting (5.15) in (5.14) and observing that it satisfies

the linearized Liouville equation for all times [24]. Hence,

$$\begin{aligned} i\Delta L(s) f_c(\mathbf{\Gamma},\zeta) &= iL(s) f_c(\mathbf{\Gamma},\zeta) \\ &= \left[\frac{\partial}{\partial \mathbf{\Gamma}}\cdot\dot{\mathbf{\Gamma}} + \dot{\mathbf{\Gamma}}\cdot\frac{\partial}{\partial \mathbf{\Gamma}} + \dot{\zeta}\frac{\partial}{\partial\zeta} + \frac{\partial}{\partial\zeta}\dot{\zeta}\right] f_c(\mathbf{\Gamma},\zeta) \\ &= \left[\sum_{i=1}^{N}\frac{\partial}{\partial \mathbf{r}_i}\cdot\mathbf{C}_i\mathbf{F}_e + \sum_{i=1}^{N}\frac{\partial}{\partial \mathbf{p}_i}\cdot\mathbf{D}_i\mathbf{F}_e\right] f_c(\mathbf{\Gamma},\zeta) \\ &\qquad + \beta\left[-\sum_{i=1}^{N}\mathbf{D}_i{}^T\frac{\mathbf{p}_i}{m} + \sum_{i=1}^{N}\mathbf{C}_i{}^T\mathbf{F}_i\right]\cdot\mathbf{F}_e f_c(\mathbf{\Gamma},\zeta) \\ &= \beta V\left[\mathbf{B}(\mathbf{\Gamma}) - \mathbf{J}(\mathbf{\Gamma})\right]\cdot\mathbf{F}_e f_c(\mathbf{\Gamma},\zeta)\,, \end{aligned} \tag{5.16}$$

where

$$\mathbf{B}(\mathbf{\Gamma}) \;=\; \frac{1}{\beta V}\left(\sum_{i=1}^{N}\frac{\partial}{\partial \mathbf{r}_i}\cdot\mathbf{C}_i^T + \sum_{i=1}^{N}\frac{\partial}{\partial \mathbf{p}_i}\cdot\mathbf{D}_i^T\right)\,, \tag{5.17}$$

and

$$\mathbf{J}(\mathbf{\Gamma}) \;=\; \frac{1}{V}\left(\sum_{i=1}^{N}\mathbf{D}_i{}^T\frac{\mathbf{p}_i}{m_i} - \sum_{i=1}^{N}\mathbf{C}_i{}^T\mathbf{F}_i\right)\,. \tag{5.18}$$

It should be noted that when $\mathbf{B} = \mathbf{0}$ and no thermostatting mechanism exists, *i.e.*, $\zeta = 0$ in (5.11), $\dfrac{\partial}{\partial\mathbf{\Gamma}}\cdot\dot{\mathbf{\Gamma}} = 0$ and hence the phase space becomes incompressible, as mentioned in Chapter 3. Therefore, the condition $\mathbf{B} = \mathbf{0}$ is called as the *adiabatic incompressibility of phase space* AIΓ, and $\mathbf{B}$ is known as the *phase space compression factor*, see [24, Chapter 5] . The variable $\mathbf{J}$ is defined as the "dissipative" flux, as it can be seen in [24, Section 5.1] that in the absence of thermostatting mechanism, the rate of change of internal energy H_0 is given by $\dot{H}_0 = -\beta\mathbf{J}\cdot\mathbf{F}_e$.

Let $\mathbf{G}(\mathbf{\Gamma}(t)) = \tilde{\mathbf{G}}(t)$ be a general phase variable. Then, the ensemble average of $\mathbf{G}$ evolving with (5.11) in the Schrödinger representation is given by

$$\langle\tilde{\mathbf{G}}(t)\rangle \;=\; \int \mathbf{G}(\mathbf{\Gamma}) f(\mathbf{\Gamma},\zeta,t)\,\mathrm{d}\mathbf{\Gamma}\,\mathrm{d}\zeta\,, \tag{5.19}$$

where $f(\mathbf{\Gamma},\zeta,t)$ is the perturbed phase-space distribution function obtained by solving (5.12). Us-

ing (5.13), (5.15) and (5.16), the ensemble average of $\tilde{\mathbf{G}}(t)$ is reduced to

$$\begin{aligned}\langle\tilde{\mathbf{G}}(t)\rangle &= \int \mathbf{G}(\mathbf{\Gamma}) f(\mathbf{\Gamma},\zeta,t)\,\mathrm{d}\mathbf{\Gamma}\,\mathrm{d}\zeta \\ &= \langle\tilde{\mathbf{G}}(0)\rangle_c + \\ &\quad \beta V\int_0^t\left(\int \mathbf{G}(\mathbf{\Gamma})\Big[\exp\big(-iL_0(t-s)\big)\Big(\big[\mathbf{J}(\mathbf{\Gamma})-\mathbf{B}(\mathbf{\Gamma})\big]\cdot\mathbf{F}_e\Big)f_c(\mathbf{\Gamma},\zeta)\Big]\,\mathrm{d}\mathbf{\Gamma}\,\mathrm{d}\zeta\right)\mathrm{d}s\,.\end{aligned} \tag{5.20}$$

The inner integral on the right-hand side of (5.20) can be written as

$$\begin{aligned}&\int \mathbf{G}(\mathbf{\Gamma})\Big[\exp\big(-iL_0(t-s)\big)\Big(\big[\mathbf{J}(\mathbf{\Gamma})-\mathbf{B}(\mathbf{\Gamma})\big]\cdot\mathbf{F}_e\Big)f_c(\mathbf{\Gamma},\zeta)\Big]\,\mathrm{d}\mathbf{\Gamma}\,\mathrm{d}\zeta \;= \\ &\qquad\qquad \int\Big(\big[\mathbf{J}(\mathbf{\Gamma})-\mathbf{B}(\mathbf{\Gamma})\big]\cdot\mathbf{F}_e\Big)f_c(\mathbf{\Gamma},\zeta)\Big[\exp\big(\mathrm{iL}_0(t-s)\big)\mathbf{G}(\mathbf{\Gamma})\Big]\,\mathrm{d}\mathbf{\Gamma}\,\mathrm{d}\zeta\end{aligned} \tag{5.21}$$

by virtue of the identity (3.29) in Chapter 3, where iL_0 is the phase-variable p-Liouvillean of the field-free equations of motion, *i.e.*, equations (5.11) with $\mathbf{F}_e=\mathbf{0}$. Also, $g(\mathbf{\Gamma},0)$ in (3.29) is chosen to be equal to $\big[\mathbf{J}(\mathbf{\Gamma})-\mathbf{B}(\mathbf{\Gamma})\big]\cdot\mathbf{F}_e f_c(\mathbf{\Gamma},\zeta)$. In equation (5.21), $\exp\big(\mathrm{iL}_0(t-s)\big)\mathbf{G}(\mathbf{\Gamma})$ is the value of $\mathbf{G}$ at time $t-s$ starting with an initial value $\mathbf{\Gamma}$ chosen from $\big[\mathbf{J}(\mathbf{\Gamma})-\mathbf{B}(\mathbf{\Gamma})\big]\cdot\mathbf{F}_e f_c(\mathbf{\Gamma},\zeta)$. Introducing the notation $\exp\big(\mathrm{iL}_0(t-s)\big)\mathbf{G}(\mathbf{\Gamma})=\tilde{\mathbf{G}}((t-s)_0;\mathbf{\Gamma})$, where the subscript '0' in $(t-s)_0$ indicates that the propagation is by field-free equations of motion, (5.21) can be rewritten as

$$\begin{aligned}&\int \mathbf{G}(\mathbf{\Gamma})\Big[\exp\big(-iL_0(t-s)\big)\Big(\big[\mathbf{J}(\mathbf{\Gamma})-\mathbf{B}(\mathbf{\Gamma})\big]\cdot\mathbf{F}_e\Big)f_c(\mathbf{\Gamma},\zeta)\Big]\,\mathrm{d}\mathbf{\Gamma}\,\mathrm{d}\zeta \\ &\qquad = \int\Big(\big[\tilde{\mathbf{J}}(\mathbf{0};\mathbf{\Gamma})-\tilde{\mathbf{B}}(\mathbf{0};\mathbf{\Gamma})\big]\cdot\mathbf{F}_e\Big)f_c(\mathbf{\Gamma},\zeta)\tilde{\mathbf{G}}((t-s)_0;\mathbf{\Gamma})\,\mathrm{d}\mathbf{\Gamma}\,\mathrm{d}\zeta \\ &\qquad = \int\Big(\tilde{\mathbf{G}}((t-s)_0;\mathbf{\Gamma})\otimes\big[\tilde{\mathbf{J}}(\mathbf{0};\mathbf{\Gamma})-\tilde{\mathbf{B}}(\mathbf{0};\mathbf{\Gamma})\big]\Big)\mathbf{F}_e f_c(\mathbf{\Gamma},\zeta)\,\mathrm{d}\mathbf{\Gamma}\,\mathrm{d}\zeta \\ &\qquad = \Big(\Big\langle\tilde{\mathbf{G}}((t-s)_0)\otimes\Big[\tilde{\mathbf{J}}(0)-\tilde{\mathbf{B}}(0)\Big]\Big\rangle_c\Big)\mathbf{F}_e\,,\end{aligned} \tag{5.22}$$

where '$\otimes$' denotes tensor product and $\left\langle\tilde{\mathbf{G}}((t-s)_0)\otimes\Big[\tilde{\mathbf{J}}(0)-\tilde{\mathbf{B}}(0)\Big]\right\rangle_c$ is the correlation function of $\mathbf{G}$ and $\mathbf{J}-\mathbf{B}$ with respect to the extended canonical distribution (5.10). Substituting (5.22) into

(5.20), the ensemble average of $\tilde{\mathbf{G}}(t)$ with respect to (5.11) becomes

$$\begin{aligned}\langle\tilde{\mathbf{G}}(t)\rangle &= \langle\tilde{\mathbf{G}}(0)\rangle_c + \beta V\int_0^t\left(\left\langle\tilde{\mathbf{G}}((t-s)_0)\otimes\left[\tilde{\mathbf{J}}(0)-\tilde{\mathbf{B}}(0)\right]\right\rangle_c\right)\mathbf{F}_e \\ &= \langle\tilde{\mathbf{G}}(0)\rangle_c + \beta V\int_0^t\left(\left\langle\tilde{\mathbf{G}}((s)_0)\otimes\left[\tilde{\mathbf{J}}(0)-\tilde{\mathbf{B}}(0)\right]\right\rangle_c\right)\mathbf{F}_e\,.\end{aligned} \tag{5.23}$$

It is noted that, since $\displaystyle\int_0^t\left(\left\langle\tilde{\mathbf{G}}((s)_0)\otimes\left[\tilde{\mathbf{J}}(0)-\tilde{\mathbf{B}}(0)\right]\right\rangle_c\right)$ in (5.23) is independent of $\mathbf{F}_e$, the ensemble average $\langle\tilde{\mathbf{G}}(t)\rangle$ corresponding to (5.11) is linearly dependent on the applied external field $\mathbf{F}_e$, as expected from the linear response theory. Now, the long-time ensemble average of $\tilde{\mathbf{G}}(t)$ can be obtained as

$$\langle\tilde{\mathbf{G}}(\infty)\rangle = \beta V\int_0^\infty\left(\left\langle\tilde{\mathbf{G}}((s)_0)\otimes\left[\tilde{\mathbf{J}}(0)-\tilde{\mathbf{B}}(0)\right]\right\rangle_c\right)\mathbf{F}_e\,. \tag{5.24}$$

Choosing the phase variable $\mathbf{G}$ to be the heat flux vector (3.65), the long time average of the heat flux vector under the perturbed equations of motion is

$$\langle\tilde{\mathbf{J}}_Q(\infty)\rangle = \beta V\int_0^\infty\left(\left\langle\tilde{\mathbf{J}}_Q((s)_0)\otimes\left[\tilde{\mathbf{J}}(0)-\tilde{\mathbf{B}}(0)\right]\right\rangle_c\right)\mathbf{F}_e\,. \tag{5.25}$$

Also, choosing the tensors $\mathbf{C}_i$ and $\mathbf{D}_i$ in (5.11) to be such that vector the $\mathbf{J}-\mathbf{B}$ is equal to the heat flux vector $\mathbf{J}_Q$, then (5.25) can be reduced to

$$\frac{\langle\tilde{\mathbf{J}}_Q(\infty)\rangle}{T} = \left(\frac{V}{k_BT^2}\int_0^\infty\left\langle\tilde{\mathbf{J}}_Q((s)_0)\otimes\tilde{\mathbf{J}}_Q(0)\right\rangle_c\right)\mathbf{F}_e\,. \tag{5.26}$$

Thus, in the linear non-equilibrium steady state, $\dfrac{\langle\tilde{\mathbf{J}}_Q(\infty)\rangle}{T}$ is proportional to the external field $\mathbf{F}_e$ with the constant of proportionality being the Green-Kubo expression for the transport coefficient $\dfrac{\mathbf{L}_{QQ}}{T^2}$ given by (3.18). In other words, the transport coefficient tensor $\dfrac{\mathbf{L}_{QQ}}{T^2}$ can be calculated by using (5.11) and tracking the response of $\dfrac{\langle\tilde{\mathbf{J}}_Q(\infty)\rangle}{T}$ to $\mathbf{F}_e$ rather than calculating the autocorrelation function directly from an equilibrium simulation as in the Green-Kubo method.

To summarize, three conditions need to be satisfied by the equations of motion (5.11), and hence $\mathbf{C}_i$ and $\mathbf{D}_i$, to apply them for the evaluation of the transport coefficient $\dfrac{\mathbf{L}_{QQ}}{T^2}$ using the HNEMD method. These are (i) equivalency of fluxes,

$$\mathbf{J}-\mathbf{B} = \mathbf{J}_Q\,, \tag{5.27}$$

(ii) preservation of zero total momentum,

$$\sum_{i=1}^{N} \mathbf{p}_i \;=\; \mathbf{0}\;, \tag{5.28}$$

and (iii) compatibility with periodic boundary conditions so as to take advantage of quick convergence with respect to system size, as in the Green-Kubo method. It should be mentioned here that the condition given by (5.27) can also be imposed by constructing $\mathbf{C}_i$ and $\mathbf{D}_i$ so that $\mathbf{B} = \mathbf{0}$ and $\mathbf{J} = \mathbf{J}_Q$. As a consequence of this alternative construction, the equations of motion (5.11) satisfy the condition of adiabatic incompressibility of phase space $\mathtt{AI}\Gamma$, as mentioned earlier. The second condition is applied to simplify the calculation of heat flux and the equivalency of fluxes (5.27) and is discussed in the following chapter. In this case, the macroscopic momentum in the heat flux vector (3.65) becomes zero and the instantaneous heat flux vector is of the form

$$\begin{aligned}\tilde{\mathbf{J}}_Q(t) \;=\; \frac{1}{V}\sum_{i_1}\Bigg[E_{i_1}\mathbf{I} + \frac{1}{2!}\sum_{i_2}\mathbf{r}_{i_1 i_2}\otimes\mathbf{F}_{i_1 i_2} + \frac{1}{6!}\sum_{i_2,i_3}[\mathbf{r}_{i_1 i_2}+\mathbf{r}_{i_1 i_3}]\otimes\mathbf{F}_{i_1 i_2 i_3} + \ldots \\ + \frac{1}{M!}\sum_{i_2,\ldots i_M}[\mathbf{r}_{i_1 i_2}+\mathbf{r}_{i_1 i_3}+\ldots+\mathbf{r}_{i_1 i_M}]\otimes\mathbf{F}_{i_1 i_2 \ldots i_M}\Bigg]\frac{\mathbf{p}_{i_1}}{m_i}\end{aligned} \tag{5.29}$$

One of the main contributions in this work is to design $\mathbf{C}_i$ and $\mathbf{D}_i$ systematically so that (5.11) can be employed to obtain the heat transport coefficient materials $\dfrac{\mathbf{L}_{QQ}}{T^2}$ for single or multi-species system modeled by complex many-body potentials. The systematic selection of $\mathbf{C}_i$ and $\mathbf{D}_i$ is presented in the following chapter.

Chapter 6

An Extended HNEMD Method for Single Species Systems

In this chapter, the expressions for the tensor variables $\mathbf{C}_i$ and $\mathbf{D}_i$ in the equations of motion (5.11) consistent with the linear response theory of Chapter 5 are given for systems consisting of single species and modeled by pair, three-body and many-body potentials. The expressions for $\mathbf{C}_i$ and $\mathbf{D}_i$ were initially given by Evans [21] for systems modeled by pair potentials (for example, Argon), however, in an ad-hoc manner. Here, a systematic procedure is outlined to construct $\mathbf{C}_i$ and $\mathbf{D}_i$ for three-body to multi-body potentials by observing the physical similarities of the quantities in the stress tensor and heat flux vector to the expressions for $\mathbf{C}_i$ and $\mathbf{D}_i$ already given in the case of pair potentials. Finally, the HNEMD method is applied to argon and silicon systems by incorporating the algorithm into a software called "Large-scale Atomic/Molecular Massively Parallel Simulator (LAMMPS)" [60].

6.1 Pair Potentials

For single species systems modeled by pair potentials, the total energy H_0 of the molecular system is obtained from (5.2) and (3.36) by putting $M = 2$, and takes the form

$$H_0 \;=\; \sum_{i=1}^{N} \frac{\mathbf{p}_i \cdot \mathbf{p}_i}{2m} + \frac{1}{2!} \sum_{i,j} u_2(\mathbf{r}_i, \mathbf{r}_j) \; . \tag{6.1}$$

Here, m is the mass of the atom corresponding to the single species. The heat flux vector in the state of zero total momentum is obtained from (3.65) as

$$\tilde{\mathbf{J}}_Q(t) \;=\; \frac{1}{V} \sum_i \left[E_i \mathbf{I} + \frac{1}{2!} \sum_j \mathbf{r}_{ij} \otimes \mathbf{F}_{ij} \right] \frac{\mathbf{p}_i}{m} \; . \tag{6.2}$$

The choice of $\mathbf{C}_i$ and $\mathbf{D}_i$ for such systems as given by Evans [24, 21] are

$$\begin{aligned}\mathbf{C}_i\mathbf{F}_e &= \mathbf{0}\,,\\ \mathbf{D}_i\mathbf{F}_e &= \left[(E_i-\bar{E})\mathbf{I}+\frac{1}{2}\sum_j \mathbf{F}_{ij}\otimes\mathbf{r}_{ij}-\frac{1}{2N}\sum_{j,k}\mathbf{F}_{jk}\otimes\mathbf{r}_{jk}\right]\mathbf{F}_e\,.\end{aligned} \tag{6.3}$$

It can be seen that

$$\sum_i \mathbf{D}_i\mathbf{F}_e = \mathbf{0}\,, \tag{6.4}$$

from (6.3), and hence $\overline{\sum_i \dot{\mathbf{p}}_i} = -\zeta\sum_i \mathbf{p}_i$ from (5.11) and (6.4). This implies that, if the initial total momentum is zero, which is usually the case in molecular dynamics simulations, the total momentum is zero at subsequent times. Therefore, the choice of $\mathbf{C}_i$ and $\mathbf{D}_i$ given by (6.3) satisfies the condition of preservation of zero total momentum (5.28). It can also be seen that (6.3) are compatible with PBCs, as atoms that leave the system from one side can enter from the opposite side with the same momentum and forces. Also, the phase space compression factor is given by

$$\begin{aligned}\mathbf{B} &= \frac{1}{\beta V}\left(\sum_{i=1}^{N}\frac{\partial}{\partial\mathbf{r}_i}\cdot\mathbf{C}_i^T+\sum_{i=1}^{N}\frac{\partial}{\partial\mathbf{p}_i}\cdot\mathbf{D}_i^T\right)\,,\\ &= \frac{1}{\beta V}\left(\sum_{i=1}^{N}\frac{\mathbf{p}_i}{m}\right)\frac{N-1}{N}\,,\\ &= \mathbf{0}\,,\end{aligned} \tag{6.5}$$

hence satisfyies the condition of adiabatic incompressibility of phase space $\mathtt{AI}\Gamma$. The dissipative flux

$$\begin{aligned}\mathbf{J} &= \frac{1}{V}\left(\sum_{i=1}^{N}{\mathbf{D}_i}^T\frac{\mathbf{p}_i}{m}-\sum_{i=1}^{N}{\mathbf{C}_i}^T\mathbf{F}_i\right)\\ &= \frac{1}{V}\left[\sum_i E_i\mathbf{I}+\frac{1}{2}\sum_j\mathbf{r}_{ij}\otimes\mathbf{F}_{ij}\right]\frac{\mathbf{p}_i}{m}-\left[\bar{E}\mathbf{I}+\frac{1}{2N}\sum_{j,k}\mathbf{r}_{jk}\otimes\mathbf{F}_{jk}\right]\left(\sum_i\frac{\mathbf{p}_i}{m_i}\right)\\ &= \mathbf{J}_Q\,,\end{aligned} \tag{6.6}$$

where the third equality in (6.6) is obtained by using the preservation of total momentum condition, and hence $\mathbf{J}-\mathbf{B}=\mathbf{J}_Q$. Therefore, all the three conditions, (5.27), (5.28) and compatibility with PBCs, described at the end of Section 5.2 are satisfied by (6.3) making them an ideal choice to apply the HNEMD method for systems modeled by pair potentials. A scalar heat conduction

coefficient κ is estimated by setting $\mathbf{F}_e = (0, 0, F_{ez})$. In this case, (5.26) reduces to

$$\frac{\langle \tilde{J}_{Qz}(\infty) \rangle}{VT} \;=\; \left(\frac{1}{Vk_BT^2} \int_0^\infty \langle \tilde{J}_{Qz}((s)_0) \tilde{J}_{Qz}(0) \rangle_c \, \mathrm{d}s \right) F_{ez} \;=\; \kappa F_{ez} \,. \tag{6.7}$$

The equations of motion (5.11) with the NH thermostat are integrated by the operator split method, as described in Appendix A. The following three methods are considered to deduce the thermal conductivity from estimates of $\langle \tilde{J}_{Qz}(\infty) \rangle$ corresponding to a set of force fields $\{F_{ez,j},\, j = 1, \ldots, n\}$:

1. *Linear extrapolation*: This is the approach used in [21], where a least squares fit of the function $\kappa + mF_{ez}$ to $\kappa_j = \dfrac{\left\langle \tilde{J}_{Qz,j}(\infty) \right\rangle}{VTF_{ez,j}}$ vs. $F_{ez,j}$ is extrapolated to $F_{ez} = 0$ to determine a value for the thermal conductivity κ. The variance in the intercept $\sigma_\kappa^2 = \dfrac{\sigma^2}{\Delta} \displaystyle\sum_{j=1}^{n} F_{ez,j}$ is used to estimate the error, with $\sigma^2 = \dfrac{1}{n-2} \displaystyle\sum_{j=1}^{n} \left(\kappa_j - \kappa - mF_{ez,j}\right)^2$ being the fit error and $\Delta = n \displaystyle\sum_{j=1}^{n} \big(F_{ez,j}\big)^2 - \big(\sum_{j=1}^{n} F_{ez,j}\big)^2$ and n being the number of samples, see [6].

2. *Gradient*: In this method, the slope of a least squares fit of the function κF_{ez} to $\dfrac{\langle \tilde{J}_{Qz,j}(\infty) \rangle}{TV}$ vs. $F_{ez,j}$ in (6.7) is identified as the thermal conductivity. A zero intercept, *i.e.*, $\lim\limits_{F_{ez} \to 0} J_{Qz} = 0$, is assumed. The error in the slope is estimated via $\sigma_\kappa^2 = \dfrac{\sigma^2}{\Delta} n$ where, again, σ^2 is the fit error and Δ is the variance of $F_{ez,j}$, see [6].

3. *Mean*: Here, the conductivity is taken to be the average over κ_j, namely $\kappa = \dfrac{1}{n} \displaystyle\sum_{j=1}^{n} \kappa_j$, and the error is estimated by $\sigma_\kappa^2 = \dfrac{1}{n} \dfrac{1}{n-1} \displaystyle\sum_{j=1}^{n} \left(\kappa_j - \kappa\right)^2$, see [6].

The HNEMD algorithm is incorporated into a software called LAMMPS. LAMMPS is a parallelizable molecular dynamics software which has all the basic subroutines, such as finding neighbor lists, time stepping, force calculation, *etc.*, that are needed for running a molecular dynamics simulation. The HNEMD algorithm is written as a separate subroutine and is then integrated with LAMMPS.

6.1.1 Argon using the Lennard-Jones Potential

As an initial test, the algorithm is applied to an argon system at its triple point (86.5 K, 5.719 Å) using a Lennard-Jones (LJ) pair potential with 256 atoms in an FCC lattice and a time step-size of $4.0\,fs$ for about 10^6 time steps. Lennard-Jones is a pair potential, where the two-body term u_2 in (3.32) is of the form

$$u_2(\mathbf{r}_i, \mathbf{r}_j) \;=\; 4\varepsilon_{ij}\left[\left(\frac{\sigma_{ij}}{r_ij}\right)^6 - \left(\frac{\sigma_{ij}}{r_ij}\right)^{12}\right], \tag{6.8}$$

where $r_{ij} = \|\mathbf{r}_i - \mathbf{r}_j\|$ is the distance between atoms i and j, ε_{ij} is the depth of the potential energy well, σ_{ij} is the distance at which the interaction potential between two particles is zero. The parameters ε_{ij} and σ_{ij} depend on the type of atoms i and j. For argon, $\varepsilon_{ij} = 1.6539 \times 10^{-21}\,J$ and $\sigma_{ij} = 3.405\,\mathring{A}$ [65], and the cut-off distance for the potential is $r_c = 13\,\mathring{A}$. Figure 6.1 shows the variation of κ_j with the external field $F_{ez,j}$. It is observed that there exists a finite range $0.04\,\mathring{A}^{-1} < F_{ez} < 0.1\,\mathring{A}^{-1}$, in which κ_j is essentially independent of F_{ez}. Outside this range, there is strong dependence of κ_j on F_{ez} and the linear response theory is not applicable. The thermal conductivity obtained by the extrapolation method using the estimates in the range of validity of the linear response theory is found to be $0.126 \pm 0.001\,W/mK$, where the experimental result is $0.126\,W/mK$. The results in Table 6.1 show that this method can also be applied to calculate the thermal conductivity at different temperatures and volumetric deformations yielding results comparable to those obtained using the Green-Kubo method, see, *e.g.*, [33].

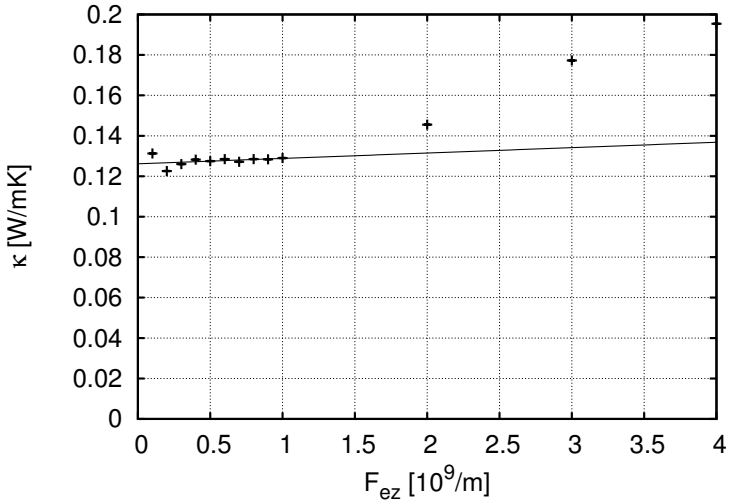

Figure 6.1: *Variation of thermal conductivity $\kappa(F_{ez})$ with F_{ez} for argon at its triple point. The intercept at $F_{ez} = 0$ is the estimate of the true thermal conductivity κ. Note that the errors in the estimates for smaller F_{ez} are small enough to make the error bars indistinguishable.*

Interatomic distance ($\mathring{A}$)	Temperature (K)	HNEMD κ (W/mK)	GK κ (W/mK)
5.376	10	1.97	1.91
5.376	20	0.86	0.95
5.376	30	0.60	0.63
5.376	50	0.37	0.39
5.719	86.5	0.13	0.13

Table 6.1: *Comparison of thermal conductivity (κ) of argon at triple point obtained by the HNEMD and GK methods at different temperatures and fictitious volumetric deformations*

6.2 Three-body Potentials

As mentioned earlier, the expressions for $\mathbf{C}_i$ and $\mathbf{D}_i$ have not been obtained systematically for systems until now modeled by pair potentials. Hence, it becomes difficult to construct $\mathbf{C}_i$ and $\mathbf{D}_i$ for higher-order potentials. In this section, similarities between the heat flux vector $\mathbf{J}_Q$ given by (3.65), stress tensor $\mathbf{T}$ given by (3.64), and $\mathbf{C}_i$ and $\mathbf{D}_i$ for pair potentials are carefully observed so as to be able to construct $\mathbf{C}_i$ and $\mathbf{D}_i$ that satisfy the three conditions of the linear response theory for systems modeled by three-body potentials.

The choice of $\mathbf{C}_i$ and $\mathbf{D}_i$ for pair potentials (6.3) can be rewritten as

$$\begin{aligned} \mathbf{C}_i\mathbf{F}_e &= \mathbf{0}\,, \\ \mathbf{D}_i\mathbf{F}_e &= \left(E_i\mathbf{I} + \frac{1}{2}\sum_j \mathbf{F}_{ij}\otimes\mathbf{r}_{ij}\right)\mathbf{F}_e - \left(\bar{E}\mathbf{I} - \frac{1}{2N}\sum_{j,k}\mathbf{F}_{jk}\otimes\mathbf{r}_{jk}\right)\mathbf{F}_e\,. \end{aligned} \tag{6.9}$$

The term $(E_i - \bar{E})\mathbf{F}_e$ in (6.9) implies that a heat current is induced by driving the particles with energy E_i greater (respectively, smaller) than the average energy $\bar{E}$ in the direction (respectively, against the direction) of the external field $\mathbf{F}_e$. The term $\frac{1}{2}\sum_j(\mathbf{F}_{ij}\otimes\mathbf{r}_{ij})\mathbf{F}_e$ implies that the heat current is also driven based on the deviation of the virial part of the stress tensor of atom i (3.54) from the average stress. It can also be observed that the tensor $\mathbf{D}_i$ coupled to the external field $\mathbf{F}_e$ also appears in the heat flux vector given by (6.2) which also says that heat flux is driven in a general system based on the energy and virial stress tensor of individual atom i. With the observations in place, one may write the expressions for $\mathbf{C}_i$ and $\mathbf{D}_i$ for systems modeled using three-body potentials by incorporating the three body terms corresponding to energy E_i and virial stress $\mathbf{T}_V$ in $\mathbf{D}_i$. Specifically, the expressions for $\mathbf{C}_i$ and $\mathbf{D}_i$ for the case of three-body potentials

take the form

$$\begin{aligned}
\mathbf{C}_i\mathbf{F}_e &= \mathbf{0}\,, \\
\mathbf{D}_i\mathbf{F}_e &= \left(E_i\mathbf{I} + \frac{1}{2}\sum_j \mathbf{F}_{ij}\otimes\mathbf{r}_{ij} + \frac{1}{3!}\sum_{j,k}\mathbf{F}_{ijk}\otimes[\mathbf{r}_{ij}+\mathbf{r}_{ik}]\right)\mathbf{F}_e \\
&\quad - \left(\bar{E}\mathbf{I} - \frac{1}{2N}\sum_{j,k}\mathbf{F}_{jk}\otimes\mathbf{r}_{jk} + \frac{1}{3!N}\sum_{i,j,k}\mathbf{F}_{ijk}\otimes[\mathbf{r}_{ij}+\mathbf{r}_{ik}]\right)\mathbf{F}_e\,.
\end{aligned} \tag{6.10}$$

Again, it can be seen that $\sum_i \mathbf{D}_i\mathbf{F}_e = \mathbf{0}$ from (6.10) and hence $\overline{\sum_i \dot{\mathbf{p}}_i} = -\zeta\sum_i \mathbf{p}_i$. If the total initial momentum is zero, the total momentum is zero for all subsequent times. Hence, (6.10) satisfies the preservation of total momentum condition (5.28). It should be noted here that the averages in (6.10) need to be subtracted in order to satisfy the condition of zero total momentum. It can also be seen that (6.10) are compatible with periodic boundary conditions, as atoms that leave the system from one side can enter it again from the opposite side with the same momentum and forces. Finally, for this choice of $\mathbf{C}_i$ and $\mathbf{D}_i$ for the three-body potentials, it follows from (5.17) that

$$\mathbf{B} = \mathbf{0}\,. \tag{6.11}$$

Therefore, the condition of adiabatic incompressibility of phase space $\mathtt{AI}\Gamma$ is satisfied. Also, the dissipative flux $\mathbf{J}$ can be obtained using (6.10) as

$$\begin{aligned}
\mathbf{J} &= \frac{1}{V}\left(\sum_{i=1}^{N}\mathbf{D}_i{}^T\frac{\mathbf{p}_i}{m_i} - \sum_{i=1}^{N}\mathbf{C}_i{}^T\mathbf{F}_i\right) \\
&= \frac{1}{V}\sum_i\left(E_i\mathbf{I} + \frac{1}{2}\sum_j\mathbf{r}_{ij}\otimes\mathbf{F}_{ij} + \frac{1}{3!}\sum_{j,k}[\mathbf{r}_{ij}+\mathbf{r}_{ik}]\otimes\mathbf{F}_{ijk}\right)\frac{\mathbf{p}_i}{m_i} \\
&\quad - \frac{1}{V}\left(\bar{E}\mathbf{I} - \frac{1}{2N}\sum_{j,k}\mathbf{r}_{jk}\otimes\mathbf{F}_{jk} + \frac{1}{3!N}\sum_{i,j,k}[\mathbf{r}_{ij}+\mathbf{r}_{ik}]\otimes\mathbf{F}_{ijk}\right)\left(\sum_i\frac{\mathbf{p}_i}{m_i}\right) \\
&= \mathbf{J}_Q\,,
\end{aligned} \tag{6.12}$$

where the third equality is obtained by using the condition of zero total momentum (5.28). Hence, $\mathbf{J}-\mathbf{B} = \mathbf{J}_Q$ and therefore all the three conditions imposed in Chapter 5 are satisfied. The linear response theory then implies that the long-time ensemble average of heat-flux vector $\mathbf{J}_Q$ under the application of the external field $\mathbf{F}_e$ is given by (5.26) and the constant of proportionality which is the thermal conductivity tensor $\boldsymbol{\kappa}$ (equivalent to $\dfrac{\mathbf{L}_{QQ}}{T^2}$ for systems consisting of single species) is obtained by tracking the (linear) dependence of $\dfrac{\langle\tilde{\mathbf{J}}_Q(\infty)\rangle}{T}$ on $\mathbf{F}_e$.

6.2.1 Silicon using the Stillinger-Weber Potential

As a test case, the HNEMD algorithm developed for three-body potentials is applied to bulk silicon (diamond crystal structure) modeled by Stillinger-Weber (SW) potential [68] consisting of both two-body and three-body terms since it is widely accepted that elastic constants, phonon dispersion curves and thermal expansion coefficients can be accurately modeled using this potential, see, *e.g.*, [37, 7, 13, 34]. The two-body and three-body terms in the SW potential are of the form

$$\begin{aligned} u_2(\mathbf{r}_i, \mathbf{r}_j) &= \varepsilon f_2\left(\frac{r_{ij}}{\sigma}\right), \\ u_3(\mathbf{r}_i, \mathbf{r}_j, \mathbf{r}_k) &= \varepsilon f_3\left(\frac{\mathbf{r}_i}{\sigma}, \frac{\mathbf{r}_j}{\sigma}, \frac{\mathbf{r}_k}{\sigma}\right), \end{aligned} \tag{6.13}$$

respectively. Here, the functions f_2 and f_3 are given by

$$f_2\left(\frac{r_{ij}}{\sigma}\right) = \begin{cases} A\left(B\left(\frac{r_{ij}}{\sigma}\right)^{-p} - \left(\frac{r_{ij}}{\sigma}\right)^{-q}\right) \exp\left[\left(\left(\frac{r_{ij}}{\sigma}\right) - a\right)^{-1}\right] & \text{for } \left(\frac{r_{ij}}{\sigma}\right) < a \\ 0 & \text{for } \left(\frac{r_{ij}}{\sigma}\right) \geq a \end{cases} \tag{6.14}$$

and

$$f_3\left(\frac{\mathbf{r}_i}{\sigma}, \frac{\mathbf{r}_j}{\sigma}, \frac{\mathbf{r}_k}{\sigma}\right) = h\left(\frac{r_{ij}}{\sigma}, \frac{r_{ik}}{\sigma}, \theta_{jik}\right) + h\left(\frac{r_{ji}}{\sigma}, \frac{r_{jk}}{\sigma}, \theta_{ijk}\right) + h\left(\frac{r_{ki}}{\sigma}, \frac{r_{kj}}{\sigma}, \theta_{ikj}\right), \tag{6.15}$$

respectively, where

$$h\left(\frac{r_{ij}}{\sigma}, \frac{r_{ik}}{\sigma}, \theta_{jik}\right) = \lambda \exp\left[\gamma\left(\left(\frac{r_{ij}}{\sigma}\right) - a\right)^{-1} + \gamma\left(\left(\frac{r_{ik}}{\sigma}\right) - a\right)^{-1}\right] \cos\left(\theta_{jik} + \frac{1}{3}\right)^2, \tag{6.16}$$

and θ_{jik} is the angle between $\mathbf{r}_j$ and $\mathbf{r}_k$ subtended at $\mathbf{r}_i$ [68]. The parameter set in the SW potential for silicon is given by

$$\begin{aligned} &A = 7.049\,, B = 0.602\,, \\ &p = 4\,, q = 0\,, a = 1.80\,, \\ &\lambda = 21.0\,, \gamma = 1.20\,, \\ &\sigma = 0.209 \text{ nm}\,, \varepsilon = 50 \text{ kcal/mol}\,, \end{aligned}$$

see [68].

Applying the HNEMD method to bulk silicon (1000 K, 5.43 Å), a sequence of simulations is performed using the Stillinger-Weber potential with 1728 atoms in a diamond cubic lattice for about 4 million time steps, each of size $0.55\,fs$. The system is chosen large enough to be free

of the size effects noted for the GK method in [67]. It is concluded from Figure 6.2 that linear response theory is valid for $0.3 \times 10^{-4}\,\mathring{A}^{-1} < F_{ez} < 2 \times 10^{-4}\,\mathring{A}^{-1}$. Since the external field

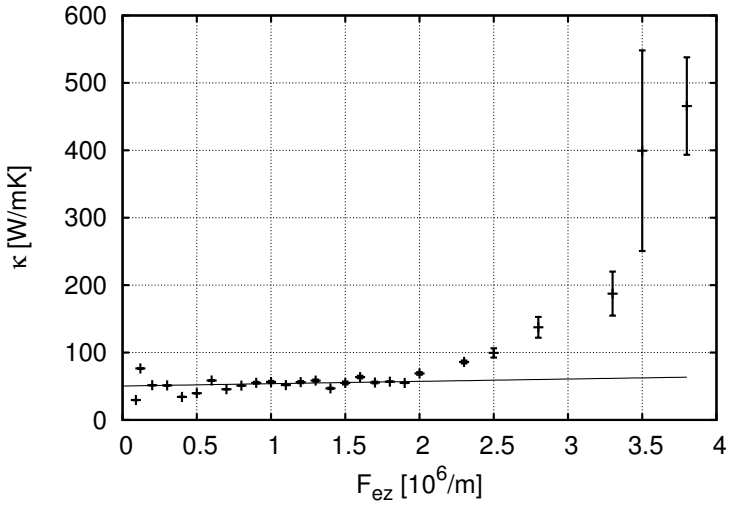

Figure 6.2: *Variation of thermal conductivity $\kappa(F_{ez})$ with F_{ez} for silicon system at $T = 1000\,K$. The intercept at $F_{ez} = 0$ is the estimate of the true thermal conductivity κ. Note that the errors in the estimates for smaller F_{ez} are small enough to make the error bars indistinguishable.*

is applied only along the z-direction, it is expected for the diamond cubic system that the average heat fluxes $\langle \tilde{J}_{Qx}(\infty) \rangle$ and $\langle \tilde{J}_{Qy}(\infty) \rangle$ in the x and y directions approach zero respectively, as shown in Figure 6.3. The value of thermal conductivity obtained by linear extrapolation to $F_{ez} \to 0$ is $50 \pm 4\,W/mK$, which is lower than but consistent with the Green-Kubo result $66 \pm 16\,W/mK$ and the direct method result $65 \pm 16\,W/mK$ [67]. The gradient method gives a conductivity estimate of $55 \pm 2\,W/mK$, see Figure 6.4. On the other hand, the mean of values in the range $0.3 \times 10^{-4}\,\mathring{A}^{-1} < F_{ez} < 1 \times 10^{-4}\,\mathring{A}^{-1}$ gives a conductivity estimate in the range $53 \pm 2\,W/mK$, see Figure 6.2. Hence, all the three approaches for evaluating κ from the HNEMD method yield consistent results.

To quantify the significance of three-body terms on deducing thermal conductivity, the simulations were repeated with only two-body terms included in the equations of motion (5.11) and (6.10), as well as in the heat flux vector $\mathbf{J}_Q(\mathbf{\Gamma})$ of (3.65). A regime of F_{ez} was found where the linear response theory is valid, as shown in Figure 6.5. The values of thermal conductivity from both the gradient and mean methods were found to be $26 \pm 1\,W/mK$ which is approximately half of the respective values obtained from simulations including three-body terms, see Figure 6.6. This clearly demonstrates the significance of the three-body terms in the equations of motion and the heat flux vector when estimating the thermal conductivity of silicon, as these ensure that the diamond crystal structure is the most stable periodic arrangement of particles [68].

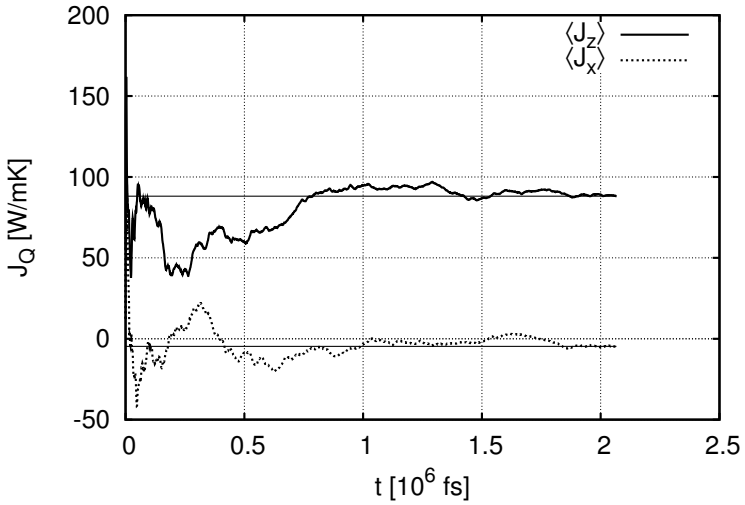

Figure 6.3: *The running average of components of the heat flux* $\mathbf{J}_Q$ *in the* x *and* z *directions for the silicon system in the non-equilibrium steady state with* $F_{ez} = 8 \times 10^{-5} \mathring{A}^{-1}$*. Note that the* y *direction is omitted for clarity.*

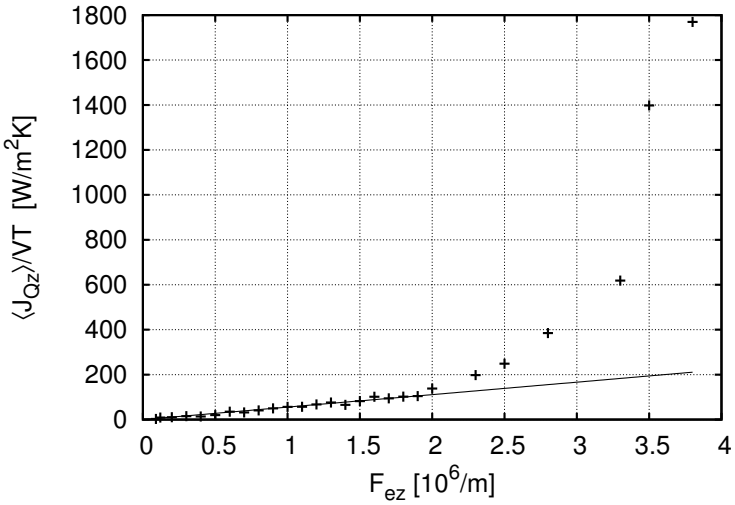

Figure 6.4: *Heat flux* J_z *as a function of* F_{ez} *used to obtain the thermal conductivity of a silicon system at* $T = 1000\,K$ *via the gradient method. It is assumed that the linear fit passes through the origin.*

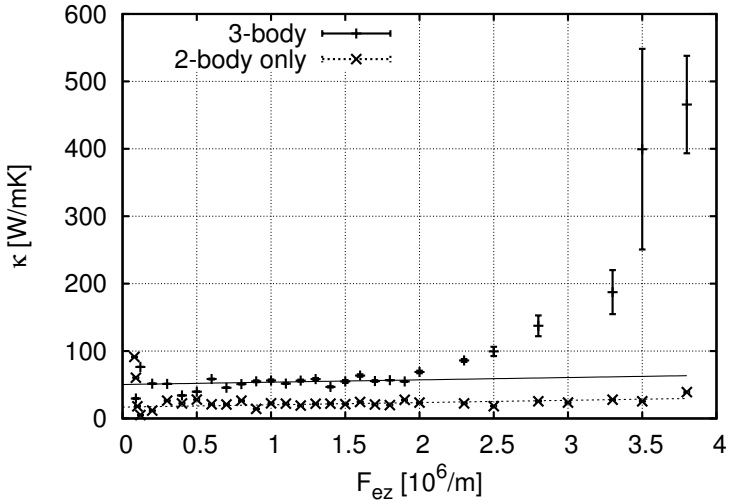

Figure 6.5: *Comparison of thermal conductivity $\kappa(F_{ez})$ variation with F_{ez} for silicon at T=1000K. The intercept at $F_{ez} = 0$ is the estimate of the true thermal conductivity κ. The method using the full heat flux and fictitious force is compared with the same method using only the two-body terms.*

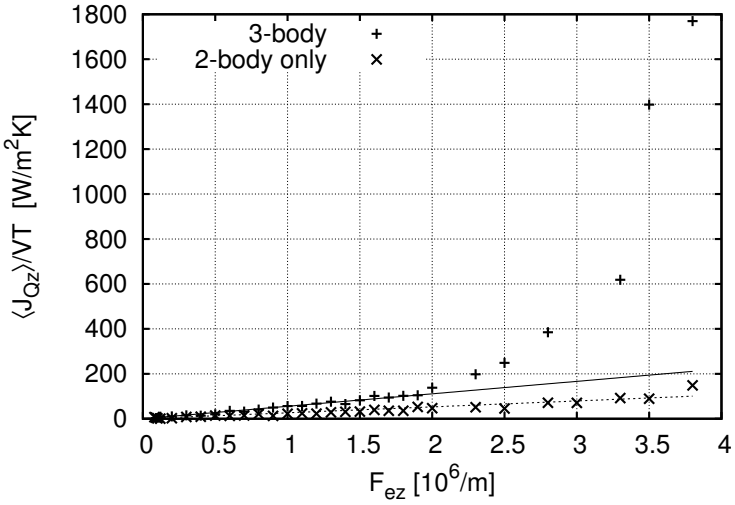

Figure 6.6: *Comparison of heat flux J_z estimates for silicon at T=1000K using the gradient method. The method using the full heat flux and fictitious force is compared with the same method using only the two body terms.*

6.3 Multi-body potentials

In this section, expressions for $\mathbf{C}_i$ and $\mathbf{D}_i$ are given for systems modeled by multi-body potentials (any M in (3.32)) [45]. Multi-body potentials with $M = 4$ (dihedral angles and torsion) are important in describing the surface and cluster phases of silicon [53]. Also, multi-body potentials are used to model many metals [16, 17].

The complex part of deriving the expressions for $\mathbf{C}_i$ and $\mathbf{D}_i$ is obtaining the expressions for stress and heat flux in the case of multi-body potentials, which have already been derived in Chapter 3, see (3.64) and (3.65). The equation for the heat flux with zero total momentum is given by

$$\begin{aligned}\tilde{\mathbf{J}}_Q(t) \;=\; \frac{1}{V}\sum_{i_1}\Bigg[E_{i_1}\mathbf{I} + \frac{1}{2!}\sum_{i_2}\mathbf{r}_{i_1i_2}\otimes\mathbf{F}_{i_1i_2} + \frac{1}{6!}\sum_{i_2,i_3}[\mathbf{r}_{i_1i_2}+\mathbf{r}_{i_1i_3}]\otimes\mathbf{F}_{i_1i_2i_3} + \ldots \\ + \frac{1}{M!}\sum_{i_2,\ldots i_M}[\mathbf{r}_{i_1i_2}+\mathbf{r}_{i_1i_3}+\ldots+\mathbf{r}_{i_1i_M}]\otimes\mathbf{F}_{i_1i_2\ldots i_M}\Bigg]\frac{\mathbf{p}_{i_1}}{m}\end{aligned} \tag{6.17}$$

Again, noting the relation between the heat-flux vector, stress tensor and $\mathbf{C}_i$ and $\mathbf{D}_i$, in analogy to the case of three body potentials, the expressions for $\mathbf{C}_i$ and $\mathbf{D}_i$ for multi-body potentials are proposed by taking in to the multi-body terms in E_i and the virial stress $\mathbf{T}_V$ as

$$\begin{aligned}\mathbf{C}_i\mathbf{F}_e \;&=\; \mathbf{0}\,,\\ \mathbf{D}_i\mathbf{F}_e \;&=\; \Bigg(E_i\mathbf{I} + \frac{1}{2!}\sum_{i_2}\mathbf{F}_{ii_2}\otimes\mathbf{r}_{ii_2} + \frac{1}{3!}\sum_{i_2,i_3}\mathbf{F}_{ii_2i_3}\otimes[\mathbf{r}_{ii_2}+\mathbf{r}_{ii_3}] + \ldots \\ &\quad + \frac{1}{M!}\sum_{i_2,\ldots,i_M}\mathbf{F}_{ii_2\ldots i_M}\otimes[\mathbf{r}_{ii_2}+\ldots+\mathbf{r}_{ii_M}]\Bigg)\mathbf{F}_e - \Bigg(\bar{E}\mathbf{I} - \frac{1}{2!N}\sum_{i_1,i_2}\mathbf{F}_{i_1i_2}\otimes\mathbf{r}_{i_1i_2} + \\ &\qquad + \frac{1}{3!N}\sum_{i_1,i_2,i_3}\mathbf{F}_{i_1i_2i_3}\otimes[\mathbf{r}_{i_1i_2}+\mathbf{r}_{i_1i_3}] + \ldots \\ &\qquad + \frac{1}{M!N}\sum_{i_1,i_2,\ldots,i_M}\mathbf{F}_{i_1i_2\ldots i_M}\otimes[\mathbf{r}_{i_1i_2}+\ldots+\mathbf{r}_{i_1i_M}]\Bigg)\mathbf{F}_e\,.\end{aligned} \tag{6.18}$$

It can be seen that this choice satisfies the zero total momentum preservation and is compatible with PBCs, as the atoms that leave the system from one side can enter it again from opposite side with the same momentum and forces. The phase space compression factor for this choice is

$$\mathbf{B} \;=\; \frac{1}{\beta V}\left(\sum_{i=1}^{N}\frac{\mathbf{p}_i}{m}\right)\frac{N-1}{N} \;=\; \mathbf{0}\,, \tag{6.19}$$

and the dissipative flux is obtained as

$$\begin{aligned}
\mathbf{J} &= \frac{1}{V}\sum_i \mathbf{D}_i{}^T\frac{\mathbf{p}_i}{m} - \sum_i \mathbf{C}_i{}^T\mathbf{F}_i \\
&= \frac{1}{V}\sum_i \Bigg[E_i\mathbf{I} + \frac{1}{2!}\sum_{i_2}\mathbf{r}_{ii_2}\otimes\mathbf{F}_{ii_2} + \frac{1}{3!}\sum_{i_2,i_3}(\mathbf{r}_{ii_2}+\mathbf{r}_{ii_3})\otimes\mathbf{F}_{ii_2i_3} + \ldots + \\
&\frac{1}{M!}\sum_{i_2,\ldots,i_M}(\mathbf{r}_{ii_2}+\ldots+\mathbf{r}_{ii_M})\otimes\mathbf{F}_{ii_2\ldots i_M}\Bigg]\frac{\mathbf{p}_i}{m} - \frac{1}{V}\Bigg[\bar{E} + \frac{1}{2!N}\sum_{i_1,i_2}\mathbf{r}_{i_1i_2}\otimes\mathbf{F}_{i_1i_2} + \\
&\frac{1}{3!N}\sum_{i_1,i_2,i_3}(\mathbf{r}_{i_1i_2}+\mathbf{r}_{i_1i_3})\otimes\mathbf{F}_{i_1i_2i_3} + \frac{1}{M!N}\sum_{i_1,i_2\ldots,i_M}(\mathbf{r}_{i_1i_2}+\ldots+\mathbf{r}_{i_1i_M})\otimes\mathbf{F}_{i_1i_2\ldots i_M}\Bigg]\left(\sum_i\frac{\mathbf{p}_i}{m}\right), \\
&= \mathbf{J}_Q\ ,
\end{aligned} \tag{6.20}$$

where the second equality is obtained by substituting (6.18), the third equality is obtained by observing that the total momentum is zero. Hence, (6.18) satisfies all the three conditions that are required for the application of the linear response theory in Chapter 5 and hence (6.18) with (5.11) may be used to obtain the thermal conductivity estimate. In the preceding derivations, it is important to note that the tensor variable $\mathbf{C}_i$ coupled with the momenta is always zero. However, $\mathbf{C}_i\mathbf{F}_e = \mathbf{0}$ need not be true in general, which is shown in the following chapter in which the equations of motion (5.11) are obtained for systems containing different species capable of diffusion, heat transport and cross effects.

6.4 Discussion

The HNEMD method for silicon requires 1-2 million time steps to obtain the thermal conductivity from a heat-flux average that is converged to within statistical uncertainties. This is a small number relative to the GK method, which requires on the order of 20-30 million time steps to reach a comparable confidence interval. In terms of CPU time, the HNEMD method requires approximately 30 hours, where as the Green-Kubo method requires on the order of 150-200 hours. This is because the GK method relies on the integration of heat flux autocorrelation functions with long decay times, where the tail might not be calculated accurately, as discussed in Chapter 4. One way to avoid long simulation times in GK method is to approximate the decay of the autocorrelation function with exponential curves. However, it is shown in [67] that exponential curves do not correctly represent the long-time decay of the autocorrelation function. Since the HNEMD method estimates the average $\langle\tilde{J}_{Qz}(\infty)\rangle$ for a range of F_{ez}, it eschews errors related to autocorrelation calculations.

The HNEMD method has two potential shortcomings. First, it requires simulations for multiple

values of F_{ez} in order to identify the range of the linear response theory. This is alleviated by the fact that such simulations are independent of each other and can be performed in parallel. Second, the method is inefficient for extremely small values of F_{ez}. In this range, the system is very close to the equilibrium state and the effect of the external force field on the system becomes comparable to the system at equilibrium. Therefore, $\langle \tilde{J}_{Qz}(\infty) \rangle$ approaches zero making it difficult to estimate the ratio $\frac{\langle \tilde{J}_{Qz}(\infty) \rangle}{TF_{ez}}$ as F_{ez} approaches zero, see Figure 6.7. Hence, it is important to determine a

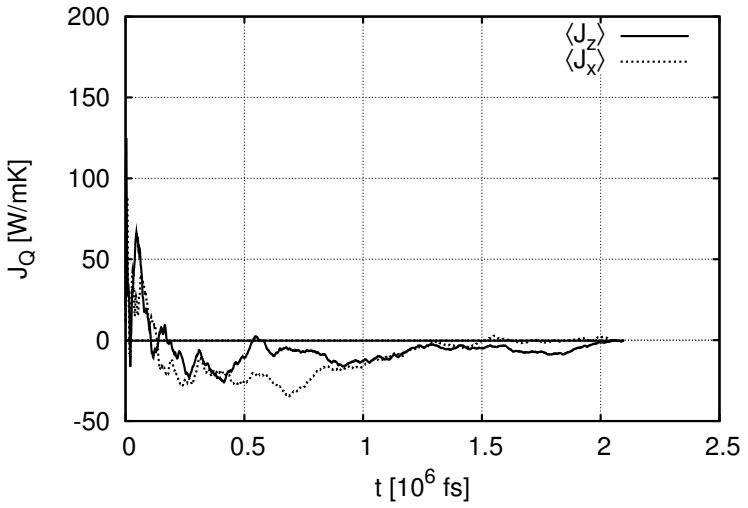

Figure 6.7: *The running average of components of the heat flux* $\mathbf{J}_Q$ *for the silicon system in the non-equilibrium steady state with* $F_{ez} = 1 \times 10^{-5} \mathring{A}^{-1}$.

range of F_{ez} that is large enough to obtain reasonable values of $\frac{\langle \tilde{J}_{Qz}(\infty) \rangle}{TF_{ez}}$ and small enough for the system to be in the linear non-equilibrium range.

The kinetic theory of gases can be employed to estimate the linear response range of a system to the external perturbation F_{ez}. It is known for the case of gases that Fourier's Law ($\mathbf{J}_Q = -\boldsymbol{\kappa} \nabla T$) is valid when the relative variation of temperature is small within a length equal to the mean-free path φ (defined as the average distance that the particle travels before colliding an other particle) [9, 62], namely

$$\varphi \frac{|\nabla T|}{T} \ll 1 \,. \tag{6.21}$$

Assuming that silicon at 1000K is a gas of phonons, (6.21) can be employed with φ being the *phonon* mean-free path. In the linear range, it can be seen from (6.7) and Fourier's law that the effect of external field F_{ez} is identical to that of a logarithmic temperature gradient, *i.e.*, $F_{ez} = \dfrac{\partial \ln T}{\partial z} = \dfrac{1}{T} \dfrac{\partial T}{\partial z}$. Therefore, appealing to (6.21), it is concluded that if the system is in

the linear range, then $F_{ez} \ll \frac{1}{\varphi}$. Hence, for silicon $F_{ez} \ll 0.0015\,\mathring{A}^{-1}$, since the phonon mean-free path of Si at 1000K is estimated from the kinetic theory to be 600 Å, see [67]. In fact, it can be observed from Figure 6.2 that the linear range of F_{ez} is approximately $1/100$ to $1/10$ of $0.0015\mathring{A}^{-1}$. It follows that the number of simulations that must be performed for different F_{ez} to obtain a reliable conductivity estimate with the HNEMD method can be significantly reduced. At a minimum, the proposed extrapolation method requires only two conductivity estimates, whereas the gradient method requires a single flux measurement in the linear range since zero flux at zero F_{ez} is assumed at the outset. The estimation of conductivity by the mean method can be also potentially accomplished with a single measurement, but it is more sensitive than the gradient method to the accurate knowledge of the lower limit of the linear range.

Chapter 7

A New HNEMD Method for Multiple Species Systems

The HNEMD equations of motion and specifically the tensors $\mathbf{C}_i$ and $\mathbf{D}_i$, developed in Chapter 6 are suitable for systems consisting of a single species, since they yield the transport coefficient $\frac{\mathbf{L}_{QQ}}{T^2}$ without requiring the calculation of any average quantities from equilibrium simulations. If these HNEMD equations of motion are employed for multi-species systems, *e.g.*, a semi-conductor gallium-nitride (GaN) system [72, 71], the long-time average of the heat flux vector $\mathbf{J}_Q$ still remains proportional to the external field. However, the constant of proportionality is not just equal to the heat transport coefficient, but involves additional correlation integrals, since the HNEMD equations do not satisfy the condition of equivalence of fluxes (5.27), as in the case of single-species systems, which is shown in the following section. Hence, these correlation integrals need to be evaluated from an equilibrium simulation in addition to running the HNEMD algorithm. An earlier attempt to obtain non-equilibrium equations of motion specifically tailored to multi-species also requires equilibrium MD simulations in addition to running the non-equilibrium algorithm as equivalency of fluxes condition is not satisfied [22]. In this chapter, the deficiency of the HNEMD method leading to additional correlation functions is shown preceding the development of M-HNEMD method. Also, expressions for $\mathbf{C}_i$ and $\mathbf{D}_i$ are developed to obtain the heat transport coefficient for multi-species systems without resorting to additional equilibrium simulations. The resulting method is termed as the Mixture-HNEMD (M-HNEMD) method.

7.1 Thermal Conductivity Estimation by the HNEMD method

In this section, it is shown that the original HNEMD method [21, 45] is not consistent for mixtures and alloys due to the non-equivalency of the fluxes $\mathbf{J}-\mathbf{B}$ and $\mathbf{J}_Q$ (*i.e.*, $\mathbf{J}-\mathbf{B} \neq \mathbf{J}_Q$). To appreciate this point, recall that $\mathbf{C}_i$ and $\mathbf{D}_i$ in the original HNEMD equations of motion [45] are given in the

form

$$\mathbf{C}_i \;=\; \mathbf{0} \quad , \quad \mathbf{D}_i \;=\; \boldsymbol{\nu}_i - \frac{1}{N}\sum_{j=1}^{N}\boldsymbol{\nu}_j \;, \tag{7.1}$$

where

$$\boldsymbol{\nu}_i \;=\; E_i\mathbf{I} + \frac{1}{2!}\sum_{i_2}\mathbf{F}_{ii_2}\otimes\mathbf{r}_{ii_2} + \frac{1}{3!}\sum_{i_2,i_3}\mathbf{F}_{ii_2i_3}\otimes(\mathbf{r}_{ii_2}+\mathbf{r}_{ii_3}) + \\ \ldots + \frac{1}{M!}\sum_{i_2,\ldots,i_M}\mathbf{F}_{ii_2\ldots i_M}\otimes(\mathbf{r}_{ii_2}+\ldots+\mathbf{r}_{ii_M})\;. \tag{7.2}$$

These choices are compatible with preservation of zero total momentum, since $\sum_i \mathbf{D}_i = \mathbf{0}$. On the other hand, in this case the fluxes $\mathbf{B}$ and $\mathbf{J}$ defined respectively in (5.17) and (5.18) are given by

$$\mathbf{B} \;=\; \frac{1}{\beta V}\left(\sum_{i=1}^{N}\frac{\mathbf{p}_i}{m_i}\right)\frac{N-1}{N} \tag{7.3}$$

and

$$\mathbf{J} \;=\; \frac{1}{V}\left(\sum_{i=1}^{N}\boldsymbol{\nu}_i^T\frac{\mathbf{p}_i}{m_i} - \frac{1}{N}\sum_{j=1}^{N}\boldsymbol{\nu}_j^T\sum_{i=1}^{N}\frac{\mathbf{p}_i}{m_i}\right) \;=\; \mathbf{J}_Q - \mathbf{A}\;, \tag{7.4}$$

where

$$\mathbf{A}(\boldsymbol{\Gamma}) \;=\; \tilde{\mathbf{A}}(t)\frac{1}{VN}\sum_{j=1}^{N}\boldsymbol{\nu}_j^T\sum_{i=1}^{N}\frac{\mathbf{p}_i}{m_i} \tag{7.5}$$

is the difference between the heat flux $\mathbf{J}_Q$ and the dissipative flux $\mathbf{J}$. It can be seen from (7.3), (7.4) and (7.5) that the difference in the fluxes $\mathbf{J}$ and $\mathbf{B}$ is not equal to the heat flux $\mathbf{J}_Q$, which violates the second condition (5.27) in Section 5.2. Therefore, in the HNMED method, the long-time average of the macroscopic heat flux vector $\mathbf{J}_Q$ in (5.25) can be expressed with the aid of (7.3) and (7.4) as

$$\frac{\langle\tilde{\mathbf{J}}_Q(\infty)\rangle}{T} \;=\; \left(\frac{V}{k_BT^2}\int_0^\infty\left\langle\tilde{\mathbf{J}}_Q((s)_0)\otimes\tilde{\mathbf{J}}_Q(0)\right\rangle_c\mathrm{d}s - \\ \frac{V}{k_BT^2}\int_0^\infty\left\langle\tilde{\mathbf{J}}_Q((s)_0)\otimes\left[\tilde{\mathbf{A}}(0)+\tilde{\mathbf{B}}(0)\right]\right\rangle_c\mathrm{d}s\right)\mathbf{F}_e \tag{7.6}$$

or

$$\frac{\left\langle\tilde{\mathbf{J}}_Q(\infty)\right\rangle}{T} \;=\; \frac{1}{T^2}(\mathbf{L}_{QQ}-\mathbf{L}_{QA}-\mathbf{L}_{QB})\mathbf{F}_e\;, \tag{7.7}$$

where

$$\mathbf{L}_{QA} \;=\; \frac{V}{k_B}\int_0^\infty \left\langle \tilde{\mathbf{J}}_Q((s)_0)\otimes\tilde{\mathbf{A}}(0)\right\rangle_c \mathrm{d}s\;, \tag{7.8}$$

and

$$\mathbf{L}_{QB} \;=\; \frac{V}{k_B}\int_0^\infty \left\langle \tilde{\mathbf{J}}_Q((s)_0)\otimes\tilde{\mathbf{B}}(0)\right\rangle_c \mathrm{d}s\;. \tag{7.9}$$

Hence, estimation of $\mathbf{L}_{QQ}$ requires the calculation of $\mathbf{L}_{QA}+\mathbf{L}_{QB}$ in addition to running the standard HNEMD algorithm to obtain $\frac{\langle\tilde{\mathbf{J}}_Q(\infty)\rangle}{T}$. These extra correlation terms need to be evaluated by means of a Green-Kubo method, which naturally involves the errors related to the integration and calculation of correlation functions. If, upon employing the Green-Kubo method, the sum $\mathbf{L}_{QA}+\mathbf{L}_{QB}$ is found to be small compared to $\mathbf{L}_{QQ}$, then it is sufficient to use the classical HNEMD method given by (7.1) for estimating $\mathbf{L}_{QQ}$.

7.2 M-HNEMD Algorithm

In this section, equations of motion, and particularly choices for $\mathbf{C}_i$ and $\mathbf{D}_i$, are derived for a system of n different species, which satisfy the three basic conditions (5.27), (5.28) and compatibilitiy with PBCs discussed in Section 5.2. In the following, a sequence of proposed forms for $\mathbf{C}_i$ and $\mathbf{D}_i$ is suggested and refined to satisfy the three conditions, hence leading to the final expressions given at the end of this section.

As observed in Section 7.1, using $\mathbf{D}_i$ in the form (7.1) violates the equivalence of fluxes (5.27). To circumvent this problem, $\mathbf{D}_i$ may be initially modified as

$$\mathbf{D}_i \;=\; \boldsymbol{\nu}_i - \frac{m_i}{\bar{m}}\sum_{j=1}^{N}\boldsymbol{\nu}_j\;, \tag{7.10}$$

where $\bar{m}=\sum_{i=1}^{N} m_i$. Using (7.10) with $\mathbf{C}_i=\mathbf{0}$, the flux vector $\mathbf{J}$ in (5.18) becomes

$$\mathbf{J} \;=\; \frac{1}{V}\sum_{i=1}^{N}\boldsymbol{\nu}_i^T\frac{\mathbf{p}_i}{m_i} - \frac{1}{\bar{m}}\Bigg(\sum_{j=1}^{N}\boldsymbol{\nu}_j^T\Bigg)\Bigg(\sum_{i=1}^{N}\mathbf{p}_i\Bigg) \tag{7.11}$$

and $\sum_{i=1}^{N}\mathbf{p}_i=\mathbf{0}$, provided that the total initial momentum is zero, hence $\mathbf{J}=\mathbf{J}_Q$. However, the flux

vector $\mathbf{B}$ in (5.17) is now equal to

$$\mathbf{B} \;=\; \frac{1}{\beta V}\left(\sum_{i=1}^{N}\frac{\mathbf{p}_i}{m_i} - \frac{1}{\bar{m}}\sum_{i=1}^{N}\mathbf{p}_i\right) \;=\; \frac{1}{\beta V}\sum_{i=1}^{N}\frac{\mathbf{p}_i}{m_i} \;\neq\; \mathbf{0}\,, \tag{7.12}$$

resulting, again, in $\mathbf{J} - \mathbf{B} \neq \mathbf{J}_Q$. One way to achieve $\mathbf{B} = \mathbf{0}$ is to choose

$$\mathbf{C}_i \;=\; -\mathbf{r}_i \otimes \frac{\mathbf{p}_i}{m_i}\,; \tag{7.13}$$

however, this choice introduces additional terms in $\mathbf{J}$, such that

$$\mathbf{J} \;=\; \mathbf{J}_Q + \sum_{i=1}^{N}\left(\frac{\mathbf{p}_i}{m_i} \otimes \mathbf{r}_i\right)\mathbf{F}_i \;\neq\; \mathbf{J}_Q\,. \tag{7.14}$$

To simultaneously eliminate $\mathbf{B}$ and set $\mathbf{J} = \mathbf{J}_Q$, one should also change $\mathbf{D}_i$ to

$$\mathbf{D}_i \;=\; \boldsymbol{\nu}_i - \frac{m_i}{\bar{m}}\sum_{j=1}^{N}\boldsymbol{\nu}_j - (\mathbf{F}_i \cdot \mathbf{r}_i)\mathbf{I} + \frac{m_i}{\bar{m}}\sum_{j=1}^{N}(\mathbf{F}_j \cdot \mathbf{r}_j)\mathbf{I}\,. \tag{7.15}$$

While (7.13) and (7.15) enforce the conditions (5.28) and (5.27), they do not satisfy frame invariance, *i.e.*, they do not yield the same behavior under arbitrary translations and rotations of the system. To impose frame invariance, one should subtract from the position vector $\mathbf{r}_i$ of every atom a suitably defined vector $\bar{\mathbf{r}}$, which convects with the body. In this case, (7.13) and (7.15) become

$$\begin{aligned}
\mathbf{C}_i \;&=\; -\left(\mathbf{r}_i - \bar{\mathbf{r}}\right) \otimes \frac{\mathbf{p}_i}{m_i}\,, \\
\mathbf{D}_i \;&=\; \boldsymbol{\nu}_i - \frac{m_i}{\bar{m}}\sum_{j=1}^{N}\boldsymbol{\nu}_j - \left(\mathbf{F}_i \cdot \left(\mathbf{r}_i - \bar{\mathbf{r}}\right) - \frac{m_i}{\bar{m}}\sum_{j=1}^{N}\mathbf{F}_j \cdot \left(\mathbf{r}_j - \bar{\mathbf{r}}\right)\right)\mathbf{I}
\end{aligned} \tag{7.16}$$

There are various possible choices for $\bar{\mathbf{r}}$ which enforce frame invariance without violating (5.28) and (5.27). One such choice is $\bar{\mathbf{r}} \;=\; \mathbf{r}_{MC} \;=\; \frac{1}{\bar{m}}\sum_{i=1}^{N} m_i\mathbf{r}_i$, namely the position vector of the mass center of the system. Other choices include the position vector of any fixed point in the system, provided that this point convects with any arbitrary translation and rotation of the whole system. One such choice would be, for example, the left-bottom corner $\mathbf{r}_a$ of the system. However, all the aforementioned choices are incompatible with periodic boundary conditions (PBCs). Indeed, in the case of PBCs, all atoms that exit the system from one side enter it again from the opposite side with the same momentum, see, e.g., [2, Section 1.5.2]. In this so-called wrapping

process, the terms (7.16) with $\bar{\mathbf{r}} = \mathbf{r}_{MC}$ or $\bar{\mathbf{r}} = \mathbf{r}_a$ create large jumps in velocities and forces, as $\mathbf{r}_i - \bar{\mathbf{r}}$ is discontinuous in time. This discontinuity can be minimized by choosing for each atom an $\bar{\mathbf{r}}$ that depends only on atoms in its neighborhood. (Empirical evidence of both of these issues is given in Section 7.3.) Here, it is assumed that the neighborhood of an atom is comprised only of atoms within the cut-off radius $r_c > 0$ of the potential. This treatment is also time-discontinuous due to neighboring atoms leaving or entering the cutoff of a given atom. For solids, these events can be quite rare and become non-existent for low enough temperatures. For dense fluids, on the other hand, an atom can change neighbors as frequently as every time-step. For this choice of $\bar{\mathbf{r}}$, equation (7.16) can be cast as

$$\begin{aligned} \mathbf{C}_i &= -\left(\mathbf{r}_i - \bar{\mathbf{r}}_i\right) \otimes \frac{\mathbf{p}_i}{m_i} \,, \\ \mathbf{D}_i &= \boldsymbol{\nu}_i - \frac{m_i}{\bar{m}} \sum_{j=1}^{N} \boldsymbol{\nu}_j - \left(\mathbf{F}_i \cdot \left(\mathbf{r}_i - \bar{\mathbf{r}}_i \right) - \frac{m_i}{\bar{m}} \sum_{j=1}^{N} \mathbf{F}_j \cdot \left(\mathbf{r}_j - \bar{\mathbf{r}}_j \right) \right) \mathbf{I} \,, \end{aligned} \tag{7.17}$$

where $\bar{\mathbf{r}}_i = \frac{1}{N_i} \sum_{\substack{j=1 \\ j \neq i}}^{N_i} \mathbf{r}_j$ and N_i is the number of atoms in the neighborhood of atom i within the cut-off radius. Despite the time-discontinuity, the choice of (7.17) preserves total momentum and also satisfies (5.28) and (5.27) with $\mathbf{B} = \mathbf{0}$ since the partial derivatives of $\mathbf{C}_i$ and $\mathbf{D}_i$ with respect to the phase variables are unaffected. Therefore, the equations of motion (5.11) with (7.17) can be used to evaluate $\mathbf{L}_{QQ}$ and are referred to as the M-HNEMD equations of motion under periodic boundary conditions. Also, $\mathbf{C}_i$ in (7.17) remains bounded with increasing system size, unlike the choice of $\bar{\mathbf{r}} = \mathbf{r}_{CM}$. Since $\mathbf{B} = \mathbf{0}$, the equations of motion also satisfy the adiabatic incompressibility of phase space, as in the case of HNEMD method for single-species systems.

A casual review reveals that, when reduced to a single-species system ($m_i = m$), the M-HNEMD algorithm is not identical to the original HNEMD algorithm. This demonstrates the non-uniqueness of the NEMD algorithms for evaluating thermal conductivity.

7.3 Results

The HNEMD and M-HNEMD algorithms are applied to estimate the thermal conductivity $\boldsymbol{\kappa}$ of Ar and GaN systems and the transport coefficient $\dfrac{\mathbf{L}_{QQ}}{T^2}$ for an Ar-Kr system. A sequence of the heat flux averages $\langle \tilde{J}_{Qx,k}(\infty) \rangle$ corresponding to a decreasing sequence of $F_{ex,k}$ is computed to determine the linear regime of the system under the action of the external field $\mathbf{F}_e = (F_{ex,k}, 0, 0)$. In this case, κ_{xx} is estimated for Ar and GaN and $\dfrac{L_{QQ,xx}}{T^2}$ is estimated for Ar-Kr systems using the gradient method described in Chapter 6 and [46]. Before the external field $\mathbf{F}_e$ is switched on, the system is equilibrated using the NH thermostat which generates the (extended) canonical ensemble given in (5.10). When the external field is applied, the duration of each of the simulations

in the sequence is chosen to make the variance of the estimated $\langle \tilde{J}_{Qx,k}(\infty) \rangle$ negligible and hence the reported error estimates are based on the regression errors. The time integration scheme used for the HNEMD method is described in [46] and is modified for the M-HNEMD method, as in Appendix B.

7.3.1 Argon

As an initial test, the M-HNEMD algorithm with (7.17) is applied to a single-species ($n = 1$) Ar system at its triple point (T = 86.5 K, face-centered cubic lattice of length 5.719 $\mathring{A}$). The system is modeled using a Lennard-Jones potential ($M = 2$ in (3.32)) with $N = 256$ atoms, cut-off radius of $r_c = 13\mathring{A}$ and periodic boundary conditions on the $4 \times 4 \times 4$ unit cells. In the Lennard-Jones potential given by (6.8), the characteristic energy is $\varepsilon_{ij} = 1.6539 \times 10^{-21}\, J$ and the characteristic length is $\sigma_{ij} = 3.405\, \mathring{A}$, see Section 6.1.1. Each run is carried out for 10^6 time steps with a step-size of $\Delta t = 4.0\, fs$.

The computationally tractable linear regime of F_{ex} is found to be between $0.001\, \mathring{A}^{-1} < F_{ex} < 0.1\, \mathring{A}^{-1}$, as shown in Figure 7.1(a), where $\kappa_{xx,k} = \dfrac{\langle \tilde{J}_{Qx,k}(\infty) \rangle}{T F_{ex,k}}$ is independent of $F_{ex,k}$. It is concluded from Figure 7.1(a) that the results from the M-HNEMD and HNEMD algorithms are practically identical, thus providing a validation of the M-HNEMD algorithm for a single-species system. The value of thermal conductivity using the M-HNEMD algorithm with the gradient method is found to be $0.1305 \pm 0.0002\, W/mK$, see Figure 7.1(b). This compares favorably to the HNEMD result $0.1302 \pm 0.0002\, W/mK$ and the Green-Kubo result $0.129\, W/mK$, see Figure 7.2.

As an aside, it is also observed that when using $\bar{\mathbf{r}} = \mathbf{r}_{CM}$ in (7.16) the thermal conductivity κ_{xx} shows a decreasing trend for increasing values of F_{ex} until it reaches a regime of severe discontinuity, see Figure 7.3. As argued in Section 7.2, the discontinuity of $\kappa_{xx}(F_{ex})$ can be attributed to the non-smooth transition during the re-mapping due to the PBCs. This problem is eliminated with the use of equation (7.17). Interestingly, the use of equation (7.17) also eliminates the decreasing trend of κ_{xx}, which facilitates the identification of a linear regime.

7.3.2 Argon-Krypton Mixture

The M-HNEMD algorithm (7.17) is applied to the binary Ar-Kr mixture system at T = 115.6 K. The system is comprised of a total of $N = 256$ atoms (128 Ar and 128 Kr) in a cube of volume $24.192^3\, \mathring{A}^3$ with PBCs. It is modeled using a Lennard-Jones potential given by (6.8), where the parameters for Ar are as in Section 7.3.1, while for Kr are $\epsilon_{ij} = 2.3056 \times 10^{-21}\, J$ and $\sigma_{ij} = 3.670\, \mathring{A}$ [54]. The two parameters for Ar-Kr pairs are determined from the Lorentz-Berthelot mixing rules [63]. The system is initially created by filling the left half of the simulation box with argon atoms and the right half with krypton. It is then equilibrated to become a liquid mixture by integrating the NH equations of motion for about 10^4 time steps with step-size $\Delta t = 4.0\, fs$. Once the system

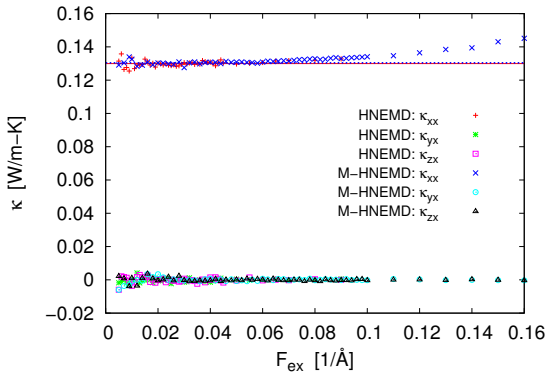

(a) *Variation of thermal conductivities κ_{xx}, κ_{yx} and κ_{zx} with F_{ex}.*

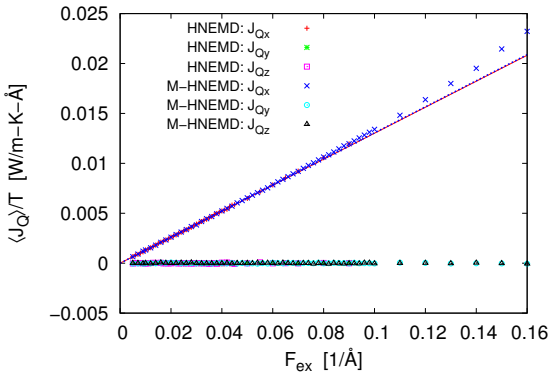

(b) *Variation of the components of $\frac{\langle \tilde{\mathbf{J}}_Q(\infty) \rangle}{T}$ with F_{ex}.*

Figure 7.1: *Comparison between the M-HNEMD and HNEMD algorithms for argon at the triple point. The dashed and solid lines correspond respectively to the M-HNEMD and HNEMD estimates of κ_{xx}.*

is equilibrated, the M-HNEMD equations of motion are solved for 10^6 time steps to obtain the heat transport coefficient $L_{QQ,xx}/T^2$.

Figure 7.4(a) shows that the linear regime is found approximately when $0.01\,\mathring{A}^{-1} < F_{ex} < 0.085\,\mathring{A}^{-1}$ for both the M-HNEMD and HNEMD algorithms. The M-HNEMD estimate for the transport coefficient $L_{QQ,xx}/T^2$ is found to be $0.08743 \pm 0.00011\,W/mK$, see Figure 7.4(b). This is in good agreement with the Green-Kubo estimate of $0.08720\,W/mK$ at a correlation time of $t = 1ps$, which is obtained by performing equilibrium molecular dynamics simulations, see Figure 7.5. The HNEMD estimate is found to be $0.08618 \pm 0.00013\,W/mK$, which is very close to the Green-Kubo and M-HNEMD estimates, see Figure 7.5. As mentioned in Section 7.1, since $\frac{L_{QA,xx} + L_{QB,xx}}{T^2} = 0.00043\,W/mK$ is small compared to the Green-Kubo estimate from Figure 7.5, either the HNEMD or the M-HNEMD algorithm may be employed to obtain an accurate estimate of $L_{QQ,xx}$ for Ar-Kr in the given state.

Figure 7.6 shows the magnitude of the discontinuities in the trajectory of a typical $\bar{\mathbf{r}}_i$ relative to the trajectory of the associated atom $\mathbf{r}_i$. These trajectories were captured before the field F_{ex} was applied to allow for comparison of $\bar{\mathbf{r}}_i$ to an unperturbed $\mathbf{r}_i$. Even in a dense fluid, it is apparent that the discontinuities are quite small relative to the normal fluctuations in position.

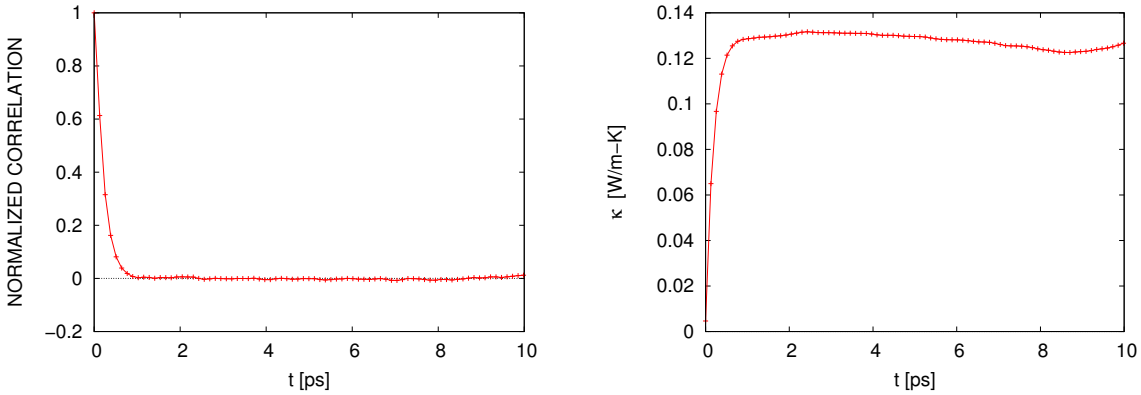

(a) *Normalized Ar auto-correlation function* $\frac{\langle \tilde{J}_{Qx}(0)\tilde{J}_{Qx}(t)\rangle}{\langle \tilde{J}_{Qx}(0)\tilde{J}_{Qx}(0)\rangle}$.

(b) *Integral of the auto-correlation function leading to thermal conductivity estimate* κ_{xx}.

Figure 7.2: *Green-Kubo estimate of the thermal conductivity of argon at triple point based on the direct integration of the heat flux auto-correlation function.*

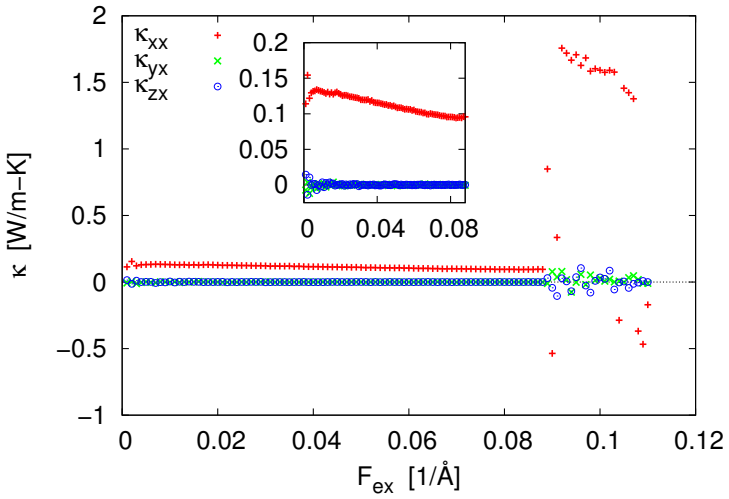

Figure 7.3: *Variation of thermal conductivities* κ_{xx}, κ_{yx} *and* κ_{zx} *with* F_{ex} *for argon at the triple point for* $\bar{\mathbf{r}} = \mathbf{r}_{CM}$, *demonstrating an instability at approximately* $F_{ex} = 0.089\,\mathring{A}^{-1}$ *and a significant decreasing trend (see inset).*

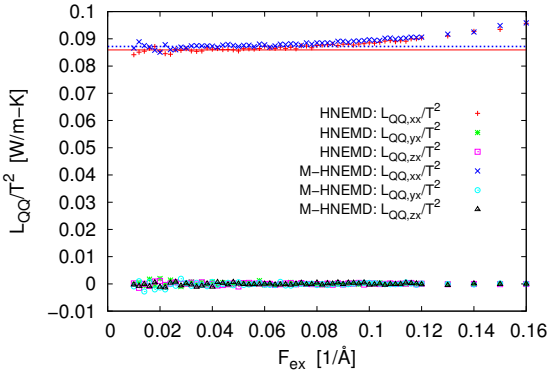

(a) *Variation of the transport coefficients $L_{QQ,xx}$, $L_{QQ,yx}$ and $L_{QQ,zx}$ with F_{ex}.*

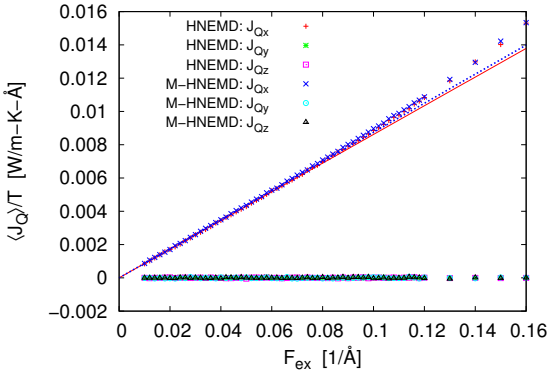

(b) *Variation of the components of the heat flux vector $\frac{\langle \tilde{\mathbf{J}}_Q(\infty) \rangle}{T}$ with F_{ex}.*

Figure 7.4: *Comparison of the M-HNEMD and HNEMD algorithms for argon-krypton mixture. The dashed and solid lines correspond respectively to the M-HNEMD method and HNEMD estimates of $L_{QQ,xx}/T^2$.*

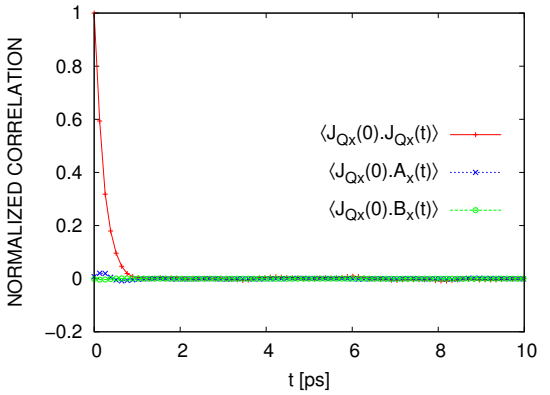

(a) *Correlations normalized by $\langle \tilde{J}_{Qx}(0)\tilde{J}_{Qx}(0) \rangle$.*

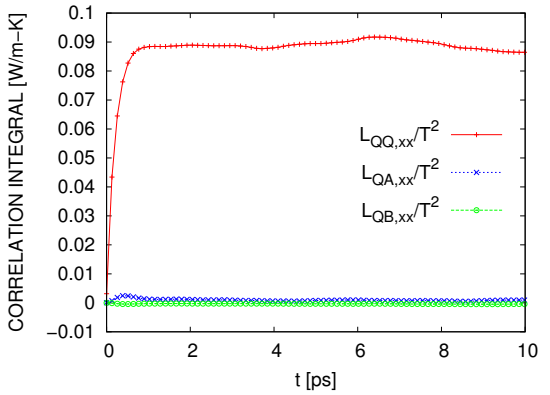

(b) *Integrals of the correlation functions.*

Figure 7.5: *Correlation functions $\langle \tilde{J}_{Qx}(0)\tilde{J}_{Qx}(t) \rangle$, $\langle \tilde{J}_{Qx}(0)\tilde{A}_x(t) \rangle$, and $\langle \tilde{J}_{Qx}(0)\tilde{B}_x(t) \rangle$, as well as integration of the correlation functions leading to $\frac{L_{QQ,xx}}{T^2}$, $\frac{L_{QA,xx}}{T^2}$ and $\frac{L_{QB,xx}}{T^2}$ estimates for argon-krypton mixture using the Green-Kubo method.*

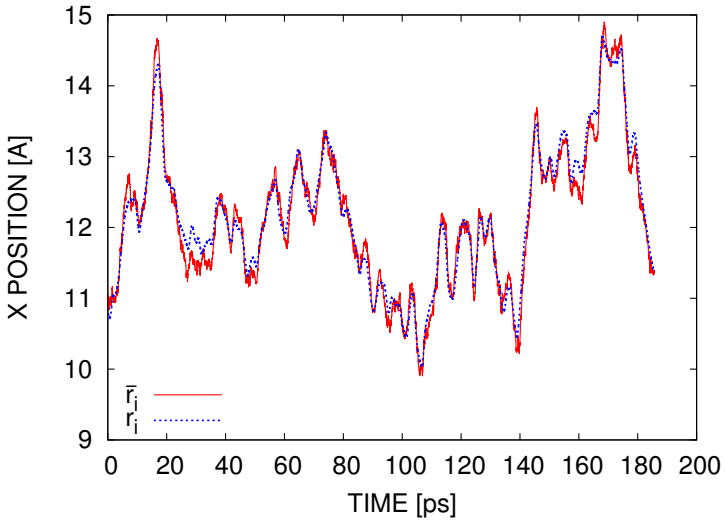

Figure 7.6: *Trajectories of* $\mathbf{r}_i$ *and* $\bar{\mathbf{r}}_i$.

7.3.3 Gallium-Nitride

The HNEMD and M-HNEMD methods are next employed to estimate the thermal conductivity of a perfect GaN system (wurtzite crystal structure) using an orthogonal cell with lattice parameters $a = 3.19\mathring{A}$ and $c = 5.20\mathring{A}$ at T=500K, see [73] for details on the lattice structure. The system is modeled using 512 atoms with 4 unit cells per direction ($4 \times 4 \times 4$) and a Stillinger-Weber potential given by (6.13)-(6.16), see [4, 5, 68], under periodic boundary conditions. It is observed that $4\times4\times4$ system is sufficient for obtaining the value of thermal conductivity using both HNEMD and M-HNEMD algorithms. A time-step of 0.5 fs is used for 8×10^6 time steps. The linear regime in the HNEMD method is found in the range $7 \times 10^{-5}\,\mathring{A}^{-1} < F_{ez} < 1.3 \times 10^{-4}\,\mathring{A}^{-1}$ and the thermal conductivity is estimated via the slope method as $133.65 \pm 2.50\,W/mK$, see Figure 7.7(a) and Figure 7.7(b).

Using the M-HNEMD method, the thermal conductivity is found to be $132.02 \pm 5.85\,W/mK$, see Figure 7.7(a) and Figure 7.7(b), which is comparable to the HNEMD result. Both the HNEMD and M-HNEMD estimates are comparable to the estimate of the direct method estimate, which is $120.59\,W/mK$ [73]. It can also be seen in Figure 7.8 that the average of the heat flux $\langle \tilde{\mathbf{J}}_Q(t) \rangle$ converges after 4×10^6 time steps for $F_{ex} = 1.0 \times 10^{-4}\mathring{A}^{-1}$ thus demonstrating that the duration of the simulations is sufficient. Finally, the Green-Kubo approach yields an estimate of $128.09\,W/mK$ using 8×10^6 time steps and 1000 atoms ($5\times5\times5$). In the Green-Kubo approach, it is observed that a system at least as large as $5 \times 5 \times 5$ is needed to obtain a thermal conductivity value. In all cases, the Green-Kubo estimate is based on the criterion of the first plateau attained by the integral of the correlation, as in [67]. Figure 7.9 shows that $\langle \tilde{\mathbf{J}}_Q(t) \otimes \tilde{\mathbf{J}}_Q(0) \rangle$ decays in a complicated manner with correlation time, unlike the Ar-Kr system, which makes this criterion somewhat ambiguous.

As seen in Figure 7.9, the noise past a correlation time of approximately $200\,ps$ is quite significant, thus requiring considerably more simulation time than the M-HNEMD method to obtain a similar quality thermal conductivity estimate. However, $\left(L_{QA,xx} + L_{QB,xx}\right)/T^2 = 0.051\,W/mK$ is extremely small compared to the Green-Kubo estimate leading to the conclusion that the HNEMD method yields comparable results for GaN.

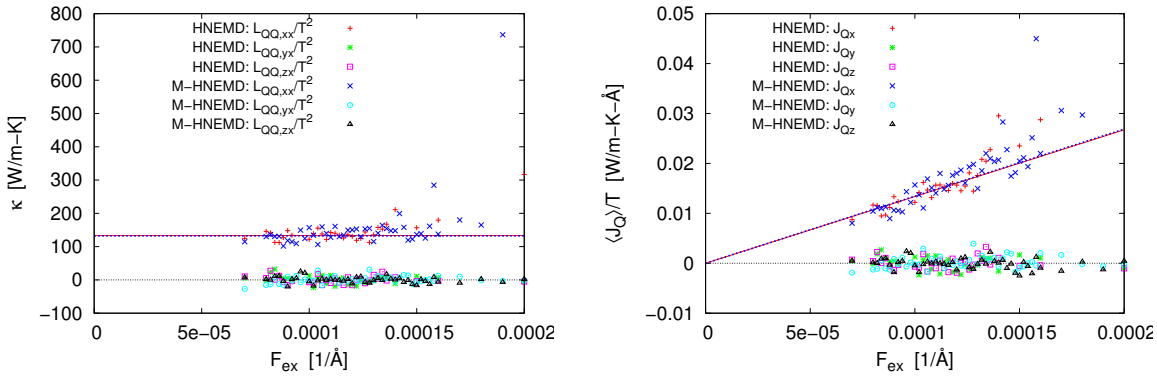

(a) *Variation of the thermal conductivities κ_{xx}, κ_{yx} and κ_{zx} with F_{ex}.*

(b) *Variation of the components of the heat flux vector $\frac{\langle \tilde{\mathbf{J}}_Q(\infty)\rangle}{T}$ with F_{ex}.*

Figure 7.7: *Comparison of the M-HNEMD and HNEMD algorithms for gallium-nitride. The dashed and solid lines correspond respectively to the M-HNEMD method and HNEMD estimates of κ_{xx}.*

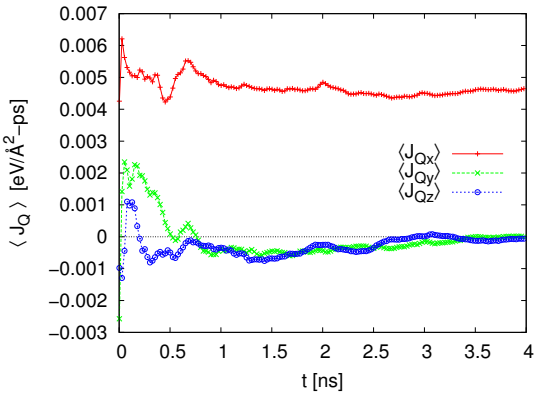

Figure 7.8: *The running average of the components of the heat flux vector $\mathbf{J}_Q$ for gallium-nitride system for $F_{ex} = 1.3 \times 10^{-4}\,\mathring{A}^{-1}$ using the M-HNEMD method.*

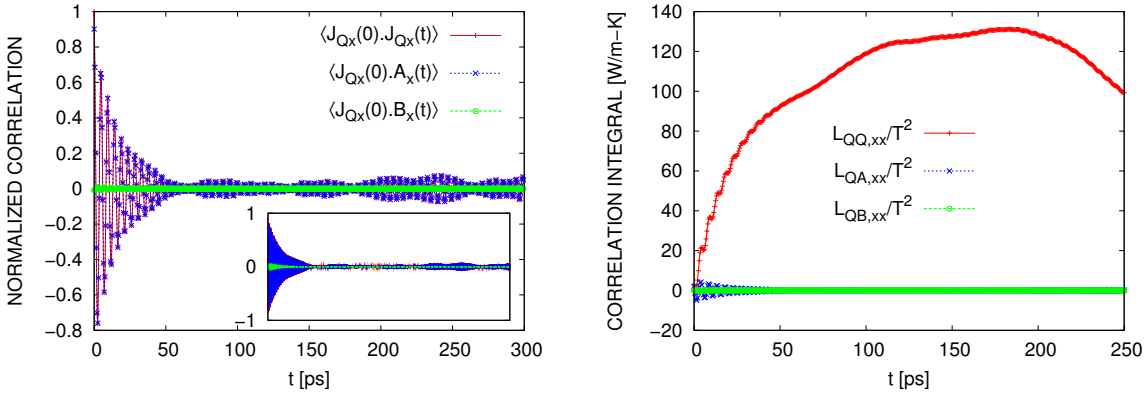

(a) *Correlations normalized by* $\langle \tilde{J}_{Qx}(0)\tilde{J}_{Qx}(0)\rangle$. **(b)** *Integrals of the correlation functions*

Figure 7.9: *Correlation functions* $\langle \tilde{J}_{Qx}(0)\tilde{J}_{Qx}(t)\rangle$, $\langle \tilde{J}_{Qx}(0)\tilde{A}_{x}(t)\rangle$ *and* $\langle \tilde{J}_{Qx}(0)\tilde{B}_{x}(t)\rangle$, *as well as integration of the correlations functions leading to* $\kappa_{xx} = \frac{L_{QQ,xx}}{T^2}$, $\frac{L_{QA,xx}}{T^2}$ *and* $\frac{L_{QB,xx}}{T^2}$ *estimates for gallium-nitride using the Green-Kubo method. Note that in (a) the data has been decimated to show each correlation clearly; the inset shows the full correlations which densely fill the envelopes described by the decimated data.*

7.4 Discussion

As observed in Section 7.3, the Green-Kubo method may not be viable for the estimation of thermal conductivity in systems like GaN. In such systems, it is difficult to establish that the complex autocorrelation function has decayed sufficiently to permit accurate integration. In addition, given that the decay of the autocorrelation function is fairly long (at least $150 - 200\,ps$ in the case of GaN, see Figure 7.9), it takes considerable simulation time using the GK method to obtain the thermal conductivity within reasonable statistical certainty. These problems may be avoided by using the HNEMD and M-HNEMD methods, thereby circumventing the integration of a noisy autocorrelation function. Also, these non-equilibrium methods yield results of reasonable accuracy for relatively small total simulation times, as the signal-to-noise ratio is high due to the action of the finite non-zero external field $\mathbf{F}_e$. Moreover, the HNEMD and M-HNEMD methods are parallelizable for a simulation corresponding to a choice of $\mathbf{F}_e$. Here, the simulation domain can be spatially decomposed into small boxes and assigned to various processors [60]. Each processor computes forces and then updates the positions and velocities of all atoms within its box. The information needed for forces at the edge of the box is obtained by communicating with the processors corresponding to the neighboring boxes [60].

For single-component systems, the HNEMD and M-HNEMD algorithms, while not mathematically identical, yield statistically identical results, which demonstrates the non-uniqueness in the construction of non-equilibrium molecular dynamics methods. Interestingly, even when ap-

plied to multi-component Ar-Kr and GaN systems, the HNEMD and M-HNEMD algorithms yield very similar results, as $\mathbf{L}_{QA} + \mathbf{L}_{QB}$ is very small compared to the heat transport coefficient tensor $\mathbf{L}_{QQ}$. However, the M-HNEMD is theoretically consistent with the linear response theory for multi-component system, in the sense that, in addition to preserving total momentum (see equation (5.28)) and being compatible with periodic boundary conditions, it also satisfies equivalency of fluxes (see equation (5.27)). In contrast, for multi-component systems the HNEMD method violates equation (5.27), thereby requiring additional equilibrium simulations to establish that $\mathbf{L}_{QA} + \mathbf{L}_{QB}$ is small compared to $\mathbf{L}_{QQ}$. Although these results have not answered the question whether the quantity $\mathbf{L}_{QA} + \mathbf{L}_{QB}$ is insignificant for all material systems under all conditions conclusively, they do suggest that the original HNEMD method can provide accurate thermal conductivity estimates without strictly satisfying the equivalence of fluxes and the incompressibility of phase space. Nevertheless, in all cases, without resorting to additional simulations to calculate expensive time-correlations, the marginally more complex M-HNEMD algorithm will provide accurate results if used in the linear regime.

As expected, the M-HNEMD method shares some of the same challenges that apply to HNEMD method. First, it requires simulations corresponding to a decreasing sequence of $\mathbf{F}_e$ to establish the linear regime. This can be alleviated by performing these simulations in parallel, as they are completely independent of each other. Second, it becomes extremely inefficient for very small $\mathbf{F}_e$, where the signal-to-noise ratio is low. In such a case, it takes simulation time on the order of a Green-Kubo estimate to obtain a reasonable estimate of $\dfrac{\langle \tilde{J}_{Qx}(\infty) \rangle}{TF_{ex}}$ as F_{ex} tends to zero. Alternately, in the very low bias regime, other NEMD methods may be attractive. For instance, the method of Ciccotti and co-workers [12, 51] employs a direct difference of heat flux between unperturbed and periodically perturbed trajectories to obtain the linear response of the system. In the M-HNEMD under consideration, it is important to set F_{ex} far enough from zero to avoid this problem, while still staying within the linear regime. An estimate of the linear regime can be obtained from prior knowledge of the phonon mean-free path [46].

Chapter 8

Conclusions and Future Work

This thesis introduces a class of homogeneous non-equilibrium molecular dynamics methods for calculating the heat transport coefficient of solids and liquids (including mixtures). The first significant contribution is the extension of the HNEMD method originally formulated for systems modeled by pair potentials, to systems modeled by many-body potentials. This extension now enables the computation of heat transport coefficient estimates across a wide range of single-species systems, such as silicon, germanium, copper, aluminum, *etc.*, which are modeled by many-body potentials [16]. As a test case, the extended HNEMD method is applied to a silicon system and it shows that the heat transport coefficient of silicon can be obtained accurately with lower overall computational cost compared to the GK and direct methods. In addition, the HNEMD method may be applied for systems with defects, such as vacancies, impurities, *etc.*, to characterize their effects on the heat transport coefficient. In such problems, since the number of atoms corresponding to equilibrium concentrations of defects are on the order of $10^5 - 10^7$, the HNEMD method may be favorable to the Green-Kubo or the direct methods due to the advantage of obtaining smaller statistical uncertainties at lower overall computational cost.

The second significant contribution documented in this thesis is a new HNEMD method for multi-species systems, referred to as the M-HNEMD method. The proposed M-HNEMD method solves the problem of computing the heat transport coefficient estimates for multi-species systems modeled by many-body potentials without resorting to additional equilibrium molecular dynamics simulations. This has remained an open problem even for the simple case of systems modeled by pair potentials. The new method is tested for argon-krypton liquid mixtures and solid gallium-nitride systems and it shows that the heat transport coefficient estimates for these systems can be obtained accurately. This method may now be applied to study a wide range of multi-species systems from crystalline In-Ga-As semiconductor thermoelectric devices, as mentioned in the introduction, to semi-flexible polymer systems such as liquid butane [14, 15].

A third contribution of this thesis is the extension of statistical mechanical theory of transport processes developed by Irving and Kirkwood to systems modeled by many-body potentials. This results in the expressions for stress tensors and heat-flux vectors for the case of many-body po-

tentials. The stress tensor thus obtained can be used to analyze metallic and non-metallic systems with cracks, dislocations, *etc.*, [74] when they are modeled by complicated many-body potentials [16, 17].

A number of new research questions can now be addressed on the strength of these new methods. For example, recent experiments [43] have shown that the thermal conductivity of individual crystalline silicon nanowires of diameters in the range of $20 - 100\,nm$ were more than one order of magnitude lower than the bulk silicon. This was attributed to the boundary effects and possible phonon spectrum modification. It was also found that, when a certain amount of roughness is added to the boundary of these nano-wires, the thermal conductivity is one order of magnitude lower than the smooth nanowires [29]. As an initial step in understanding these effects, the HNEMD method may be applied to obtain the thermal conductivity values. Since the nanowires have free surfaces and to capture the effects of these free surfaces, it is not appropriate to apply periodic boundary conditions. In these systems, the numbers of atoms required to obtain an estimate of thermal conductivity are on the order of 3×10^6 and it is hoped that the HNEMD method, with its advantage of yielding better statistical averages with lower computational cost, may be suitable. Since the Green-Kubo method is based on the validity of Fourier' law and Onsager' regression hypothesis, this class of problems presents an opportunity to test their validity in the case of nanowires.

Bibliography

[1] N. C. Admal and E. B. Tadmor. A unified interpretation of stress in molecular systems. *J. Elasticity*, 100:63–143, 2010.

[2] M. P. Allen and D. J. Tildesley. *Computer Simulation of Liquids*. Oxford University Press, New York, 1987.

[3] N. W. Ashcroft and N. D. Mermin. *Solid State Physics*. Brooks Cole, New York, 1976.

[4] A. Bere and A. Serra. Atomic structure of dislocation cores in GaN. *Phys. Rev. B*, 65:205323, 2002.

[5] A. Bere and A. Serra. On the atomic structures, mobility and interactions of extended defects in GaN: dislocations, tilt and twin boundaries. *Philos. Mag*, 86:2152–2192, 2006.

[6] P. R. Bevington and D. K. Robinson. *Data Reduction and Error Analysis for the physical sciences*. McGraw-Hill, Boston, 3rd edition, 2003.

[7] J. Q. Broughton and X. P. Li. Phase diagram of silicon by molecular dynamics. *Phys. Rev. B*, 35:9120–9127, 1987.

[8] D. Chandler. *Introduction to Modern Statistical Mechanics*. Oxford University Press, Inc., New York, 1987.

[9] S. Chapman and T. G. Cowling. *The Mathematical Theory of Non-uniform Gases*. Cambridge University Press, New York, 1939.

[10] A. J. Chorin and O. Hald. *Stochastic Tools in Mathematics and Science*. Springer, New York, 2006.

[11] G. Ciccotti, G. Jacucci, and I. R. McDonald. Thermal response to a weak external field. *J. Phys. C : Solid State Phys.*, 11:L509–L513, 1978.

[12] G. Ciccotti, G. Jacucci, and I. R. McDonald. Thought-experiments by molecular-dynamics. *J. Stat. Phys.*, 21:1–22, 1979.

[13] S. J. Cook and P. Clancy. Comparison of semiempirical potential functions for silicon and germanium. *Phys. Rev. B*, 47:7686–7699, 1993.

[14] P. J. Daivis and D. J. Evans. Nonequilibrium molecular-dynamics calculation of thermal-conductivity of flexible molecules - Butane. *Molecular Physics*, 81(6):1289–1295, 1994.

[15] P. J. Daivis and D. J. Evans. Temperature dependence of the thermal conductivity for two models of liquid Butane. *Chemical Physics*, 198(1-2):25–34, 1995.

[16] M. S. Daw and M. I. Baskes. Embedded-atom method: Derivation and application to impurities, surfaces, and other defects in metals. *Phys. Rev. B*, 29:6443–6453, 1984.

[17] M. S. Daw, S. M. Foiles, and M. I. Baskes. The embedded-atom method: a review of theory and applications. *Mat. Sci. Rep.*, 9:251–310, 1993.

[18] S. R. de Groot. *Thermodynamics of Irreversible Processes*. Interscience Publishers Inc., New York, 1951.

[19] S. R. de Groot and P. Mazur. *Non-Equilibrium Thermodynamics*. Dover, New York, 1984.

[20] T. M. Tritt Ed. *Thermal conductivity: theory, properties and applications*. Kluwer Academic, New York, 2004.

[21] D. J. Evans. Homogeneous NEMD algorithm for thermal conductivity–application of non-canonical linear response theory. *Phys. Let. A*, 91(9):457 – 460, 1982.

[22] D. J. Evans and P. T. Cummings. Non-equilibrium molecular dynamics algorithm for the calculation of thermal diffusion in simple fluid mixtures. *Mol. Phys.*, 72(4):893–898, 1991.

[23] D. J. Evans and B. L. Holian. The Nose-Hoover thermostat. *J. Chem. Phys.*, 83:4069–4074, 1985.

[24] D. J. Evans and G. P. Morris. *Statistical Mechanics of Non-equilibrium Liquids*. Academic Press, 1990.

[25] M. J. Gillan and M. Dixon. The calculation of thermal conductivities by perturbed molecular dynamics simulation. *J. Phys. C*, 16(5):869–878, 1983.

[26] A. E. Green and P. M. Naghdi. Aspects of the second law of thermodynamics in the presence of electromagnetic effects. *Q. Jl. Appl. Math*, 37:179–193, 1984.

[27] A. E. Green and P. M. Naghdi. A re-examination of the basic postulates of thermomechanics. *Proc. R. Soc. Lond. A*, 432:171–194, 1991.

[28] M. S. Green. Markoff random processes and the statistical mechanics of time-dependent phenomena. 2. Irreversible processes in fluids. *J. Chem. Phys.*, 22:398–413, 1954.

[29] A. I. Hochbaum, R. Chen, R. D. Delgado, W. Liang, E. C. Garnett, M. Najarian, A. Majumdar, and P. Yang. Enhanced thermoelectric performance of rough silicon nanowires. *Nature*, 451:163–167, 2008.

[30] W. G. Hoover. Canonical dynamics: Equilibrium phase-space distributions. *Phys. Rev. A*, 31:1695–1697, 1985.

[31] W. G. Hoover. *Computational Statistical Mechanics*. Elsevier, Amsterdam, 1991.

[32] J. H. Irving and J. G. Kirkwood. The statistical mechanical theory of transport processes. IV. The equations of hydrodynamics. *J. Chem. Phys.*, 18:817–829, 1950.

[33] H. Kaburaki, J. Li, S. Yip, and H. Kimizuka. Dynamical thermal conductivity of argon crystal. *J. Appl. Phys.*, 102:043514, 2007.

[34] J. S. Kallman, W. G. Hoover, C. G. Hoover, A. J. DeGroot, S. M. Lee, and F. Wooten. Molecular-dynamics of silicon indentation. *Phys. Rev. B.*, 47:7705–7709, 1993.

[35] L. J. T. M. Kempers. A comprehensive thermodynamic theory of the soret effect in a multicomponent gas, liquid, or solid. *J. Chem. Phys.*, 115(14):6330–6341, 2001.

[36] W. Kim, J. Zide, A. Gossard, D. Klenov, S. Stemmer, A. Shakouri, and A. Majumdar. Thermal conductivity reduction and thermoelectric figure of merit increase by embedding nanoparticles in crystalline semiconductors. *Phys. Rev. Lett.*, 96:045901–1–045901–4, 1931.

[37] M. D. Kluge, J. R. Ray, and A. Rahman. Molecular dynamic calculation of elastic constants of silicon. *J. Chem. Phys.*, 85:4028–4031, 1986.

[38] R. Kubo. Statistical-mechanical theory of irreversible processes. 1. General theory and simple applications to magnetic and conduction problems. *J. Phys. Soc. Jpn.*, 12:570–586, 1957.

[39] R. Kubo. *Statistical Mechanics*. Interscience Publishers, New York, 1965.

[40] R. Kubo, M. Yokota, and S. Nakajima. Statistical-mechanical theory of irreversible processes. II. Response to thermal disturbance. *J. Phys. Soc. Jpn.*, 12:1203–1211, 1957.

[41] L. D. Landau and E. M. Lifshitz. *Statistical Physics*. Pergamon, Oxford, 1980.

[42] D. Levesque, L. Verlet, and J. Kürkijarvi. Computer "Experiments" on classical fluids. iv. transport properties and time-correlation functions of the lennard-jones liquid near its triple point. *Phys. Rev. A*, 7:1690–1700, 1973.

[43] D. Li, Y. Wu, P. Kim, P. Yang, and A. Majumdar. Thermal conductivity of individual silicon nanowires. *Appl. Phys. Lett.*, 83:2934–2936, 2003.

[44] A. Majumdar. Thermoelectricity in semiconductor nanostructures. *Science*, 303(5659):777–778, 2004.

[45] K. K. Mandadapu, R. E. Jones, and P. Papadopoulos. Generalization of the homogeneous non-equilibrium molecular dynamics method for calculating thermal conductivity to multi-body potentials. *Phys. Rev. E*, 80:047702–1–4, 2009.

[46] K. K. Mandadapu, R. E. Jones, and P. Papadopoulos. A homogeneous non-equilibrium molecular dynamics method for calculating thermal conductivity with the three-body potential. *J. Chem. Phys.*, 130:204106–1–9, 2009.

[47] K. K. Mandadapu, R. E. Jones, and P. Papadopoulos. A homogeneous nonequilibrium molecular dynamics method for calculating the heat transport coefficient of mixtures and alloys. *J. Chem. Phys.*, 133:034122–1–11, 2010.

[48] G. Marechal and J.-P. Ryckaert. Atomic versus molecular description of transport properties in polyatomic fluids: n-Butane as an illustration. *Chemical Physics Letters*, 101(6):548–54, 1983.

[49] J. W. Martin. Many-body forces in metals and the Brugger elastic constants. *J. Phys. C: Solid State Phys.*, 8:2837–2857, 1975.

[50] G. J. Martyna, M. E. Tuckerman, D. J. Tobias, and M. L. Klein. Explicit reversible integrators for extended systems dynamics. *Mol. Phys.*, 87:1117–1157, 1996.

[51] C. Massobrio and G. Ciccotti. Lennard-Jones triple-point conductivity via weak external fields. *Phys. Rev. A*, 30:3191–3197, 1984.

[52] P. D. Maycock. Thermal conductivity of silicon, germanium, iii-v compounds and iii-v alloys. *Solid-State Electron.*, 10:161–168, 1967.

[53] A. D. Mistriotis, G. E. Froudakis, P. Vendras, and N. Flytzanis. Model potential for silicon clusters and surfaces. *Phys. Rev. B*, 47:10648–10653, 1993.

[54] M. Moosavi and E. K. Gaharshadi. Molecular dynamics simulations of some thermodynamic properties of mixtures of argon with neon, krypton and xenon using two-body and three-body interaction potentials. *Fluid Phase Equilibria*, 274:51–58, 2008.

[55] I. Müller. *Thermodynamics*. Pitman, London, 1985.

[56] S. Nosé. A molecular dynamics method for simulations in the canonical ensemble. *Mol. Phys.*, 52(2):255–268, 1984.

[57] L. Onsager. Reciprocal relations in irreversible processes. I. *Phys. Rev.*, 37(4):405–426, 1931.

[58] L. Onsager. Reciprocal relations in irreversible processes. II. *Phys. Rev.*, 38(12):2265–2279, 1931.

[59] L. Onsager and S. Machlup. Fluctuations and irreversible processes. *Phys. Rev.*, 91(6):1505–1512, 1953.

[60] S. J. Plimpton. Fast parallel algorithms for short-range molecular dynamics. *J. Comp. Phys.*, 117:1–19, 1995. See also http://lammps.sandia.gov/.

[61] I. Prigogine. *Introduction to Thermodynamics of Irreversible Processes*. Wiley-Interscience, New York, 1967.

[62] I. Prigogine. *Introduction to Thermodynamics of Irreversible Processes*. John Wiley and Sons, New York, 1967.

[63] R. C. Reid, J. M. Prausnitz, and B. E. Poling. *The Properties of Gases and Liquids*. McGraw-Hill, New York, 4th edition, 1987.

[64] F. Reif. *Fundamentals of Statistical and Thermal Physics*. McGraw-Hill, Inc., New York, 1965.

[65] L. A. Rowley, D. Nicholson, and N. G. Parsonage. Monte Carlo grand canonical ensemble calculation in a gas-liquid transition for 12-6 Argon. *J. Chem. Phys*, 17:401 – 414, 1975.

[66] R. L. Rowley and F. H. Horne. The Dufour effect. II. experimental confirmation of the onsager heatmass reciprocal relation for a binary liquid mixture. *J. Chem. Phys.*, 68(1):325–326, 1978.

[67] P. K. Schelling, S. R. Phillpot, and P. Keblinski. Comparison of atomic-level simulation methods for computing thermal conductivity. *Phys. Rev. B*, 65:144306–12, 2002.

[68] F. H. Stillinger and T. A. Weber. Computer-simulation of local order in condensed phases of silicon. *Phys. Rev. B*, 31:5262–5271, 1985.

[69] A. Tenenbaum, G. Ciccotti, and R. Gallico. Stationary nonequilibrium states by molecular dynamics. fourier's law. *Phys. Rev. A*, 25:2778–2787, 1982.

[70] S. G. Volz and G. Chen. Molecular-dynamics simulation of thermal conductivity of silicon crystals. *Phys. Rev. B*, 61:2651–2656, 2000.

[71] Z. Wang, F. Gao, J. P. Crocombette, X. T. Zu, L. Yang, and W. J. Weber. Thermal conductivity of GaN nanotubes simulated by nonequilibrium molecular dynamics. *Physical Review B*, 75:153303–1–153303–4, 2007.

[72] Z. Wang, X. Zu, F. Gao, W. J. Weber, and J.-P. Crocombette. Atomistic simulation of the size and orientation dependences of thermal conductivity in GaN nanowires. *Appl. Phys. Lett.*, 90(16):161923, 2007.

[73] X. W. Zhou, S. Aubry, R. E. Jones, A. Greenstein, and P. K. Schelling. Towards more accurate molecular dynamics calculation of thermal conductivity: Case study of GaN bulk crystals. *Phys. Rev. B*, 79:115201, 2009.

[74] J. A. Zimmerman, E. B. Webb III, J. J. Hoyt, R. E. Jones, P. A. Klein, and D. J. Bammann. Calculation of stress in atomistic simulation. *Modelling Simul. Mater. Sci. Eng.*, 12:S319–S332, 2004.

[75] R. Zwanzig. Elementary derivations of time-correlation formulas for transport coefficients. *J. Chem. Phys.*, 40:2527–2533, 1964.

Appendix A

Numerical Integration Algorithm for HNEMD Method

The governing system of equations (5.11) and (6.18) with the addition of a Nosé-Hoover (NH) thermostat can be decomposed into

$$\frac{d}{dt}\begin{bmatrix}\mathbf{r}_i\\ \mathbf{p}_i\\ \zeta\end{bmatrix} = \begin{bmatrix}\mathbf{0}\\ \mathbf{0}\\ \frac{1}{Q}\left(\bar{T}(\mathbf{p})/T-1\right)\end{bmatrix} + \begin{bmatrix}\mathbf{0}\\ -\zeta\mathbf{p}_i\\ \mathbf{0}\end{bmatrix} + \begin{bmatrix}\mathbf{0}\\ \mathbf{D}_i(\mathbf{r},\mathbf{p},\mathbf{F}(\mathbf{r}))\mathbf{F}_e\\ \mathbf{0}\end{bmatrix} + \begin{bmatrix}\mathbf{0}\\ \mathbf{F}_i(\mathbf{r})\\ \mathbf{0}\end{bmatrix} + \begin{bmatrix}\frac{1}{m}\mathbf{p}_i\\ \mathbf{0}\\ \mathbf{0}\end{bmatrix} \quad \text{(A.1)}$$

where $\bar{T}(\mathbf{p}) = \sum_i \frac{\mathbf{p}_i \cdot \mathbf{p}_i}{2m}$, T is the expected temperature, ζ is the NH control variable, $\mathbf{D}_i\mathbf{F}_e$ is the Evans bias force (6.18), and $\mathbf{F}_i$ is the interatomic force. To integrate this system of ordinary differential equations, the operator-split method [50] is employed. This method is based on the decomposition of the p-Liouvillean operator that propagates the initial state

$$\mathbf{\Gamma}(t) = \exp(\mathrm{iL}t)\mathbf{\Gamma}(0) \quad \text{(A.2)}$$

into $\mathrm{L} = \mathrm{L}_\zeta + \mathrm{L}_{p_1} + \mathrm{L}_{p_2} + \mathrm{L}_{p_3} + \mathrm{L}_x$ which correspond to sequence of vectors on the right-hand side of (A.1), so that

$$\begin{aligned}\exp(\mathrm{iL}\Delta t) = \exp\left(\mathrm{iL}_\zeta\frac{\Delta t}{2}\right)\exp\left(\mathrm{iL}_{p_3}\frac{\Delta t}{2}\right)\exp\left(\mathrm{iL}_{p_2}\frac{\Delta t}{2}\right)\exp\left(\mathrm{iL}_{p_1}\frac{\Delta t}{2}\right)\exp(\mathrm{iL}_x\Delta t)\\ \exp\left(\mathrm{iL}_{p_1}\frac{\Delta t}{2}\right)\exp\left(\mathrm{iL}_{p_2}\frac{\Delta t}{2}\right)\exp\left(\mathrm{iL}_{p_3}\frac{\Delta t}{2}\right)\exp\left(\mathrm{iL}_\zeta\frac{\Delta t}{2}\right) + h.o.t.\,.\end{aligned} \quad \text{(A.3)}$$

In applying the operator split methodology the action of each of the evolution operators $\mathrm{L}_\zeta, \mathrm{L}_{p_1}\ldots$ on $\{\mathbf{r}_i, \mathbf{p}_i, \zeta\}$ is integrated in turn, preferrably exactly; however, in the case of the Evans force $\mathbf{D}_i\mathbf{F}_e$, which depends on $\mathbf{p}$ only through the energy E_i, it is possible but not feasible to integrate

$\dot{\mathbf{p}} = \mathbf{D}_i(\mathbf{r}, \mathbf{p}, \mathbf{F}(\mathbf{r}))\mathbf{F}_e$ exactly given the quadratic dependence of $\mathbf{D}_i\mathbf{F}_e$ on $\mathbf{p}$. Therefore, given the relative expense of the operations, where the interatomic force evaluation is the most expensive followed by the Evans force, the integration of $\mathbf{D}_i\mathbf{F}_e$ is lumped with $\mathbf{F}$, see (A.8) and (A.9) below. With this choice, the resulting update is essentially the same as in the NVT algorithm in [50, Equation 26], namely

$$\zeta_{n+1/2} = \zeta_n + \frac{\Delta t}{2Q}\left(\frac{\bar{T}(\mathbf{p}_n)}{T_0} - 1\right) , \tag{A.4}$$

$$\tilde{\mathbf{p}}_n = \exp\left(\frac{\Delta t}{2}\zeta_{n+1/2}\right)\mathbf{p}_n , \tag{A.5}$$

$$\mathbf{p}_{n+1/2} = \tilde{\mathbf{p}}_n + \frac{\Delta t}{2m}\mathbf{F}_n , \tag{A.6}$$

$$\mathbf{r}_{n+1} = \mathbf{r}_n + \frac{\Delta t}{m}\mathbf{p}_{n+1/2} , \tag{A.7}$$

$$\tilde{\mathbf{F}}_{n+1} = \mathbf{F}(\mathbf{r}_{n+1}) , \tag{A.8}$$

$$\mathbf{F}_{n+1} = \tilde{\mathbf{F}}_{n+1} + \mathbf{D}(\mathbf{r}_{n+1}, \tilde{\mathbf{F}}_{n+1}, \mathbf{p}_{n+1/2})\mathbf{F}_e , \tag{A.9}$$

$$\mathbf{p}_{n+1} = \tilde{\mathbf{p}}_{n+1} + \frac{\Delta t}{2m}\mathbf{F}_{n+1} , \tag{A.10}$$

$$\tilde{\mathbf{p}}_{n+1} = \exp\left(\frac{\Delta t}{2}\zeta_{n+1/2}\right)\mathbf{p}_{n+1/2} , \tag{A.11}$$

$$\zeta_{n+1} = \zeta_{n+1/2} + \frac{\Delta t}{2Q}\left(\frac{\bar{T}(\mathbf{p}_{n+1})}{T_0} - 1\right) , \tag{A.12}$$

where (A.4) and (A.12) are the exact integration of L_ζ over $\frac{\Delta t}{2}$. Likewise, (A.5) and (A.11) are the exact integration of L_{p_3} over $\frac{\Delta t}{2}$, (A.6) and (A.10) are the integration of $L_{p_2+p_1}$ over $\frac{\Delta t}{2}$ and, finally, (A.7) is the exact integration of L_x over Δt. Here, the subscripts enumerate time-steps. It also should be noted that this operator-split method is not second-order accurate, unlike the similar schemes in [50], due to its inability to integrate the Evans force $\mathbf{D}_i\mathbf{F}_e$ exactly. However, the method does preserve momentum exactly, assuming the total initial momentum is zero. By summing either (A.5) or (A.11) over the atoms, it is clear that the exponential factor merely scales the original momentum, *i.e.*, zero, and therefore does not change it. Likewise, (A.6) and (A.10) do not change the total momentum since both the interatomic and field-dependent forces sum to zero. The sum of the interatomic forces $\mathbf{F}(\mathbf{r})$ is zero since the system is periodic and the sum of the field-dependent forces $\mathbf{D}(\mathbf{r}, \mathbf{F}, \mathbf{p})\mathbf{F}_e$ is zero since these forces are formulated as a deviation from an average.

This algorithm was incorporated into the MD code LAMMPS [60].

Appendix B

Numerical Integration Algorithm for M-HNEMD Method

Following Appendix A, the governing system of equations (5.11) can be decomposed into

$$\frac{d}{dt}\begin{bmatrix}\mathbf{r}_i\\ \mathbf{p}_i\\ \zeta\end{bmatrix} = \underbrace{\begin{bmatrix}\mathbf{0}\\ \mathbf{0}\\ \frac{1}{Q}\left(\frac{\bar{T}(\mathbf{p})}{T}-1\right)\end{bmatrix}}_{L_1} + \underbrace{\begin{bmatrix}\mathbf{0}\\ -\zeta\mathbf{p}_i\\ \mathbf{0}\end{bmatrix}}_{L_2} + \underbrace{\begin{bmatrix}\mathbf{0}\\ \mathbf{D}_i(\mathbf{r},\mathbf{p})\mathbf{F}_e\\ \mathbf{0}\end{bmatrix}}_{L_3} + \underbrace{\begin{bmatrix}\mathbf{0}\\ \mathbf{F}_i(\mathbf{r})\\ \mathbf{0}\end{bmatrix}}_{L_4} + \underbrace{\begin{bmatrix}\frac{1}{m}\mathbf{p}_i\\ \mathbf{0}\\ \mathbf{0}\end{bmatrix}}_{L_5} + \underbrace{\begin{bmatrix}\mathbf{C}_i(\mathbf{r},\mathbf{p})\mathbf{F}_e\\ \mathbf{0}\\ \mathbf{0}\end{bmatrix}}_{L_6} \tag{B.1}$$

where $\bar{T}(\mathbf{p}) = \dfrac{1}{3Nk_B}\sum_{i=1}^{N}\dfrac{\mathbf{p}_i\cdot\mathbf{p}_i}{m_i}$. The operator-split method in [50] is employed to integrate the preceding system of ordinary differential equations. In this method, the propagation

$$\mathbf{\Gamma}(t) \;=\; \exp(\mathrm{iL}t)\mathbf{\Gamma}(0) \tag{B.2}$$

of the initial state is approximated according to

$$\begin{aligned}\exp(\mathrm{iL}\Delta t) = \exp\left(\mathrm{iL}_1\frac{\Delta t}{2}\right)\exp\left(\mathrm{iL}_2\frac{\Delta t}{2}\right)\exp\left(i\mathrm{L}_{3+4}\frac{\Delta t}{2}\right)\exp\left(i\mathrm{L}_5\frac{\Delta t}{2}\right)\exp(\mathrm{iL}_6\Delta t)\\ \exp\left(\mathrm{iL}_5\frac{\Delta t}{2}\right)\exp\left(\mathrm{iL}_{3+4}\frac{\Delta t}{2}\right)\exp\left(\mathrm{iL}_2\frac{\Delta t}{2}\right)\exp\left(\mathrm{iL}_1\frac{\Delta t}{2}\right) + h.o.t.\,,\end{aligned} \tag{B.3}$$

where iL is the p-Liouvillean [24, Section 3.3] . The update formulae for the individual steps are defined as

$$L_1: \quad \zeta_{n+1/2} = \zeta_n + \frac{\Delta t}{2}\frac{1}{Q}\left(\frac{\bar{T}(\mathbf{p}_n)}{T} - 1\right) \tag{B.4}$$

$$L_2: \quad \tilde{\mathbf{p}}_{n+1/2} = \exp\left(-\frac{\Delta t}{2}\zeta_{n+1/2}\right)\mathbf{p}_n \tag{B.5}$$

$$L_{3+4}: \quad \mathbf{p}_{n+1/2} = \tilde{\mathbf{p}}_{n+1/2} + \frac{\Delta t}{2m}\mathbf{F}_n \tag{B.6}$$

$$L_5: \quad \mathbf{r}_{n+1/2} = \mathbf{r}_n + \frac{\Delta t}{2m}\mathbf{p}_{n+1/2} \tag{B.7}$$

$$L_6: \quad \tilde{\mathbf{r}}_{n+1} = \mathbf{r}_{n+1/2} + \Delta t\,\mathbf{C}(\mathbf{r}_{n+1/2}, \mathbf{p}_{n+1/2})\,\mathbf{F}_e \tag{B.8}$$

$$L_5: \quad \mathbf{r}_{n+1} = \tilde{\mathbf{r}}_{n+1} + \frac{\Delta t}{2m}\mathbf{p}_{n+1/2} \tag{B.9}$$

$$\tilde{\mathbf{F}}_{n+1} = \mathbf{F}(\mathbf{r}_{n+1}) \tag{B.10}$$

$$\mathbf{F}_{n+1} = \tilde{\mathbf{F}}_{n+1} + \mathbf{D}(\mathbf{r}_{n+1}, \mathbf{p}_{n+1/2}, \tilde{\mathbf{F}}_{n+1})\mathbf{F}_e \tag{B.11}$$

$$L_{3+4}: \quad \tilde{\mathbf{p}}_{n+1} = \mathbf{p}_{n+1/2} + \frac{\Delta t}{2m}\mathbf{F}_{n+1} \tag{B.12}$$

$$L_2: \quad \mathbf{p}_{n+1} = \exp\left(-\frac{\Delta t}{2}\zeta_{n+1/2}\right)\tilde{\mathbf{p}}_{n+1} \tag{B.13}$$

$$L_1: \quad \zeta_{n+1} = \zeta_{n+1/2} + \frac{\Delta t}{2}\frac{1}{Q}\left(\frac{\bar{T}(\mathbf{p}_{n+1})}{T} - 1\right) \tag{B.14}$$

where, in the interest of brevity, all the i subscripts referring to atoms have been omitted. Here the subscript n refers to the time-step. Also note that $\mathbf{F}_0$ is defined as $\mathbf{F}_0 = \mathbf{F}(\mathbf{r}_0)$, given initial conditions $\mathbf{r}_0$ and $\mathbf{p}_0$.

All the steps of this algorithm involve exact integration of the respective propagators, with the exception of (B.8) and (B.12) which involve integration of the forces $\mathbf{C}_i\mathbf{F}_e$ and $\mathbf{D}_i\mathbf{F}_e$. Indeed, (B.12) is exact except for the part of $\mathbf{D}_i$ that depends on kinetic energy and, consequently, on terms involving squares of the components of $\mathbf{p}_i$. Moreover, $\mathbf{D}_i$ involves the momenta of each atom through the average kinetic energy embedded in $\mathbf{D}_i$. Likewise, (B.8) is inexact due to the dependence of $\mathbf{C}_i$ on a set of $\mathbf{r}_j$, which couples the integration for atom i to the motions of its neighboring atoms.

This algorithm was incorporated into the MD code LAMMPS [60].